GEOCHEMICAL EVOLUTION OF HAWAIIAN GROUNDWATER

DISSERTATION SUBMITTED TO THE GRADUATE DIVISION OF THE UNIVERSITY OF HAWAI'I AT MĀNOA IN PARTIAL FULFILLMENT OF THE REQUIREMENTS FOR THE DEGREE OF

DOCTOR OF PHILOSOPHY

IN

GEOLOGY AND GEOPHYSICS

AUGUST 2016

By

Joseph K. Fackrell

Dissertation Committee:

Craig Glenn, Chairperson
Roger Babcock
Henrietta Dulai
Aly El-Kadi
Brian Popp

Keywords: Groundwater, dissolved inorganic nutrients, DIC, stable isotopes, wastewater, West Maui, West Hawai‘i

ACKNOWLEDGEMENTS

I thank my advisor, Craig Glenn, and my committee members for providing me the opportunity, means, and assistance necessary to see this dissertation project through to completion.

I would like to thank Scott Rollins with the Maui County Wastewater Division and Watson Okubo at the Hawai‘i State Department of Health for providing the monitoring data used in Chapter 2 of this dissertation. I would also like to thank the Kīholo community, Justin Lottig, David Chai, Charles Dawrs, Mary Metcalf, Steve Patterson, Keith Olson, Justin Rose, and Bob Ravenscraft for providing access and support for water sampling as well as George Wilkins, Britt Craven, Joshua Vandemark, Adam Sibley, and Jeremy Kimura for providing access to precipitation collector locations. I additionally thank Jacque Kelly, Christine Waters, George Bugarin, James Bishop, Joseph Kennedy, and Christopher Shuler for their assistance with sampling and analysis as well as Bob Whittier and Don Thomas for sharing their experience and insight on groundwater in Hawai‘i.

This project has been funded by grants from the NSF Hawai‘i EPSCoR Program through the National Science Foundation under award number EPS-0903833, WRRIP grant numbers 2014HI434B and 2015HI442B through the University of Hawai‘i Water Resources Research Center, the United States Environmental Protection Agency through the Hawai‘i State Department of Health (grant number INF20110364), the United States Army Engineer Research and Development Center (grant number INF20110342), and by a grant/cooperative agreement to Craig Glenn from the National Oceanic and Atmospheric Administration, Project R/HE-17, which is sponsored by the University of Hawai‘i Sea Grant College Program, SOEST, under Institutional Grant No. NA09OAR4170060 from NOAA Office of Sea Grant, Department of Commerce. The views expressed herein are those of the author(s) and do not necessarily reflect the views of any of the agencies listed.

Finally, I would like to thank my family and my girlfriend for all of their understanding and support throughout this process.

ABSTRACT

Groundwater in Hawai‘i is heavily utilized for domestic, industrial, and agricultural purposes and additionally serves as a delivery mechanism of dissolved nutrients and inorganic C to coastal waters via submarine groundwater discharge (SGD). An understanding of the factors that control dissolved nutrient and inorganic C concentrations in groundwater is vital to sustainable use of this economically and ecologically important resource. In order to better understand the dynamics of dissolved nutrients and inorganic C in Hawaiian groundwater I investigated the biogeochemistry of a subsurface wastewater effluent plume in West Maui and used H and O isotopic composition of water to develop groundwater conceptual models and flow paths for the West Hawai‘i region which I then used to evaluate relationships between terrestrial controls and groundwater geochemical parameters.

I utilized N and C species concentration data along with $\delta^{15}N$ values of NO_3^- and $\delta^{13}C$ values of dissolved inorganic C to evaluate the stoichiometry of biogeochemical reactions (mineralization, nitrification, anammox, denitrification) occurring within a subsurface wastewater plume that originates as treated wastewater injection and enters the coastal waters of West Maui as SGD via several submarine springs. Additionally, I compared wastewater time-series data, injection rates, and treatment history with submarine spring time-series data to assess correlation between input and output variables. I found that heterotrophic denitrification is the primary mechanism of N loss within the groundwater plume and that chlorination for pathogen disinfection suppresses microbial activity responsible for N loss, resulting in increased coastal ocean N loading. Replacement of chlorination with UV disinfection may restore biogeochemical reactions responsible for N loss within the aquifer and return N-attenuating conditions in the effluent plume, reducing N loading to coastal waters.

I characterized the local meteoric water line (LMWL) and relationship between $\delta^{18}O$ values in precipitation and elevation for the West Hawai‘i region utilizing a network of 8 cumulative precipitation collectors sampled at 6-month intervals over a 2 year period. Additionally, I determined $\delta^{2}H$ and $\delta^{18}O$ values for groundwater samples across the study area. I then utilized these data to develop new conceptual models of groundwater flow and characterized groundwater flow paths in this complex and poorly understood hydrogeologic setting. The West Hawai‘i LMWL indicates a primary source of oceanic moisture from the lee of the island, while the $\delta^{18}O$-elevation relationship resembles that determined for the trade-wind

potion of the Hawai‘i Volcano region. I developed updated conceptual models on groundwater occurrence and flow in the West Hawai‘i region incorporating subsurface geological features that I utilized in conjunction with $\delta^{18}O$ values for groundwater samples to determine that groundwater flow paths in the West Hawai‘i region generally originate at high elevations in the island’s interior

I measured PO_4^{3-}, SiO_4^{4-}, NO_3^-, and DIC concentrations as well as $\delta^{15}N$ of NO_3^- and $\delta^{13}C$ of DIC values for groundwater samples collected throughout the West Hawai‘i study area. I then used the Spearman’s rank correlation test to aid in the assessment of the effects of land use/land cover, wastewater effluent discharge, and geothermal activity along flow paths determined for each groundwater sample on the measured parameters. I found that geothermal activity was significantly correlated to elevated groundwater SiO_4^{4-}, NO_3^-, and DIC concentrations and that wastewater effluent discharge along with urban and park land use was significantly correlated to elevated groundwater NO_3^- concentrations. Additionally, land use and land cover types associated with greater precipitation and soil development were significantly correlated to elevated PO_4^{3-} concentrations.

TABLE OF CONTENTS

LIST OF TABLES

LIST OF FIGURES

CHAPTER 1. INTRODUCTION

Background

Understanding terrestrial origins and delivery mechanisms of dissolved species (and particularly bio-active nutrients and dissolved inorganic carbon (DIC)) to the coastal ocean is vital to recognizing which natural and anthropogenic factors on land most impact coastal ecosystems. Submarine groundwater discharge (SGD), which can be enriched in nutrients relative to marine surface waters, has been shown to be the primary transport mechanism of land-derived nutrients and other dissolved components to coastal waters even in areas with significant surface water discharge (Moore, 2006). Furthermore, SGD was found to contribute 80-160% the amount of freshwater river flux to the Atlantic Ocean (Moore, 2008). On large tropical islands, such as those of the Hawaiian archipelago where this study is based, SGD generally comprises a greater fraction of freshwater coastal discharge than on continents due to abundant rainfall, high relief, and highly permeable fractured rock aquifers (Zektser, 2000). On the dry leeward sides of high islands such as Maui and Hawai‘i, surface water discharge is minor to nearly non-existent, and thus SGD clearly dominates the freshwater flux to the coastal ocean (e.g. Johnson et al., 2008). The geochemical composition of SGD on large tropical islands can be affected by multiple natural and anthropogenic factors from its origin as meteoric water to its eventual discharge at the coast. The overarching goal of my research is to gain a greater understanding of the factors controlling the groundwater geochemistry and, in particular, the spatial and temporal flow of groundwater-borne nutrients and DIC to the coastal ocean. This information may fundamentally influence policy decisions regarding land and water use practices.

Field Sites

I investigated two field locations for my dissertation research. The first location and subject of Chapter 2 is the Kā‘anapali region of West Maui, with particular emphasis on an injected wastewater effluent plume originating at the Lahaina Wastewater Reclamation Facility (LWRF) and discharging from submarine springs at nearby Kahekili Beach. The second location and subject of Chapters 3 and 4 is much broader and consists of a large part of the western portion of the island of Hawai‘i, roughly bounded by the peaks of Mauna Kea and Mauna Loa in the east and coastline between Kīholo and Kealakekua Bays in the west.

West Maui

The landscape of the Kā‘anapali region of West Maui is characterized by a variety of past and present land use practices including intensive sugar cane and pineapple agriculture, golf course and resort development, and wastewater disposal via effluent injection. The injection of wastewater effluent at the Lahaina Wastewater Reclamation Facility (LWRF) is particularly important because it has a unique geochemical fingerprint that is easily traced in the subsurface and facilitates the identification of effluent-sourced groundwater as SGD. The effects of land use on the occurrence of invasive algal blooms and coral reef degradation in proximal near shore waters has been the subject of several recent studies described in greater detail below.

The Kā‘anapali region is located on the relatively dry, lightly dissected leeward portion of the West Maui volcano (1.2-1.6 Ma.) The geology of this area is dominated by the shield building Wailuku Volcanic series overlain by a thin veneer of later stage Honolua Volcanic series lavas in the northern portion of the study area. The rejuvenated stage Lahaina Volcanic series (age unknown) occurs as vents at Pu‘u Keka‘a (Black Rock) and further south near Lahaina town (Stearns and Macdonald, 1942). A narrow band of poorly characterized coastal alluvium, likely consisting of both terrestrial and marine sediments, fronts the coast at most locations in the study area. The area’s groundwater exists primarily as an unconfined basal lens with low hydraulic gradients due to the high hydraulic conductivity of the basaltic aquifer (Stearns and Macdonald, 1942, Gingerich et al., 2012). Though locally confining conditions may exist in the coastal alluvium, they are not widespread enough to create a discernible effect on the larger scale water table levels of the basal lens (Souza, 1981). Dike confined high-level groundwater exists in the far upland portion of the study area near Pu‘u Kukui (the summit of the West Maui volcano), where the area’s rainfall and groundwater recharge rates are highest (Engott and Vana, 2007).

Land use in the Kā‘anapali area was long dominated by intensive sugar cane cultivation south of Honokowai stream and pineapple cultivation north of Honokowai stream, but recently both industries have declined, with sugar cane and pineapple cultivation ceasing entirely in 1999 and 2009, respectively. The Kā‘anapali area now consists primarily of resort, golf course, and light commercial development along the coastline with former agricultural fields on the lower slopes (to about 400 m elevation) and state forest reserves on the upper slopes (above about 400 m elevation). Wastewater from the Kā‘anapali area is processed at LWRF and disposed of via 4

on-site injection wells drilled to roughly 60 m below sea level at injection rates of approximately 3 million gallons per day (MGD) (Glenn et al., 2012). LWRF is located approximately 0.5 km inland from Kahekili Beach. This facility has undergone several expansions and treatment upgrades since its inception in 1975. The processing capacity of LWRF was increased from 3.2 to 6.7 MGD by construction of an additional plant onsite in 1985 (Tetra Tech, 1993), and in 1995 biological nutrient removal and UV disinfection capabilities were instituted to further treat wastewater before injection (Scott Rollins, County of Maui Wastewater Reclamation Division, personal communication). LWRF is currently capable of treating effluent to irrigation (R1) quality and delivers 0.7-1.5 MGD of R1 water to Kā‘anapali Golf Course and 0.185 MGD to the Honua Kai resort for reuse in addition to the roughly 3 MGD of effluent disposed of via on-site injection (Glenn et al., 2012).

The occurrence of large scale algal blooms in the Kā‘anapali area during the late 1980s raised concerns regarding the impacts of land use practices on the coastal environment. It was thought that SGD carrying nutrients from intensively fertilized and irrigated sugarcane and pineapple agriculture, resort and golf course development, the domestic use of cesspools and septic tanks, and effluent injection at LWRF was contributing to coastal nuisance algal blooms. Several studies, including an inconclusive dye tracer injection test at the LWRF injection wells (Tetra Tech, 1994), were conducted to examine the contribution various land use practices had on nutrient delivery to the coastal ocean (e.g. Tetra Tech, 1993; Dollar and Andrews, 1997). Various modeling approaches combined with in situ measurements were used to assess the contributions of various land use activities to coastal nutrient delivery from both ground and surface waters (Tetra Tech, 1993; Soicher, 1996; Soicher and Peterson, 1997). Dollar and Andrews (1997) and Laws (2004) examined the area’s coastal water quality by comparing nutrient concentrations across various locations. Dollar and Andrews (1997) also measured N isotopic composition of algal tissue in an attempt to determine the contribution of terrestrially derived N to this tissue. More recently, analysis of wastewater indicator chemicals, nutrient species, and stable isotopic compositions of water and dissolved NO_3^- (Hunt and Rosa, 2009), N isotopic composition in algal tissue (Dailer et al., 2010, 2012), and analysis of trace metals, radon, nutrient species, and subsurface electrical resistivity (Swarzenski et al., 2012, 2015) were used to ascertain pathways of nutrient delivery to coastal waters. These studies identified a stretch of coastal ocean along Kahekili Beach Park roughly 1 km southwest of the LWRF

injection wells characterized by elevated $\delta^{15}N$ values in algal tissue, higher temperatures, and water with lower pH values relative to adjacent areas. These findings were interpreted as evidence for injected effluent discharging into coastal waters along this stretch of coastline. The detection of wastewater indicator compounds (carbamazepine and sulfamethoxazole) in submarine springs along this stretch of coastline (Hunt and Rosa, 2009) lent further support to this interpretation. Most recently, dye tracer and natural tracer geochemical methods were used to confirm the hydrological connection between injected LWRF effluent and submarine springs located just offshore of Kahekili beach park (Glenn et al., 2012; Glenn et al., 2013). In addition, a large plume of anomalously warm seawater in the vicinity of submarine springs at Kahekili Beach Park was found using aerial thermal infrared imagery (Glenn et al., 2012).

West Hawai‘i

The geology and hydrology of West Hawai‘i contrast markedly to West Maui as it is comprised of young, relatively unweathered and uneroded lavas, and lacks both cap rock and coastal alluvium. In further contrast to the West Maui region, the West Hawai‘i region is characterized by well documented copious SGD (e.g. Johnson et al., 2008; Peterson et al., 2009), a lack of intensive agriculture, a large proportion of bare land, high relief, and drastically varied climatic regimes.

The West Hawai‘i study area is located on the relatively undissected flanks of the historically active Hualālai and Mauna Loa volcanoes as well as the dormant Mauna Kea volcano. The Hualālai volcano dominates the central and coastal portions of the study area and contains a prominent rift zone trending northwest from its main vents. The volcano’s structure consists of subsurface tholeiitic lavas (exposed only in boreholes and submarine deposits) overlain by the Waa Waa Trachyte Member, emplaced approximately 114-92 ka, and the younger alkalic Hualālai volcanic series (Sherrod et al., 2007). Hualālai is unique among Hawaiian volcanoes in that its dense substructure, which is presumed to mark the eruptive pathways of the volcano’s tholeiitic shield building stage, is displaced by 4 km from its surficial vents and rift zones (Kauahikaua et al., 1998). Hualālai has also experienced large-scale mass wasting in the form of the North Kona Slump (>130 ka) which left a large offshore escarpment subsequently draped with younger lavas (Moore and Clague, 1992).

Groundwater in the West Hawai‘i study area occurs as both a thin lens of basal groundwater under Ghyben-Herzberg conditions within several kilometers of the coast and as high-level groundwater further inland. The basal groundwater is characterized by low hydraulic gradients due to the lack of confining coastal sediments and high hydraulic conductivities of the young lava flows. It also exhibits a strong response to tidal cycling (Oki, 1999), illustrating its hydraulic connectivity to the ocean. The structures responsible for the presence of high-level groundwater in this area are not well understood, but available drilling log, water level, and pump test data suggests that both dense impermeable flows impounding water under artesian conditions and buried dikes impeding horizontal flow may be important factors (Oki, 1999; Bauer, 2003, Thomas et al., 2015). Drilling log and depth profile data acquired from boreholes drilled through the basal lens in the North Keauhou aquifer suggest that (1) cold, intermediate depth seawater circulates through the basal lens in this region, possibly entering at the steep submerged headwall of the North Kona Slump and (2) fresh water under artesian conditions, possibly related to the high-level water found further inland, underlies the basal lens in this area and is hydraulically connected to the ocean (Bowles, 2007; Nance, 2013). Recent work by Fackrell and Glenn, (2014) and Tillman et al., (2014) used H and O isotopic composition of water to demonstrate that high-level water is hydraulically connected to and recharges basal groundwater in this region. Most recently, Kelly and Glenn (2015) used CFC dating and H and O isotopic composition of water to characterize fractions of “old” vs. “young” recharge as well as groundwater flow paths for portions of the study area.

The West Hawai‘i study area covers a wide variety of ecosystems and land use types and is well known for its characteristic groundwater-fed coastal anchialine ponds. The portion of the study area north of Hualālai’s northwest rift is relatively arid and dominated by bare lava, grassland, and scrubland. It is currently lightly developed, with conservation land at higher elevations, current and former ranch land at middle elevations, and localized resort and golf course development along the coast. The portion of the study area south of Hualālai’s northwest rift zone contains the Kailua-Kona urban center and is considerably more developed than the portion of the study area north of Hualālai’s northwest rift zone. Relative to its higher elevations, the coastal portion of this region is arid and contains a wide variety of land use types including an airport, an experimental industrial park, Kaloko-Honokōhau National Historical Park, the Kealakehe wastewater treatment plant effluent disposal site, and the urban development of

Kailua-Kona. As the majority of residences in this region are not connected to centralized sewer systems, most wastewater is disposed of via on-site sewage disposal systems (OSDS) (Whittier and El-Kadi, 2009). The middle elevations of this area (roughly 400-1500 m) comprise Kona's famous "coffee belt" and receive relatively high rainfall driven by the interaction of moisture-laden daytime sea breezes with the steep and high elevation western slope of the Hualālai volcano (Giambelluca et al., 2013). Land use at these middle elevations consists primarily of forest, pasture, coffee plantations, and light residential development. At elevations >1500 m, the region receives progressively less rainfall with increasing elevation and is dominated by conservation and pasture lands.

Numerous previous studies have shed light on groundwater geochemistry and the role of SGD in delivering dissolved nutrients to the ocean in West Hawai‘i. Swain (1973) analyzed basic water parameters and major dissolved ion concentrations in several West Hawai‘i wells in conjunction with a statewide groundwater quality survey. Kay et al. (1977) used a volumetric approach combined with nutrient analyses to estimate SGD-driven nutrient fluxes in the northern portion of the region. Thomas, (1986) conducted dissolved ion analyses of West Hawai‘i groundwater in support of geothermal resource assessment and found evidence for potential thermal alteration of groundwater near Hualālai's northwest rift zone. Dollar and Atkinson, (1992) considered fertilizer application and leaching rates to demonstrate that fertilizer applied to two golf courses in the region could result in increased delivery of dissolved N and P species to the adjacent coastal ocean via SGD. Oki, (1999) and Bauer, (2003) analyzed available borehole log, water level, and pump test data to describe the occurrence of groundwater in West Hawai‘i and speculate regarding the nature of the subsurface structures responsible for the impoundment of high-level groundwater south of the Hualālai northwest rift zone. Bowles, (2007) and Nance, (2013) cited anomalously low basal groundwater temperatures and a negative correlation between salinity and temperature in boreholes in the Northern Keauhou aquifer as evidence for the recirculation of cold, intermediate depth seawater in this area. Other recent studies have used radiochemical tracers (e.g. Street et al., 2008; Peterson et al. 2007, 2009) and aerial thermal infrared imagery (Johnson et al., 2008) combined with nutrient analyses of groundwater and SGD to quantify the magnitude of SGD and its associated nutrient fluxes at various locations along the West Hawai‘i coast. Important outcomes of these studies include identification of the spatially and temporally variable nature of SGD in this region and the determination of locally

consistent linear relationships between nutrient concentrations and salinity in groundwater and associated SGD plumes. Knee et al., (2010) attempted to spatially link nutrient concentrations in SGD and up-gradient groundwater with land use in West Hawai‘i, but were not able to establish conclusive relationships. Hunt, (2014) measured nutrient concentrations and wastewater indicator compounds in the vicinity of Kaloko-Honokōhau national historical park and found evidence for wastewater and fertilizer nutrient contributions.

Objectives

The overall goal of this research has been to better understand the most important forcing factors and transformative mechanisms responsible for the ultimate inorganic nutrient and DIC compositions of SGD in my study sites. My objectives in support of this goal were to: (1) utilize geochemical tracers to determine groundwater recharge areas, (2) assess the origins of dissolved nutrients and DIC in groundwater, and (3) evaluate the biogeochemical reactions that may influence down-gradient geochemical evolution of groundwater prior to its discharge to the ocean. Differences in scale, data availability, and characterization by previous research necessitated emphasizing different objectives between my study sites. My research in West Maui, which was focused on a relatively compact wastewater effluent plume with well characterized inputs and outputs (Glenn et al., 2012, 2013), allowed concentrated efforts on objective (3) in detail (Chapter 2). My research in West Hawai‘i, which took place over a much larger area with poorly constrained hydrogeological characteristics, required first accomplishing objective (1) (Chapter 3) before moving on to objective (2) (Chapter 4).

Chapter 2 is focused on understanding the nature and temporal variability of biogeochemical reactions occurring within the LWRF wastewater effluent plume from subsurface injection to discharge to the coastal ocean in support of objective (3). Specifically, I sought to characterize the biogeochemical processes responsible for the attenuation of N within the effluent plume as well as understand the mechanisms responsible for the temporal variability of N species concentrations in the effluent plume's coastal discharge. I utilized LWRF effluent and submarine spring N species data along with $\delta^{15}N$ values of dissolved NO_3^-, C species concentrations, and $\delta^{13}C$ values of DIC to evaluate the stoichiometry of biogeochemical reactions occurring within the subsurface effluent plume. Additionally, I considered as a whole LWRF effluent and submarine spring N species data collected over the last several years to

examine how changes in effluent injection rate as well as treatment and disinfection practices control the temporal variability in the extent of N species transformation and loss occurring within the effluent plume and, consequently, the variability of N flux to coastal waters from this source.

Chapter 3 examines groundwater recharge and flow in West Hawai‘i using H and O isotopic composition of water as a tracer in support of objective (1). I first characterized δ^2H and $\delta^{18}O$ values in precipitation and groundwater on a regional scale over several years utilizing a network of precipitation collectors and groundwater sampling locations. I then used these data in conjunction with insight gained by previous investigations to develop new conceptual models of groundwater occurrence and flow in West Hawai‘i and determine plausible groundwater flow paths for different regions of the study area based on these conceptual models.

Chapter 4 seeks to better understand the relationship between natural and anthropogenic terrestrial factors and groundwater nutrient and DIC concentrations in the West Hawai‘i study area in support of objectives (2) and (3). I utilized Spearman's rank correlation to assess the effects of land use/land cover, wastewater effluent discharge, and geothermal activity along the groundwater flow paths determined in Chapter 3 on groundwater nutrient and DIC concentrations. Additionally, I measured $\delta^{15}N$ values of NO_3^- and $\delta^{13}C$ values of DIC to aid in nutrient and DIC source identification and, where possible, examine biogeochemical transformations occurring during groundwater infiltration and flow.

Significance

The study areas chosen and the scope of research for this dissertation project were motivated by both scientific and practical considerations. As such, the findings of this work have implications for regulators responsible for land use and water resource policies as well as for scientists working in the fields of groundwater geochemistry and biogeochemistry.

In Chapter 2, I employed the novel approach of using stepwise stoichiometric analysis to provide insight into the presence and extent of various biogeochemical processes within a subsurface wastewater effluent plume. This approach may be of use for future workers seeking to understand and quantify biogeochemical processes along similarly well-constrained flow paths. Additionally, I found that chlorination of injected LWRF effluent beginning in October 2011 likely adversely affected microbial populations in the aquifer responsible for N attenuation,

resulting in an increase in observed submarine spring N flux offshore of Kahekili Beach beginning in February 2013. This finding provides insight for regulators and wastewater treatment plant operators into the potential consequences of chlorination of wastewater at facilities utilizing underground effluent injection.

Chapter 3 proposes new conceptual models for groundwater occurrence and flow as well as groundwater flow paths for the West Hawai‘i region based on insight gained from analyzing δ^2H and $\delta^{18}O$ values in precipitation and groundwater. The new conceptual models illustrate the importance of subsurface geological structures in controlling groundwater occurrence and flow throughout the region. The groundwater flow paths developed in conjunction with these conceptual models tend to originate in the upper elevations of the Mauna Loa and Mauna Kea volcanoes as opposed to the much smaller Hualālai volcano, with long travel distances implying correspondingly long travel times. These findings confirm the utility of H and O isotopic composition of water as an excellent source of insight into poorly understood groundwater systems and may serve to guide future efforts at better understanding and sustainably utilizing groundwater resources in this region.

In Chapter 4, I assessed the effects of land use/land cover, geothermal activity, and wastewater effluent discharge along previously determined groundwater flow paths (Chapter 3) on groundwater nutrient concentrations, DIC concentrations, $\delta^{15}N$ of NO_3^- values, and $\delta^{13}C$ of DIC values in West Hawai‘i. I found that (1) geothermal activity related to Hualālai’s recently active northwest rift zone is responsible for the elevated SiO_4^{4-}, NO_3^-, and DIC concentrations in groundwater in the Ka‘ūpūlehu region, (2) both wastewater effluent and fertilizer associated with urban and park land use contribute to elevated NO_3^- concentrations in groundwater in the Keauhou Coastal region, and (3) differences in land use/land cover associated with precipitation and soil development contribute to differences in PO_4^{3-} concentration, $\delta^{13}C$ of DIC values, and $\delta^{15}N$ of NO_3^- values observed between the Kīholo and Keauhou Upland regions. These findings provide much new insight into the factors responsible for the geochemical variability of groundwater in West Hawai‘i and illustrate the utility of using groundwater flow paths to assess relationships between terrestrial factors and groundwater geochemical parameters on regional scales in complex hydrogeological environments. Additionally, these findings should be of use to policy makers in better understanding the potential effects of land use decisions on the

sustainability of groundwater resources and the coastal environments they affect via SGD in West Hawai‘i and elsewhere.

Dissertation Organization

Objectives and significance of Chapters 2, 3, and 4 are discussed above. Chapter 5 discusses the major conclusions of my research as well as potential topics for future work to expand on the findings presented here. Appendix 1 presents the raw data collected and compiled from the West Maui study area while Appendix 2 presents the raw data collected and compiled from the West Hawai‘i study area.

CHAPTER 2. WASTEWATER INJECTION, AQUIFER BIOGEOCHEMICAL REACTIONS, AND RESULTANT GROUNDWATER N FLUXES TO COASTAL WATERS: KĀʻANAPALI, MAUI, HAWAIʻI

Joseph K. Fackrell, Craig R. Glenn, Brian N. Popp, Robert B. Whittier, and Henrietta Dulai

In press at *Marine Pollution Bulletin* (Available online 6/20/2016, http://dx.doi:10.1016/j.marpolbul.2016.06.050)

Abstract

We utilize N and C species concentration data along with δ15N values of NO3- and δ13C values of dissolved inorganic C to evaluate the stoichiometry of biogeochemical reactions (mineralization, nitrification, anammox, and denitrification) occurring within a subsurface wastewater plume that originates as treated wastewater injection and enters the coastal waters of Maui as submarine groundwater discharge. Additionally, we compare wastewater effluent time-series data, injection rates, and treatment history with submarine spring discharge time-series data. We find that heterotrophic denitrification is the primary mechanism of N loss within the groundwater plume and that chlorination for pathogen disinfection suppresses microbial activity in the aquifer responsible for N loss, resulting in increased coastal ocean N loading. Replacement of chlorination with UV disinfection may restore biogeochemical reactions responsible for N loss within the aquifer and return N-attenuating conditions in the effluent plume, reducing N loading to coastal waters.

Introduction

The introduction of excess anthropogenic N to coastal waters from the terrestrial environment is recognized as a major driver of coastal ocean eutrophication, whose effects include mass algae blooms, the development of hypoxic "dead zones," and degradation of original habitat (e.g. Paerl, 1997; Scavia and Bricker, 2006; Bricker et al., 2007; Howarth and Marino, 2006). Coral reef ecosystems are in decline worldwide as a result of a variety of environmental stressors (Bruno and Selig, 2007; Wilkinson, 2008) and, while the relative contribution of N pollution to this decline with respect to other stressors such as global warming and ocean acidification can be debated (Szmant, 2002), there is clear evidence that corals can be susceptible to damage from N-fuelled algae blooms, which can smother reefs and block light from reaching coral's symbiotic algae (e.g. Smith et al., 1981; Littler et al., 2006; Paytan et al.,

2006; DeGeorges et al., 2010). Common sources of N to coastal waters include fertilizer and municipal and industrial wastewater, which can be transported to the ocean via surface runoff and through the subsurface as submarine groundwater discharge (SGD).

SGD is commonly enriched in nutrients relative to ocean surface waters and can transport the majority of land-derived N and other nutrients to coastal waters, even in areas where significant surface water discharge occurs (Burnett et al., 2003; Garrison et al., 2003; Moore, 2006; Kwon et al., 2014). SGD consists of both fresh water and recirculated seawater and typically enters coastal waters via a brackish zone of subsurface mixing termed the subterranean estuary (Moore, 1999). The subterranean estuary is a hydraulically dynamic and geochemically reactive zone in which biogeochemical transformations involving N and other dissolved species occur (e.g. Slomp and Van Cappellen, 2004; Kroeger and Charette, 2008; Spiteri et al., 2008). Because N transformations in the subterranean estuary can govern the spatial and temporal changes in the rate of N species delivery to coastal waters, understanding the nature and extent of these reactions is necessary to characterizing N flux from this complex zone.

NO_3^- reduction, the bacterially mediated stepwise transformation of aqueous NO_3^- to N_2 gas, is the primary means of bioactive N loss in groundwater (Kendall, 1998). The reaction typically requires suboxic conditions, the presence of an electron donor, and a population of denitrifying bacteria (Kehew, 2000). Factors that affect these requirements have the potential to disrupt the NO_3^- reduction reaction. NO_3^- $\delta^{15}N$ values can be diagnostic of NO_3^- source provenance and various transformative processes in the N cycle (e.g. Kendall, 1998; Granger and Sigman, 2008). N isotope values have been used in groundwater studies (e.g. Aravena and Robertson, 1998) and marine studies (e.g. Sigman et al., 2005) to trace the sources and evolution of NO_3^-. In this study we use NO_3^- $\delta^{15}N$ values and NO_3^- concentrations as indicators of NO_3^- reduction. The microorganisms responsible for denitrification preferentially reduce $^{14}NO_3^-$ into N_2, leaving the remaining NO_3^- relatively enriched in ^{15}N (Kendall, 1998).

Dissolved organic C (DOC) is a key species in facilitating NO_3^- reduction in groundwater. DOC is a source of sustenance for heterotrophic microorganisms that preferentially utilize available dissolved O_2 (DO) as an electron acceptor in aerobic respiration due to its high energy yield. When DOC remains in excess as DO concentrations become suboxic, capable microorganisms shift to anaerobic respiration using available NO_3^- as an electron acceptor (reducing NO_3^- to N_2 gas) to facilitate the oxidation of organic C to dissolved inorganic C (DIC)

(Froelich et al., 1979; Stumm and Morgan, 1996; Kehew, 2000). Species such as Fe^{2+} may also be oxidized in NO_3^- reduction in subterranean estuaries with DOC poor conditions (Kroeger and Charette, 2008). $\delta^{13}C$ values of DIC, when considered in conjunction with DOC and DIC concentrations, can be a useful tool in identifying DIC produced by the NO_3^- reduction (Aravena and Robertson, 1998) as well as evaluating NO_3^- reduction stoichiometry and the potential for the participation of electron donors other than DOC in the reaction.

The purpose of this study is to evaluate the mechanisms controlling the N flux from SGD from submarine springs offshore of Kahekili Beach Park on the island of Maui, Hawai‘i. These submarine springs have been demonstrated to discharge treated wastewater effluent injected underground at Lahaina Wastewater Reclamation Facility (LWRF), approximately 0.5 km inland (Hunt and Rosa, 2009; Glenn et al., 2012, 2013). In this work we utilize LWRF effluent and submarine spring N species data along with $\delta^{15}N$ values of dissolved NO_3^-, C species concentrations, and $\delta^{13}C$ values of DIC to evaluate the stoichiometry of biogeochemical reactions occurring within the subsurface effluent plume. Additionally, we consider as a whole LWRF effluent and submarine spring N species data collected over the last several years to examine how changes in effluent injection rate as well as treatment and disinfection practices control the temporal variability in the extent of N species transformation and loss occurring within the effluent plume and, consequently, the variability of N flux to coastal waters from this source.

Study Area/Background

Study Area Description

The Kā‘anapali region (Figure 2.1) is located on the relatively dry, lightly dissected leeward portion of the West Maui volcano (1.2-1.6 Ma.) The geology of this area is dominated by the shield building Wailuku Volcanic series overlain by a thin veneer of later stage Honolua Volcanic series lavas in the northern portion of the study area. The rejuvenated stage Lahaina Volcanic series (age unknown) occurs as vents at Pu‘u Keka‘a (Black Rock) and further south near the town of Lahaina (Stearns and Macdonald, 1942). A narrow band of coastal alluvium, consisting of both terrestrial and marine sediments, fronts the coast at most locations in the study area. The area’s groundwater exists primarily as an unconfined basal lens with low hydraulic gradients due to the high hydraulic conductivity of the basaltic aquifer (Stearns and Macdonald,

1942; Gingerich et al., 2012). Although locally confining conditions may exist in the coastal alluvium, they are not widespread enough to create a discernible effect on the larger scale water table levels of the basal lens (Souza, 1981). Dike confined high-level groundwater exists in the far upland portion of the study area near the summit of the West Maui volcano, where the area's rainfall and groundwater recharge rates are highest (Engott and Vana, 2007).

The marine portion of the study area is located within the Kahekili Herbivore Fisheries Management area, established in July 2009 to restore a healthy population of algae grazing fishes to the region. Though a fringing reef is present near the shore, the seafloor slopes rapidly to depths over 30 m just 500 m offshore. Coral cover at depths of 3 m and 7 m have declined from ca. 50-60% in 1994 to ca. 20-30% in 2005, a reduction more dramatic than the average observed decline during this period for Maui study sites as a whole. Additionally, macroalgae cover at 3 m increased from near 0% to over 20% for the same period (Williams and Sparks, 2008).

Land use in the Kā‘anapali area was long dominated by intensive sugar cane cultivation south of Honokōwai stream and pineapple cultivation north of Honokōwai stream, but recently both industries have declined, with sugar cane and pineapple cultivation ceasing entirely in 1999 and 2009, respectively. The area now consists primarily of resort, golf course, and light commercial development along the coastline with former agricultural fields on lower slopes (to about 400 m elevation) and state forest reserves on the slopes above. Wastewater is processed at the LWRF, located approximately 0.5 km inland from Kahekili Beach, and disposed of via 4 vertical on-site injection wells drilled to roughly 60 m below sea level. This facility has undergone several expansions and treatment upgrades since its inception in 1975. The capacity of LWRF was increased from 3.2 to 6.7 MGD by construction of an additional plant onsite in 1985 (Tetra Tech, 1993), and in 1995 biological nutrient removal and partial UV disinfection capabilities were instituted to further treat wastewater before injection (County of Maui Wastewater Reclamation Division, personal communication). LWRF effluent was disinfected using chlorination under an EPA mandate from October 2011 to May 2014, when full UV disinfection capabilities were certified. The facility is currently capable of treating effluent to irrigation (R-1) quality using UV disinfection and had mean injection and reuse flows of 3.3 and 0.9 MGD, respectively, in the period from January 2011 to July 2014

Background

The occurrence of periodic large scale algal blooms in the Kā‘anapali area beginning in the 1980s has raised concerns regarding the impacts of land use practices on the coastal environment. Several studies, including an inconclusive dye tracer injection test at the LWRF injection wells (Tetra Tech, 1994), were conducted to address these concerns (e.g. Tetra Tech, 1993; Dollar and Andrews, 1997). Various modeling approaches combined with in situ measurements were used to assess the contributions of land use activities to coastal nutrient delivery from both ground and surface waters (Tetra Tech, 1993; Soicher, 1996; Soicher and Peterson, 1997). Dollar and Andrews (1997) and Laws et al. (2004) examined the area's coastal water quality by comparing nutrient concentrations across various locations. Dollar and Andrews (1997) also measured the N isotopic composition of algal tissue in an attempt to determine the contribution of terrestrially-derived N. More recently, analysis of nutrient species, and stable isotopic compositions of water and dissolved NO_3^- (Hunt and Rosa, 2009), N isotopic composition in algal tissue (Dailer et al., 2010, 2012), and analysis of trace metals, radon, nutrient species, and subsurface electrical resistivity (Swarzenski et al., 2012) were used to ascertain pathways of nutrient delivery to coastal waters. These studies found that the coastal ocean along Kahekili Beach Park roughly 1 km southwest of the LWRF injection wells was characterized by elevated $\delta^{15}N$ values in algal tissue, higher temperatures, and lower water pH values relative to adjacent areas. These findings were interpreted as evidence for injected effluent discharging into coastal waters along this coastline. The detection of wastewater indicator compounds in warm, relatively fresh submarine spring discharge along this stretch of coastline (Hunt and Rosa, 2009) lent further support to this interpretation.

Most recently, dye tracer and natural tracer geochemical methods were used to confirm the direct hydrological connection between the main LWRF effluent injection wells 3 and 4 with a patchwork of hundreds of small (~5 cm^2) submarine springs located just offshore of Kahekili Beach and to quantify SGD and associated nutrient fluxes in the area (Glenn et al., 2012, 2013). Other significant findings of that study were that (1) the discharge of the submarine springs off Kahekili beach park consists primarily (64%) of injected LWRF effluent, with a mean travel time of roughly 14 months, and (2) a large (but temporally variable) portion of N in the injected effluent is removed during subsurface transit via microbial nitrate reduction prior to its discharge at the coast. In addition, a large (~ 674,000 m^2) plume of anomalously warm seawater in the

vicinity of submarine springs at Kahekili Beach Park was found using aerial thermal infrared imagery and associated with the warm discharging effluent (Glenn et al., 2012). Monthly monitoring of the submarine spring discharge by the State of Hawai‘i Department of Health (HDOH) commenced in January 2012 and has since yielded new insights into the temporal variability of N concentrations in these waters.

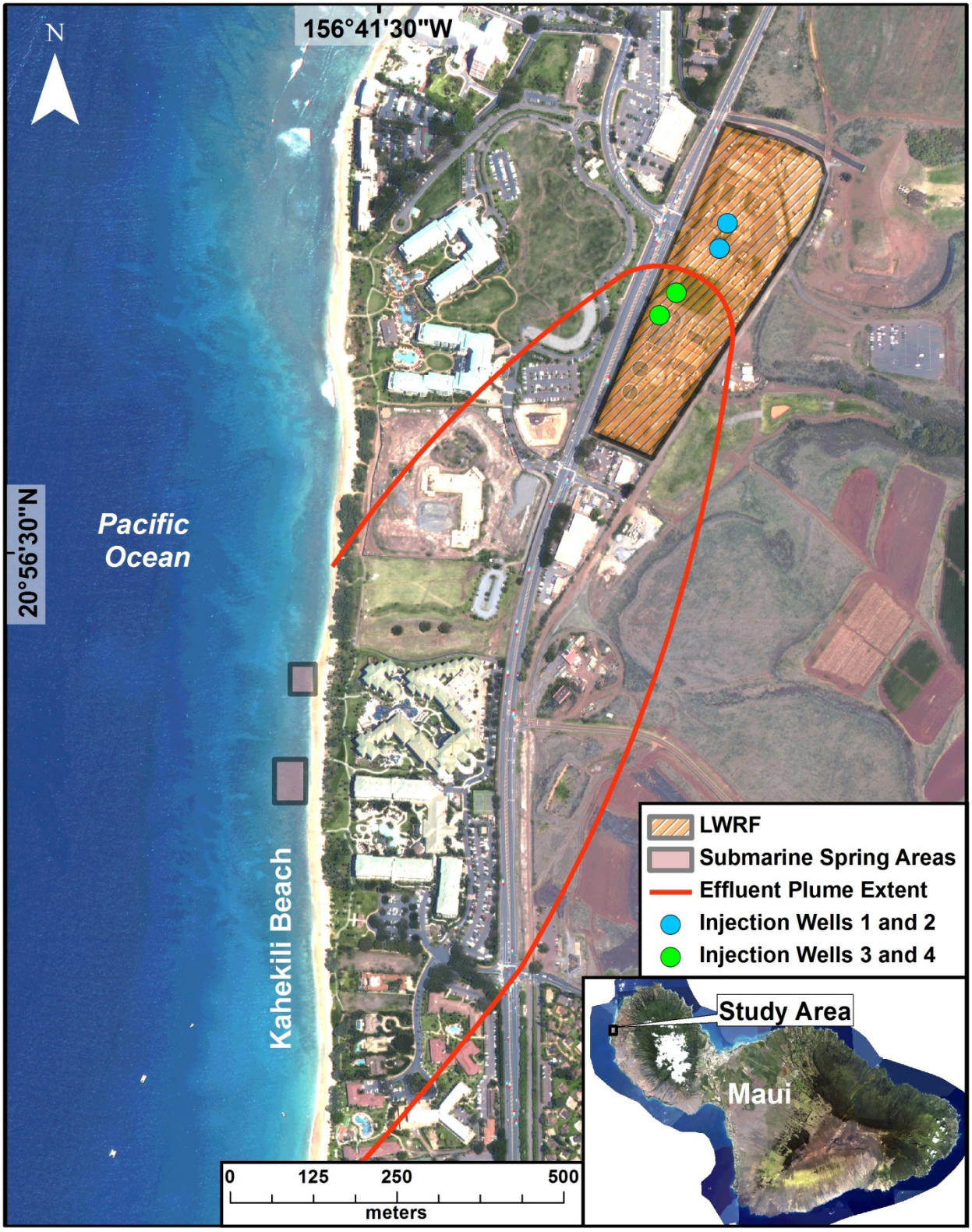

Figure 2.1. Kā‘anapali study area overview showing LWRF injections wells, Wells 3 and 4 effluent plume extent assessed by dye tracer in Glenn et al., 2013, and submarine spring area locations.

Methods

N species and $\delta^{15}N$ values of dissolved NO_3^-

To best assess the N species evolution between LWRF input and submarine spring output, we considered all available LWRF effluent and submarine spring N species concentrations and $\delta^{15}N$ values of dissolved NO_3^- available in both published literature and regulatory agency records; Table 2.1 provides a summary of data considered from these sources. Weekly LWRF N species concentration data collected for regulatory purposes (NH_4^+, NO_2^-+ NO_3^-, organic N, and total N) were obtained for the period of January 2008 through May 2013 along with monthly effluent Total Residual Chlorine (TRC) values from the period October 2011 through July 2014 from the County of Maui Wastewater Division. Discrete LWRF N species concentrations and $\delta^{15}N$ of dissolved NO_3^- values are from Hunt and Rosa (2009) and Glenn et al. (2012). Submarine spring N species data is from Hunt and Rosa (2009), Swarzenski et al. (2012), Glenn et al. (2012), and from monthly HDOH monitoring from January 2012 to July 2014. TRC is reported for several HDOH submarine spring samples. Submarine spring $\delta^{15}N$ values of dissolved NO_3^- are from Hunt and Rosa (2009) and Glenn et al., 2012). Except for TRC, which is reported in units of mg/L, dissolved species concentrations are reported in units of μM. $\delta^{15}N$ values of dissolved NO_3^- are reported in units of ‰ relative to AIR. LWRF and HDOH samples were analyzed in accordance with applicable USEPA procedures and can be assumed to have a maximum relative standard deviation of 10% for N species concentrations and 15% for TRC.

Table 2.1. Summary of N species and $\delta^{15}N$ of dissolved NO_3^- data collected from published works and regulatory agencies. The abbreviations LWRF and SS are used to denote LWRF effluent and submarine spring discharge sample types in this and all subsequent tables.

Sample Information			Parameters Reported				
Source	Type	Collection Date(s)	Salinity	DO	TRC	N Species	$\delta^{15}N$ of NO_3^-
LWRF Monitoring Program	LWRF	1/2005 to 5/2013[1]			X	X	
Hunt and Rosa, 2009	LWRF	5/2008	X			X	X
	SS	5/2008	X			X	X
Swarzenski et al., 2012	SS	7/2010	X	X		X	
Glenn et al., 2012	LWRF	6/2011, 9/2011	X	X		X	X
	SS	6/2011, 9/2011, 1/2012	X			X	X
HDOH Monitoring Program	SS	2/2012 to 7/2014[2]	X	X	X	X	

[1] Weekly sampling frequency [2]Monthly sampling frequency, with some months skipped.

C species and $\delta^{13}C$ values of DIC

Water samples for C species analysis were split into 60 mL HDPE bottles from filtered LWRF effluent and submarine spring samples collected in June and September 2011 were kept chilled during transport before being frozen for storage prior to analysis. Samples were analyzed at the University of Hawai‘i Water Resources Research Center Analytical Laboratory using a Shimadzu TOC-V Organic Carbon Analyzer. Samples were run separately for non-purgeable organic C (NPOC) and total C. Inorganic C values were obtained by subtracting NPOC from total C. Since the samples run were filtered through 0.45 micron cellulose acetate filters, the values obtained for NPOC, total C and inorganic C are represented as DOC, total dissolved carbon (TDC), and DIC, respectively. The 2σ values for analytical precision were 29 μM for DOC, 60 μM for TDC, and 67 μM for DIC (propagated error as a derived quantity).

$\delta^{13}C$ of DIC samples were collected in September 2011 with minimal headspace in 20 mL borosilicate glass vials, crimp-sealed with aluminum caps and butyl rubber septa, and immediately poisoned via syringe with 0.5 mL of saturated $HgCl_2$ solution. These samples were stored at room temperature to minimize the potential for leakage by the septa. Samples were analyzed at the University of Hawai‘i Stable Isotope Bioigeochemistry laboratory with a ThermoFinnigan Delta^{Plus}V mass spectrometer coupled to a GasBench II peripheral using the

method of Salata et al., 2000. Results are reported in units of ‰ relative to PDB and normalized to the standards NBS-18 and NBS-19 using the accepted values of -5.04‰ VPDB and 1.95‰ VPDB, respectively. The 2σ value for analytical precision determined by duplicate sample analysis was 0.4‰.

Salinity Unmixing of Submarine Spring Discharge Samples

For purposes of comparison with each other and with LWRF effluent, the highly variable salinities of the submarine spring samples considered in this study can be assumed to be a result of the dilution of the fresh component of the discharge with pore waters with normal ambient marine salinity. In order to normalize the DO, N species, and C species concentrations to the fresh water component of the submarine spring samples, the following equation was used to un-mix the ambient ocean water component of the samples:

$$C_1 = C_{mix} + (C_{mix} - C_2) \times (S_{mix} - S_1) / (S_2 - S_{mix}) \quad (1)$$

where C_1 is the concentration of component 1, the hypothetical "source;" C_2 is the concentration of component 2, in this case seawater; C_{mix} is the concentration in the mixed sample being evaluated; S_1 is the salinity of component 1, set equal to the suspected parent water; S_2 is the salinity of component 2, in this case seawater; and S_{mix} is the salinity of the mixed sample being evaluated. In order to ensure consistency with previous studies of this system, we utilized the same seawater end member salinity and N species concentrations as Hunt and Rosa, (2009) and Glenn et al., (2012), originally reported by Dollar and Andrews, (1997). These samples were collected approximately 500 m offshore of the study area coastline over a time period of 6 months and as such represent the best seawater end member concentrations for these parameters available for this region. End member DOC, TDC, and DIC values were taken from the arithmetic mean values of these parameters for marine samples collected in September 2011 in support of Glenn et al., 2012. End member DO concentrations were taken from the arithmetic mean of the marine samples collected by HDOH in January, 2012 and reported in Glenn et al., 2012. End member TRC was set at 0 based on the lack of natural free chlorine in the marine environment. The salinity of the treated wastewater effluent (here, the arithmetic mean salinity of the LWRF treated wastewater effluent samples measured in Glenn et al., 2012) was used as the hypothetical source salinity for ease of comparing unmixed submarine spring sample values

with LWRF effluent sample values. The parameter values utilized for Equation (1) are listed in Table 2.2.

Table 2.2. End member parameters used in salinity unmixing of submarine spring discharge samples.

Parameter	Value	Reference
S_1	1.10	Glenn et al., 2012
S_2	34.93	Dollar and Andrews, 1997
C_2 (DO)	225 µM	Glenn et al., 2012
C_2 (NH_4^+)	0.19 µM	Dollar and Andrews, 1997
C_2 (NO_2^-+ NO_3^-)	0.13 µM	Dollar and Andrews, 1997
C_2 (TN)	6.84 µM	Dollar and Andrews, 1997
C_2 (DON)	6.53 µM	Dollar and Andrews, 1997
C_2 (DOC)	176 µM	Glenn et al., 2012
C_2 (TDC)	1815 µM	Glenn et al., 2012
C_2 (DIC)	1631 µM	Glenn et al., 2012
C_2 (TRC)	0 mg/L	N/A

Results

Wastewater Effluent and Submarine Spring Discharge Data

Table 2.3 shows the results of LWRF and submarine spring samples analyzed for C species concentrations and (for September 2011 samples) $\delta^{13}C$ values of DIC. Submarine spring samples (n=5) had DOC values ranging from 22 to 262 µM, with an average value of 109 µM, while LWRF effluent samples (n=3) had a higher average value (529 µM) over a smaller range (458-618 µM). In contrast, submarine spring DIC values (average=2538 µM, range 2106-2804 µM) were elevated with respect to the LWRF effluent values (average=1616 µM, range 1432-1925 µM). Submarine spring TDC values (average=2647 µM, range 2301-2918 µM) were generally higher than LWRF effluent TDC values (average 2171 µM, range 1800-2542 µM) as well. With respect to the receiving ocean water (average DOC, DIC, and TDC = 176, 1631, and 1815 µM, respectively), submarine spring samples were generally depleted in DOC and enriched in DIC and TDC. $\delta^{13}C$ values of DIC was measured for two submarine spring samples as well as LWRF effluent and R-1 (irrigation quality effluent) samples collected in September 2011. The two submarine spring samples yielded identical $\delta^{13}C$ values of DIC of -11.1 ‰ VPDB while the LWRF effluent and R-1 samples had similar $\delta^{13}C$ values of DIC values of -11.2 and -10.5 ‰, respectively. Unmixed DO and N species results as well as $\delta^{15}N$ values of dissolved NO_3^- for submarine spring and LWRF effluent samples reported in previous studies (excluding State of

Hawai‘i Department of Health monitoring data, which are treated separately below) are presented in Table 2.4.

Table 2.3. Submarine Spring and LWRF C species and $\delta^{13}C$ of DIC data. **Bold** text indicates mean values.

Sample Information				Unmixed C Species (μM)			
Sample Date	Sample Name	Type	Salinity	DOC	DIC	TDC	$\delta^{13}C$ of DIC (‰ VPDB)
6/2011	Seep 1 Piez 1	SS	2.0	114	2804	2918	
6/2011	Seep 2 Piez 1	SS	6.8	22	2778	2800	
6/2011	Seep 3 Piez 1	SS	5.0	61	2787	2848	
9/2011	Seep 3-2 Piez	SS	4.8	262	2106	2368	-11.1
9/2011	Seep 1-2 Piez	SS	2.9	85	2216	2301	-11.1
	Mean	**SS**	**4.3**	**109**	**2538**	**2647**	**-11.1**
6/2011	LWRF-1	LWRF	1.1	618	1925	2543	
9/2011	LWRF-EFF	LWRF	1.1	510	1432	1942	-11.2
9/2011	LWRF-R1	LWRF	1.1	458	1492	1950	-10.5
	Mean	**LWRF**	**1.1**	**529**	**1616**	**2145**	**-10.9**

Table 2.4. Submarine Spring and LWRF DO, N species, and $\delta^{15}N$ of dissolved NO_3^- data from previous studies, excluding regulatory data. **Bold** text indicates mean values.

Sample Information					Unmixed DO and N species (μM)					
Study	Sample Date	Sample Name	Type	Salinity	DO	TN	NO_3^- + NO_2^-	NH_4^+	DON	$\delta^{15}N$ of NO_3^- (‰ VAIR)
Hunt and Rosa, 2009	5/2008	L1	SS	26.7			218.9	23.7		39.3
		L2	SS	29.7			228.5	104.5		39.7
		L5	SS	26.0			235.1			39.8
Swarzenski et al., 2012	6/2010	T1-800-GW	SS	4.4	16.6	12.0	11.6	0.3	0.1	
		T2-900-GW	SS	1.7	55.6	49.7	39.1	0.1	10.5	
		T3-1000-GW	SS	2.7	30.6	55.1	44.1	0.1	10.9	
		T4-1100-GW	SS	1.5	19.4	52.7	42.7	0.1	9.8	
		T5-1200-GW	SS	2.8	24.4			0.1		
		T6-1300-GW	SS	2.5	15.6	54.6	43.9	0.1	10.6	
		T7-1400-GW	SS	2.9	24.7	57.4	44.2	0.1	13.2	
		T8-1500-GW	SS	2.9	26.9	55.5	44.0	0.0	11.5	
		T9-1600-GW	SS	3.0	25.6	53.9	44.2	0.2	9.5	
		T10-1700-GW	SS	3.3	35.3	53.3	44.4	0.1	8.9	
		T11-1800-GW	SS	3.4	20.9	32.7	30.1	2.4	0.2	
Glenn et al., 2012	6/2011	Seep 1 Piez 1	SS	2.0		40.8	28.7	0.4	11.6	86.5
		Seep 1 Piez 2	SS	2.1		47.7	29.2	0.5	18.0	77.8
		Seep 2 Piez 1	SS	6.8		26.6	13.6	0.3	12.7	47.6
		Seep 3 Piez 1	SS	5.0		32.0	20.5	0.4	11.1	83.9
	9/2011	Seep 3-2 Piez	SS	4.8		125.2	8.5	0.5	116.2	93.1
		Seep 1-2 Piez	SS	2.9		122.1	13.0	0.5	108.6	83.0
	1/2012	North Seep A	SS	3.7	108.8	16.4	15.0	0.1	1.3	112.2
		North Seep B	SS	4.8	117.5	6.7	7.5	0.1		123.4
		North Seep C	SS	4.6	70.9	4.5	3.7	0.1	0.7	115.5
		South Seep A	SS	2.8	79.1	4.8	1.7	0.1	3.0	144.8
		South Seep B	SS	4.1	80.9	4.5	3.4	0.1	1.0	130.1
		South Seep C	SS	17.9	36.9	0.4	6.2	0.2		135.9
		Mean	**SS**	**6.7**	**46.5**	**41.3**	**48.9**	**5.4**	**18.5**	**90.2**
Hunt and Rosa, 2009	8-May	L12	LWRF	1.1		437.0	176.0	189.0	72.0	22.7
Glenn et al., 2012	Jun-11	LWRF-1	LWRF	1.1	193.8	516.9	226.2	93.2	197.5	29.3
	Sep-11	LWRF-EFF	LWRF	1.1		457.9	282.9	11.1	163.9	30.9
		LWRF-R1	LWRF	1.1		432.6	256.6	19.0	157.0	31.5
		Mean	**LWRF**	**1.1**	**193.8**	**461.1**	**235.4**	**78.1**	**147.6**	**28.6**

Long term monitoring of wastewater effluent N species and total residual chlorine

Table 2.5 shows summary statistics of average monthly LWRF effluent N species, injection flow rates, and TRC concentrations for the periods with available data from January 2005 to July 2014. Though all LWRF effluent N species concentrations show considerable variation, NO_3^- + NO_2^- (median 259.8 μM) typically constitutes the bulk of dissolved N in the

injected effluent, with lesser proportions of NH_4^+ (median 69.0 μM) and DON (median 96.3 μM). The large disparity between median and mean LWRF NH_4^+ values reflects occasional plant upsets characterized by abnormally high NH_4^+ values (Figure 2.2) and consequently high proportion of TN as NH_4^+. These plant upsets or "ammonia spikes" are related to maintenance and personnel factors at LWRF (County of Maui Wastewater Division, personal communication). Injection wells 3 and 4, which have been shown to be hydrologically connected to the submarine springs via dye tracer test (Glenn et al., 2012, 2013), had a median effluent injection rate of 2.6 MGD which was 81.3% of the total the median effluent injection rate of 3.2 MGD during the period considered (Figure 2.3). During the period of LWRF effluent chlorination (October 2011 through July 2014), effluent TRC concentrations varied widely with a median value of 1.4 mg/L (Figure 2.5).

Table 2.5. Summary statistics for monthly average LWRF N species, injection flow rate, and TRC

	LWRF Effluent N Species 1/2005 through 5/2013 (μM)				LWRF Injection Flow Rates 1/2011 through 7/2014 (MGD)		LWRF TRC 10/2011 through 7/2014 (mg/L)
Statistic	TN	$NO_3^- + NO_2^-$	NH_4^+	DON	Wells 3+4	Total	
Minimum	179.9	21.5	0.0	17.5	1.2	2.1	0.04
Median	459.3	259.8	69.0	96.3	2.6	3.2	1.42
Mean	466.0	270.2	104.6	97.7	2.5	3.3	1.90
Maximum	1380.9	554.5	1065.0	271.3	3.6	4.6	6.01
Standard Deviation	172.4	110.2	144.7	34.3	0.5	0.6	1.47

Long term monitoring of submarine spring discharge N species and total residual chlorine

Table 2.6 shows summary statistics of average monthly submarine spring N species and unmixed TRC data for available periods from February 2012 to July 2014. All median submarine spring N species concentrations for this period were all over an order of magnitude less than those measured for the LWRF effluent reported above. The submarine spring N species distribution was dominated by $NO_3^- + NO_2^-$ (median 57.0%) and DON (median 39.3%), containing relatively little NH_4^+ (median 0.9%). Submarine spring unmixed TRC concentrations (Figure 2.5) were also over an order of magnitude less than their LWRF effluent counterparts, with a median and mean value of 0.09 mg/L. The large disparities between the median and mean N species concentrations reflect a dramatic increase in submarine N species concentrations beginning in March 2013 (Figure 2.4).

Table 2.6. Summary statistics for monthly average submarine spring N species and unmixed TRC

	Submarine Spring N Species 2/2012 through 7/2014 (uM)				Submarine Spring Unmixed TRC 2/2012 through 7/2014 (mg/L)
Statistic	TN	$NO_3^- + NO_2^-$	NH_4^+	DON	
Minimum	3.6	0.1	0.0	3.1	0.05
Median	22.1	12.6	0.2	8.7	0.09
Mean	93.3	61.9	0.4	35.5	0.09
Maximum	387.8	251.6	2.2	179.6	0.17
Standard Deviation	121.6	78.0	0.4	48.9	0.03

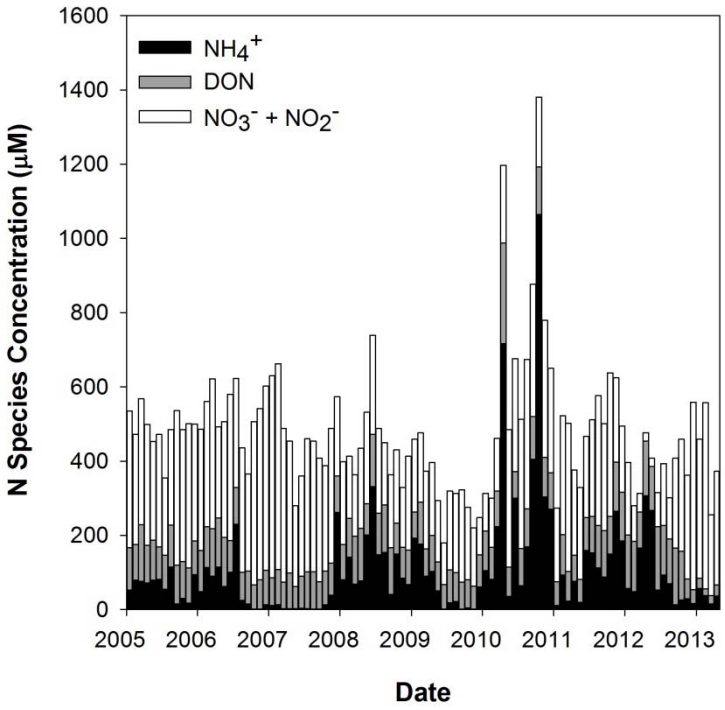

Figure 2.2: LWRF effluent monthly average N species concentrations from January 2005 to May 2013. Note that the anomalously high TN values are generally associated with high NH_4^+ concentrations.

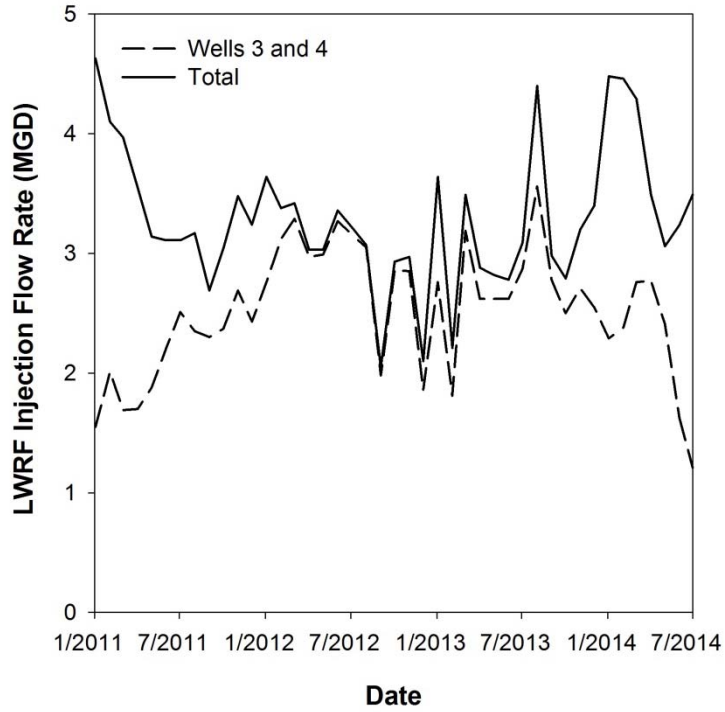

Figure 2.3: Total LWRF injection rate shown with injection rate for wells 3 and 4. Wells 3 and 4 have a proven hydrologic connection to the submarine springs and receive the majority of LWRF effluent flow. Values are monthly averages.

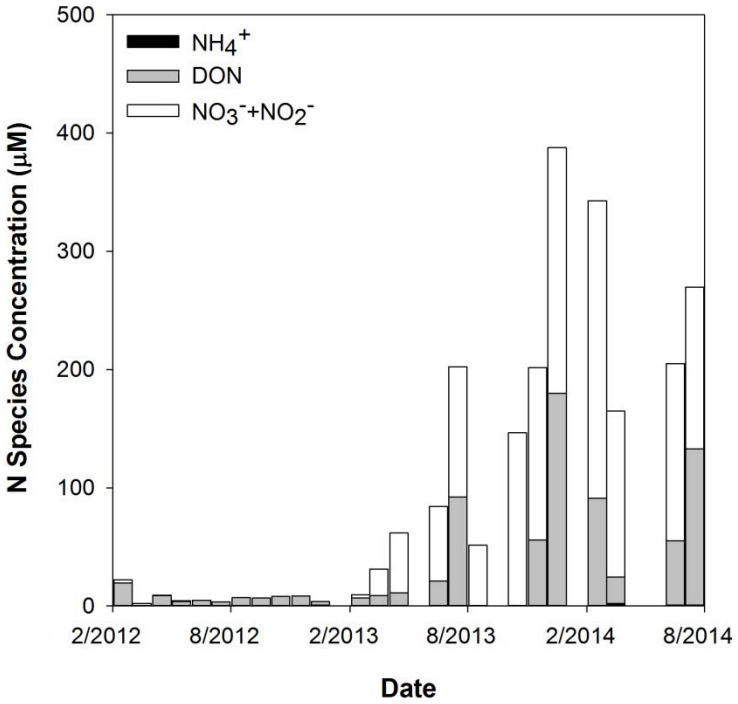

Figure 2.4: Monthly average submarine spring N species concentrations from February 2012 to July 2014. TN values began to increase dramatically in March 2013.

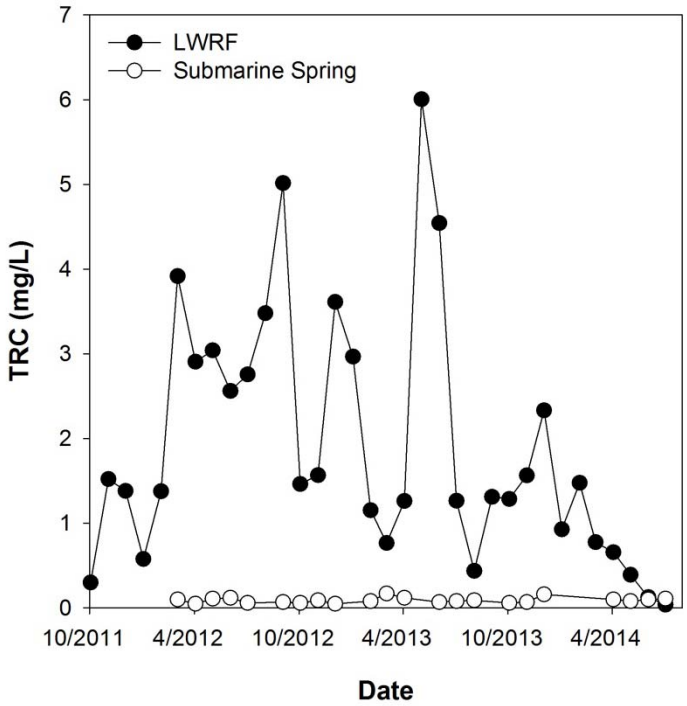

Figure 2.5: LWRF and Submarine Spring TRC concentrations from the start of effluent chlorination at LWRF in October 2011 through July 2014. LWRF effluent chlorination was commenced in October 2011 and ceased in May 2014 after UV disinfection facilities were approved for use.

Discussion

Effluent Plume Biogeochemical Reaction Stoichiometry

N species transformations and attenuation within the STE are important modulators of SGD N flux. The presence and extent of these reactions can vary over small spatial and temporal scales and are governed by the complex interplay of hydrologic and geochemical forcing mechanisms. Previous studies examining N transformations in STEs have generally utilized a series of sampling points at multiple depths across the freshwater-seawater interface (e.g. Beck et al., 2007; Kroeger and Charette, 2008; Gonneea et al., 2014). In this study, however, we are limited to considering samples collected at the input (LWRF effluent) and output (submarine spring discharge) of the STE under investigation, complicating the evaluation of N transformations occurring within the effluent plume. In order to facilitate this evaluation, we consider the effluent plume as a closed system after accounting for seawater dilution of the submarine spring discharge via salinity unmixing as described above. LWRF effluent species constitute the inputs, while submarine spring discharge species represent the outputs. The samples used to calculate the mean and standard deviations for submarine spring DOC, DIC,

TDC, TN, NO_3^- + NO_2^-, NH_4^+, and DON concentrations are from June 2011 and September 2011 (n=5, Tables 2.2 and 2.3). Mean and standard deviation values for these species concentrations in LWRF effluent were calculated from June and September 2011 samples (n=3; Tables 2.3 and 2.4). DO mean and standard deviation values were calculated using the June 2010 measurements of Swarzenski et al. (2012) and January 2012 HDOH measurements of Glenn et al. (2012) (n=17, Table 2.3). LWRF effluent mean DO was represented by a single measurement taken in June 2011 (n=1). From these data, Table 2.7 and Figure 2.6 provide a summary of the difference in unmixed concentrations for DO as well as C and N species between the LWRF effluent and submarine spring discharge samples.

Table 2.7. Calculated mean changes in unmixed DO, N species, and C species concentrations between injected LWRF effluent and submarine spring (SS) discharge.

		DO and C Species (μM)				N Species (μM)			
		DO	DOC	DIC	TDC	TN	NO_3^- + NO_2^-	NH_4^+	DON
SS	Mean	47	109	2538	2647	69	17	0	52
	Standard Deviation	33	92	347	289	50	8	0	55
LWRF	Mean	194	529	1616	2145	469	255	41	173
	Standard Deviation	NA	82	269	345	43	28	45	22
LWRF-SS Δ	Mean	-147	-420	922	502	-400	-238	-41	-121
	Standard Deviation	33	123	439	450	66	29	45	59

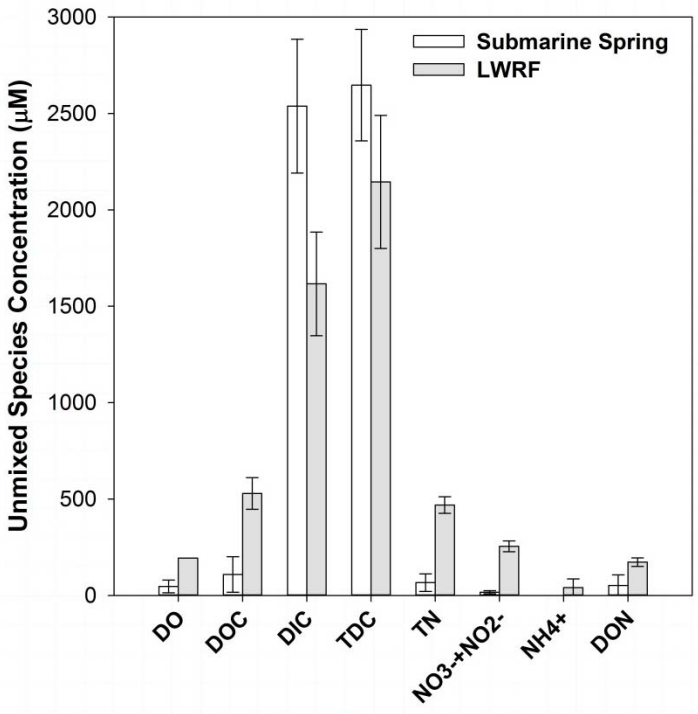

Figure 2.6: Graphical representation of changes in unmixed DO, N species, and C species between LWRF effluent and submarine spring discharge. Error bars represent one standard deviation from the mean.

Figure 2.6 shows that submarine spring discharge is enriched in DIC and TDC relative to the LWRF effluent, but depleted in all the other species considered (DO, DOC, TN, $NO_3^- + NO_2^-$, NH_4^+, and DON). Although various N speciation and other biogeochemical reactions are likely occurring simultaneously within the effluent plume, for quantitative evaluation we consider them here as occurring separately in a stepwise fashion. We first consider a typical set of reactions (Table 2.8) observed in both natural systems (e.g. Kendall, 1998) and wastewater treatment plants (e.g. Henze et al., 2002). The ammonification of DON to NH_4^+ is followed by the oxidation of NH_4^+ to NO_3^- and the subsequent reduction of NO_3^- to N_2 gas, utilizing DOC as an electron donor (heterotrophic denitrification). $NO_3^- + NO_2^-$ is considered as NO_3^- for the purposes of the denitrification reaction, since NO_2^- represents an intermediate step in the process. Table 2.8 shows the theoretical progress of this set of reactions starting with LWRF species compositions and utilizing the actual differences observed in species concentrations as the quantity of available reactant where applicable.

Table 2.8. Hypothetical stepwise changes in LWRF effluent composition through ammonification, nitrification, and denitrification processes based on reaction stoichiometry. The column heading 'Limit' refers to the species used as limiting reagent in the step considered in this and subsequent tables.

Step	Equation	Limit	DO	DOC	DIC	TDC	TN	NO_3^- + NO_2^-	NH_4^+	DON
Observed LWRF mean			194	529	1616	2145	469	255	41	173
Ammonification	$RNH_2+H_2O+H^+ \rightarrow ROH+NH_4^+$	DON	194	529	1616	2145	469	255	162	52
Nitrification	$NH_4^+ + 2O_2 \rightarrow NO_3^- + H_2O + 2H^+$	DO	47	529	1616	2145	469	329	89	52
Denitrification	$4\ NO_3^- + 5DOC + 2\ H_2O \rightarrow 2N_2 + 4HCO_3^- + CO_2$	NO_3^-	47	140	2005	2145	158	17	89	52
Observed Submarine Spring mean			47	109	2538	2647	69	17	0	52
Δ (Predicted - Observedl)			0	31	-533	-502	89	0	89	0

Table 2.8 shows that utilizing the differences between LWRF and submarine spring DON, DO, and NO_3^- + NO_2^- as limiting reagents for ammonification, nitrification, and heterotrophic denitrification, respectively, predicts the submarine spring DO concentration to within one standard deviation of its measured mean concentration (cf. Table 2.6). Predicted DIC and TDC concentrations are, however, 533 and 502 μM lower than the actual submarine spring measured mean concentrations, but this discrepancy is very likely due to the dissolution of carbonate minerals to produce DIC within the alluvium along the LWRF-submarine spring flow path, as discussed below. There also exists a large difference between the predicted submarine spring discharge NH_4^+concentration of 89 μM and the observed mean NH_4^+ concentration of 0 μM. This difference results from the LWRF effluent having insufficient DO available to facilitate the complete nitrification of the 162 μM of NH_4^+ modeled to be present following the ammonification step in Table 7. There are several potential explanations for this discrepancy. First, it remains possible for NH_4^+ to be partially oxidized to NO_2^- (utilizing 1.5 moles of DO per mole NH_4^+ converted) or N_2O (utilizing 1 mole of DO per mole NH_4^+ converted). Partial oxidation of NH_4^+ to NO_2^- instead of NO_3^- would result in a slightly lowered predicted submarine spring NH_4^+ concentration of 64 μM, while partial oxidation of NH_4^+ to N_2O instead of NO_3^- would result in changes to the predicted submarine spring species concentrations for DOC, DIC, TN, and NH_4^+ to 232, 1914, 82, and 13 μM, respectively. While bringing the predicted N species values closer to the observed, these reactions would result in predicted C

species values even farther from observed. A second and more likely explanation is that the Table 2.8 calculations overlook anaerobic ammonia oxidation, or anammox, which is the conversion of NO_2^- and NH_4^+ to N_2 gas and H_2O under anaerobic conditions. This reaction, first reported in wastewater systems (Mulder et al., 1995; Kuenen, 2008), has been integrated into engineered wastewater treatments and has also since been reported from a wide variety of natural oxygen-poor environments (e.g. Kuypers et al., 2005; Rich et al., 2008; Santoro, 2010; Terada et al., 2011; Zhu et al., 2013). Fresh groundwater environments in particular were identified by Sonthiphand et al. (2014) as ideal locations to study N-loss via anammox. The potential occurrence of anammox in the LWRF effluent plume was also suspected as based on observed nutrient and stable isotope parameters by Hunt and Rosa (2009).

Table 2.9. Hypothetical stepwise changes in LWRF effluent composition through ammonification, nitrification, anammox, and denitrification processes.

Step	Equation	Limit	DO	DOC	DIC	TDC	TN	NO_3^- + NO_2^-	NH_4^+	DON
Observed LWRF mean			194	529	1616	2145	469	255	41	173
Ammonification	$RNH_2+H_2O+H^+ \rightarrow ROH+NH_4^+$	DON	194	529	1616	2145	469	255	162	52
Nitrification	$NH_4^+ + 2O_2 \rightarrow NO_3^- + H_2O + 2H^+$	DO	47	529	1616	2145	469	329	89	52
Anammox	$NH_4^+ + NO_2^- \rightarrow N_2 + 2H_2O$	NH_4^+	47	529	1616	2145	292	240	0	52
Denitrification	$4NO_3^- + 5DOC + 2H_2O \rightarrow 2N_2 + 4HCO_3^- + CO_2$	NO_3^-	47	250	1895	2145	69	17	0	52
Observed Submarine Spring mean			47	109	2538	2647	69	17	0	52
Δ (Predicted-Observed)			0	141	-648	-502	0	0	0	0

The inclusion of anammox in the stepwise reactions (Table 2.9) allows us to more precisely account for the observed N species concentrations in the submarine spring effluent. Predicted DOC values and DIC values fall farther from the observed values (141 and -648 μM, respectively) than those predicted in Table 7 (31 and -533 μM, respectively), but these discrepancies can be improved by substituting, as above, the partial nitrification of NH_4^+ to NO_2^- for the complete nitrification of NH_4^+ to NO_3^-. This substitution results in predicted DOC and DIC values of 162 and 1983 μM, respectively, moving the predicted DOC value to within one standard deviation of the mean of the observed values.

The stepwise stoichiometric analysis of hypothetical biogeochemical reactions occurring within the effluent plume can reasonably account for the observed concentrations of DO, C species, and N species in the submarine spring discharge within the constraints of this exercise. Nonetheless, many caveats still apply. It is important to note, for example, that the distributions of N and C species used here represent a small set of observations limited to June and September of 2011 and that both LWRF effluent and submarine spring discharge N and C species concentrations have been shown to exhibit considerable temporal variation (see Figures 2.2 and 2.4 above). Due to the limited data available this analysis also did not consider variations in effluent injection rate, the estimated mean 14 month travel time from effluent injection to submarine spring discharge (Glenn et al., 2013), or the potential for admixture of groundwater from non-LWRF or marine sources (Glenn et al., 2012). The chemical equations used here to represent biogeochemical processes, while accurate enough for the large tolerances of this exercise, are simplified versions of more complex reactions (e.g. Zhou, 2007). Additionally, biogeochemical reactions not considered above that have been observed in subterranean estuaries, such as autotrophic denitritication (e.g. Kroeger and Charette, 2008), may also be occurring within the effluent plume and affecting final submarine spring species concentrations. Further measurement of LWRF and submarine spring C and N species as well as other dissolved species potentially involved in biogeochemical processes would be useful in characterizing the temporal variation in biogeochemical processes within the effluent plume and identifying additional biogeochemical reactions that may be occurring.

$\delta^{13}C$ values of DIC and $\delta^{15}N$ values of NO_3^-

$\delta^{13}C$ of DIC is a useful tracer of C sources in groundwater due to the large isotopic variations in potential source C reservoirs (Clark and Fritz, 1997). Within the LWRF effluent plume, the primary potential sources of DIC include both the DIC produced from heterotrophic consumption DOC within the effluent during processing and after injection, as well as DIC liberated from the dissolution of carbonate rocks found in borings along portions of the effluent's flow path. The typical $\delta^{13}C$ value of wastewater DOC is about -26.0‰ VPDB (Griffith et al., 2009), while $\delta^{13}C$ of marine limestone is typically near 0‰ VPDB (Clark and Fritz, 1997) and measured values of Pleistocene carbonates in Hawai‘i are similar (Fletcher et al., 2005). Since we have measured $\delta^{13}C$ of DIC as well as DIC and DOC concentrations for LWRF effluent and

submarine spring samples, we can utilize the following isotope mass balance to determine if the excess DIC observed in the submarine spring discharge has a $\delta^{13}C$ of DIC value consistent with a marine limestone source:

$$[DIC]_{LWRF}\ \delta^{13}C_{LWRF} + [DIC]_{DOC}\ \delta^{13}C_{DOC+} + [DIC]_{EX}\ \delta^{13}C_{EX} = [DIC]_{SS}\ \delta^{13}C_{SS} \quad (2)$$

Where the variables above are defined as:

$[DIC]_{LWRF}$ = mean concentration of LWRF effluent DIC (1616 μM)

$\delta^{13}C_{LWRF}$ = mean LWRF effluent $\delta^{13}C$ of DIC (-10.9‰ VPDB)

$[DIC]_{DOC}$ = concentration of DIC from DOC consumption (420 μM, $[DOC]_{LWRF}$-$[DOC]_{SS}$)

$\delta^{13}C_{DOC}$ = typical value of $\delta^{13}C$ of DIC from wastewater DOC (-26.0‰ VPDB)

$[DIC]_{EX}$ = concentration of excess DIC (502 μM, $[DIC]_{SS}$-$[DIC]_{LWRF}$-$[DIC]_{DOC}$)

$\delta^{13}C_{EX}$ = value of $\delta^{13}C$ of excess DIC (unknown)

$[DIC]_{SS}$ = mean concentration of LWRF effluent DIC (2538 μM)

$\delta^{13}C_{SS}$ = mean submarine spring $\delta^{13}C$ of DIC -11.1‰ VPDB)

Solving equation (2) for $\delta^{13}C_{EX}$ yields a value of $\delta^{13}C$ of DIC value of 0.7‰ VPDB, which is consistent with a marine limestone source and especially close to the 0.78‰ VPDB value measured for a beachrock on the neighboring island of Molokai by Fletcher et al., (2005). If the equilibrium fractionation factor of 9.0‰ (Clark and Fritz, 1997) is applied to the conversion of the CO_2 produced by the heterotrophic denitrification reaction to HCO_3^-, the $\delta^{13}C_{DOC}$ value becomes -24.2‰. Substitution of this value into equation (2) yields a $\delta^{13}C_{EX}$ value of -0.8 ‰ VPDB, also well within the range of marine limestone sources. This simple sensitivity analysis of the isotope mass balance model strongly support our simplified assumption that dissolution of carbonate materials along the effluent plume's flow path is the source of the measured submarine spring DIC values in excess of those predicted by summation of DIC originally in the LWRF effluent and DIC produced by the consumption of DOC between LWRF effluent injection and submarine spring discharge. Figure 2.7 shows a graphical representation of the evolution of DIC and $\delta^{13}C$ of DIC values within the effluent plume.

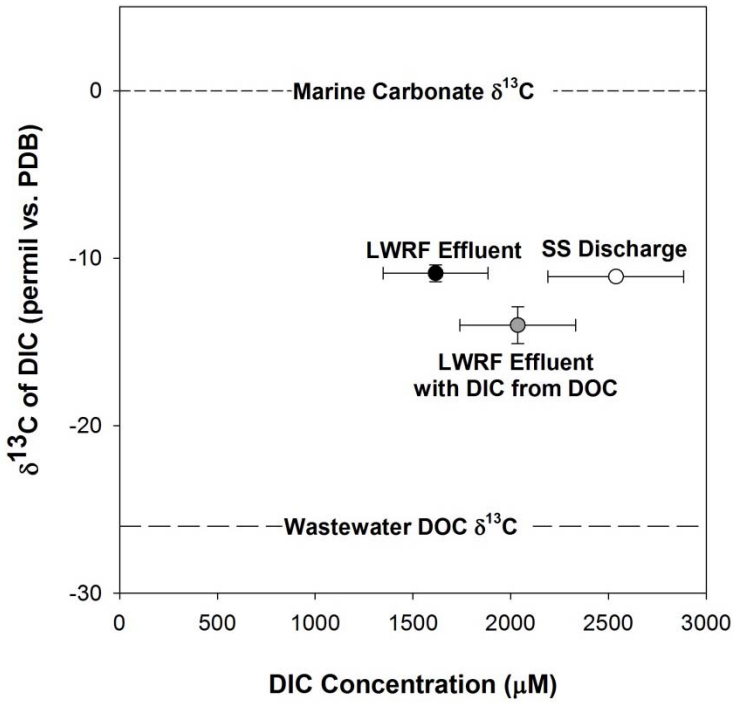

Figure 2.7: The submarine spring discharge is augmented in DIC relative to the LWRF effluent via addition of DIC from consumption of DOC in heterotrophic processes (primarily denitrification) as well as dissolution of marine-derived carbonate within the aquifer. The data point for LWRF effluent with DIC from DOC is a hypothetical, calculated quantity. Error bars represent one standard deviation from the mean.

The occurrence of temporally variable but extremely high $\delta^{15}N$ of NO_3^- values in submarine spring discharge samples (mean 90.2‰ VAIR) was discussed at length in Glenn et al., 2012. It was determined that these high values, in conjunction with the drastic reduction in $NO_3^- + NO_2^-$ concentrations along the LWRF-submarine spring flow path, were indicative of extensive, though temporally variable, denitrification of original LWRF $NO_3^- + NO_2^-$ prior to submarine spring discharge. Although the stoichiometric analyses in Tables 2.8 and 2.9 above indicate that ammonification, nitrification, and potentially anammox play key roles in determining the ultimate N species composition of the submarine spring discharge, they also suggest that denitrification is responsible for the majority of N loss within the effluent plume. Significant N loss via denitrification has been frequently documented in subsurface wastewater plumes (e.g Aravena and Robertson, 1998; Kroeger et al., 2006). This phenomena may be attributed to organic C in wastewater effluent fueling the heterotrophic consumption of O_2 resulting in low O_2 conditions favorable to denitrification. Figure 2.8 provides an overview of the relationship of TN and $\delta^{15}N$ values of NO_3^- in LWRF effluent and submarine spring samples. As explored below, future stable isotope measurements of NO_3^- as well as other N species in the

LWRF effluent and submarine spring discharge will be useful in further understanding the dynamics of the various biogeochemical N transformations occurring within this effluent plume through time.

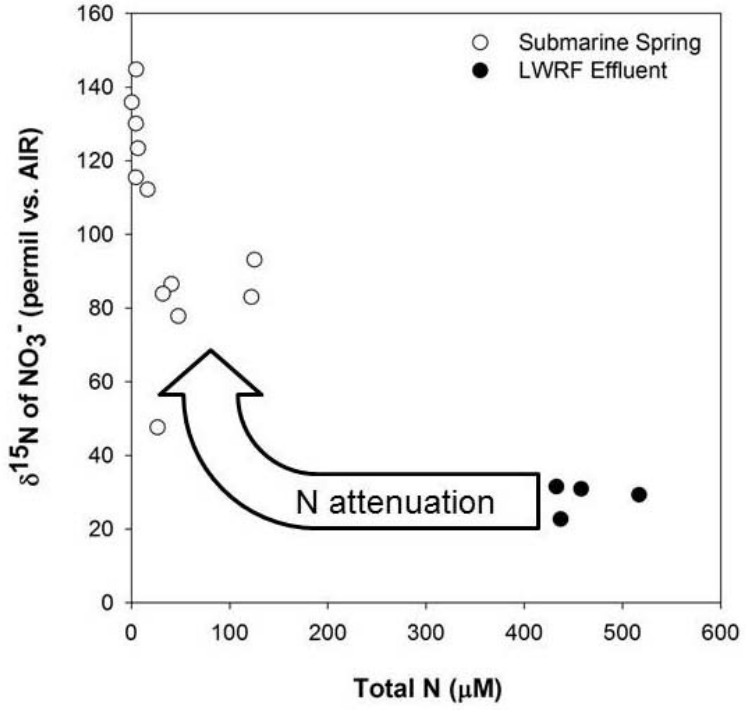

Figure 2.8: Submarine spring discharge during the period these samples were taken (June 2011-January 2012, prior to the arrival of chlorinated effluent at the submarine springs) is characterized by low Total N concentrations and high $\delta^{15}N$ of NO_3^- values relative to injected LWRF effluent. This is primarily the result of denitrification within the effluent plume, which preferentially reduces N-14 to N_2 gas, leaving the remaining N enriched in N-15.

Temporal Variation in Effluent N Fluxes vs. Submarine Spring Discharge N Fluxes

Comparison of LWRF effluent injection and submarine spring discharge N species fluxes provides a useful means for evaluating the dominant factors controlling effluent plume biogeochemistry. LWRF effluent injection N fluxes (Figure 2.9), were calculated by multiplying mean monthly N species concentrations by mean monthly injection well 3 and 4 flows. Wells 1 and 2 flows were discounted due to their comprising a small percentage of total flow. Submarine spring N fluxes (Figure 2.10) were calculated by multiplying the mean monthly salinity-unmixed N species concentrations by the single mean fresh SGD flux of 1.73 MGD determined for the submarine springs via radon mass balance (Glenn et al., 2013). These submarine spring N fluxes do not account for injected LWRF effluent entering the ocean via diffuse seepage at locations other than the submarine spring discharge locations shown in Figure 2.1 and thus likely represent

minimum N fluxes to the ocean from this source. Additionally, due to a lack of long-term SGD monitoring data, our calculated submarine spring N fluxes do not account for variations in SGD rate.

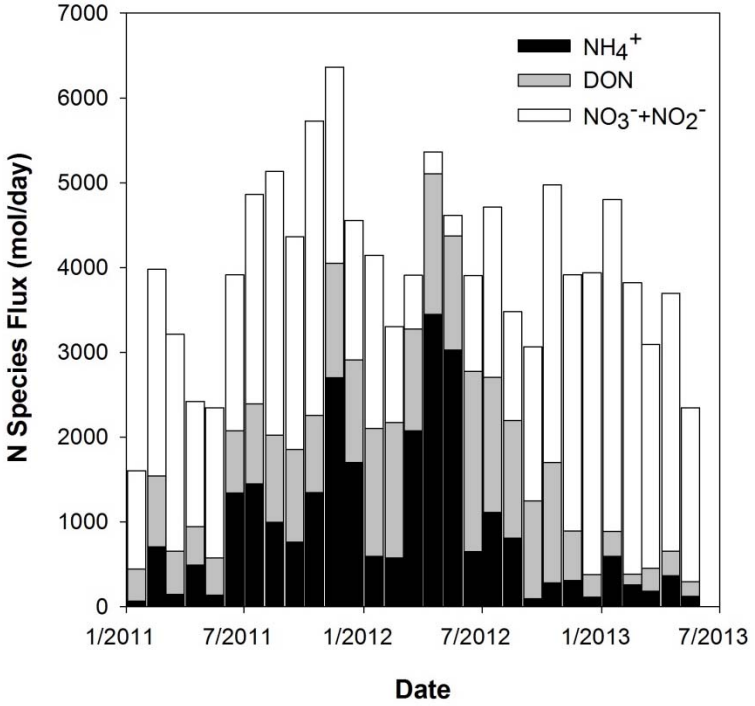

Figure 2.9: LWRF effluent N-species fluxes from January 2011 to June 2013.

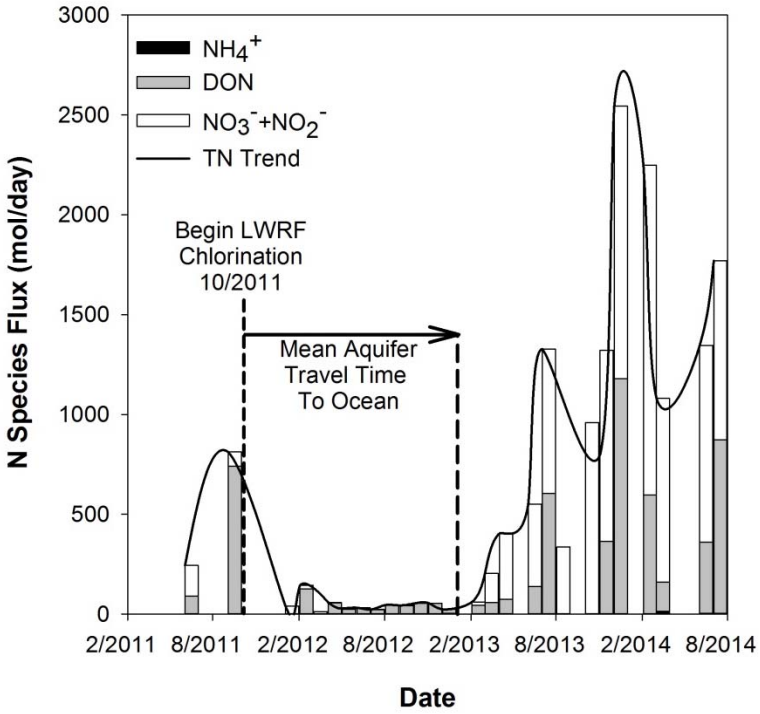

Figure 2.10: Submarine Spring N species flux from February 2011 to August 2014. Dates without bars indicate no available data. Note the marked increase in submarine spring TN flux to coastal ocean beginning about February 2013, roughly 14 months after the commencement of wastewater chlorination at the LWRF. 14 months corresponds to the mean transit time determined for the LWRF injection to submarine spring discharge flow path (Glenn, 2013).

In order to directly compare input LWRF N species fluxes with output submarine spring N species fluxes on a temporally adjusted basis, we divided the submarine spring N species fluxes by the LWRF N species fluxes determined for 14 months prior (Figure 2.11). This time shift accounts for the observed mean 14 month travel time between LWRF effluent injection and submarine spring discharge determined by Glenn et al., 2013. If LWRF effluent N species flux is the only control on submarine spring N species flux, these ratios should appear consistent over time. In reality, calculated SS/LWRF N species flux ratios remain relatively low and consistent through February 2013, after which date all N species ratios except for NH_4^+ increase dramatically. This is indicative of a sudden alteration in the effluent plume to conditions much less favorable to N loss. The most parsimonious explanation is a reduction in the rates of DON ammonification as well as denitrification and/or anammox in the effluent plume. This explanation is consistent with results of stiochiometric modelling of aquifer biogeochemical reactions. Relatively constant near-zero values of the SS/LWRF flux ratio suggest that NH_4^+ removal capabilities remained intact.

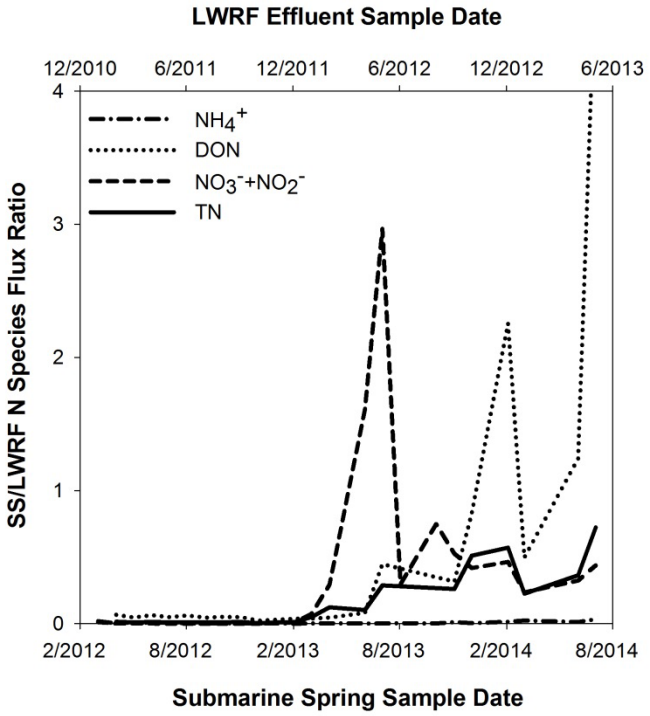

Figure 2.11: Ratios obtained by dividing submarine spring N species flux by LWRF N species flux determined 14 months prior to the indicated date to account for travel time. The ratios of all N species fluxes except for NH_4^+ increase dramatically after February 2013.

Chlorination of LWRF effluent prior to injection, which began in October 2011, roughly 16 months prior to the observed increase in SS/LWRF N species flux ratio, is consistent with a decrease in aquifer biogeochemical reactions. The purpose of wastewater chlorination is to kill waterborne pathogens (USEPA, 1999a). Chlorine gas (Cl_2) reacts with water to produce the strongly oxidizing hypochlorous acid (HOCl). HOCl may further dissociate to the hypochlorite ion (OCl^-), another oxidizing compound. At the near neutral pH values measured in the LWRF effluent (Glenn et al., 2012), HOCl, the stronger oxidant, is the dominant aqueous species produced by the chlorination of water. We suggest that chlorination also adversely affected microbial activity in the aquifer, specifically that of microbes responsible for ammonification, nitrification, anammox, and denitrification within the effluent plume. Considering the mean aquifer transit time of approximately 14 months determined by fluorescein tracer dye testing (Glenn et al., 2012, 2013), the suppression of this microbial activity would thus explain the increase in the submarine spring discharge flux of TN, DON, and $NO_3^- + NO_2^-$ beginning roughly 16 months after chlorination of injected LWRF effluent commenced. The lack of a simultaneous increase in submarine spring discharge NH_4^+ flux during this same period implies

an abiotic control on NH_4^+ attenuation within the effluent plume. One possible abiotic NH_4^+ attenuation mechanism may be the stepwise reaction of HOCl with NH_4^+ to produce chloramines and ultimately N_2 gas, a process known as "breakpoint chlorination" or "superchlorination" (Faust and Aly, 1998). We illustrate the past and possible future temporal correspondence between wastewater chlorination and its 14-month travel time delay on the resultant SS/LWRF TN flux ratio in Figure 2.12. The increase in LWRF effluent TRC shifted 14 months forward closely parallels the increase in SS/LWRF TN flux ratio and attendant increase in TN discharged to the ocean from the submarine springs. The consistently low TRC values in submarine spring discharge suggest that the Cl demand within the effluent plume is sufficiently high to exhaust the disinfecting capabilities of the Cl_2 added to the LWRF effluent prior to its discharge.

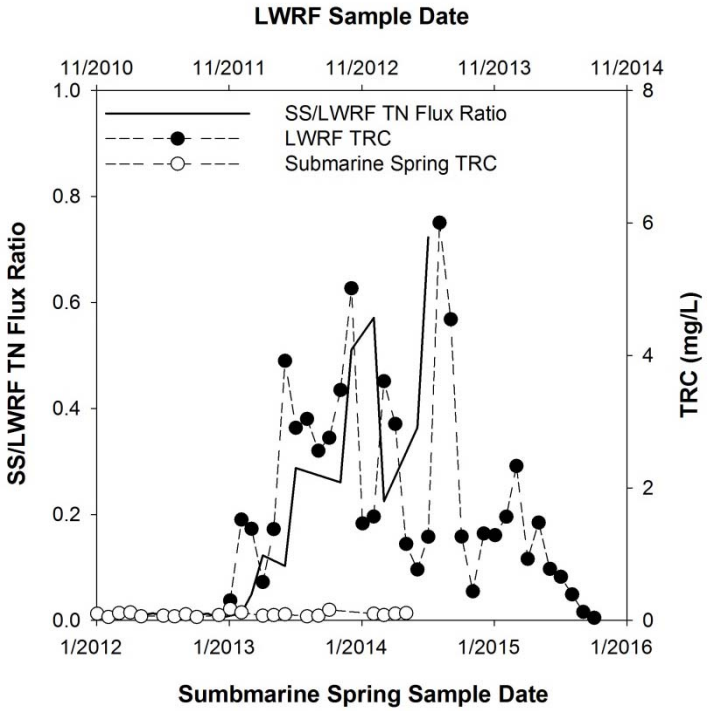

Figure 2.12: The increase in SS/LWRF TN flux ratio closely parallels the increase in TRC concentration in the injected LWRF effluent when LWRF TN has been shifted forward 14 months to account for travel time.

Following HDOH approval of upgraded UV disinfection capabilities, LWRF effluent chlorination ended in May of 2014 (County of Maui Wastewater Division, Personal Communication). Unlike chlorination, UV disinfection does not result in the persistence of strong oxidants in the effluent plume following injection (USEPA, 1999b) and thus should not have an adverse effect on microbial populations within the effluent plume. Given the known residence time of the effluent plume in the aquifer, the submarine spring discharge should be

largely free of previously chlorinated effluent by late 2015. We hypothesize that effluent plume microbial populations will recover, restoring effluent plume biogeochemical processes to those observed prior chlorination (see Section 5.1 above). Continued monitoring of submarine spring discharge will be vital to confirming that chlorination was indeed responsible for the increase in N flux from the submarine springs after February 2013 as well as understanding the speed and extent of the recovery process if observed.

Conclusions

This study has yielded two major conclusions. First, stepwise stoichiometric analysis using input and output N and C species concentrations, stable isotope values, and DO concentrations can provide significant insight into the presence and extent of various biogeochemical processes within a subsurface wastewater plume with a well-characterized flow path and transit time. This insight includes the findings that heterotrophic denitrification plays a key role in N attenuation within the effluent plume, and that anammox very likely also contributes to this net N attenuation as well. Second, chlorination of injected LWRF effluent beginning in October 2011 likely adversely affected microbial activity in the aquifer, resulting in an increase in observed submarine spring N flux offshore of Kahekili Beach beginning in February 2013. Continued monitoring of the submarine spring discharge can confirm that effluent chlorination caused increased N flux as well as provide understanding of the dynamics of a potential future restoration of the initially observed strongly N-attenuating biogeochemical conditions. These findings provide an accessible approach for workers seeking to understand and quantify biogeochemical processes within subsurface wastewater plumes with limited monitoring points and data as well as insight for regulators and wastewater treatment plant operators into potential consequences of chlorination of wastewater at facilities utilizing underground effluent injection.

CHAPTER 3. DEVELOPMENT AND HYDROGEOLOGIC APPLICATION OF A LOCAL METEORIC WATER LINE FOR WEST HAWAIʻI, USA

Joseph K. Fackrell, Craig R. Glenn, Donald Thomas, Robert Whittier, and Brian N. Popp

Prepared for submission to *Journal of Hydrology: Regional Studies*

Abstract

Local meteoric water lines (LMWL) and corresponding relationships between δ^2H and $\delta^{18}O$ values in precipitation and elevation are useful tools for assessing groundwater recharge areas and flow paths. We characterized the LMWL and relationship between $\delta^{18}O$ values in precipitation and elevation for the West Hawaiʻi region utilizing a network of 8 cumulative precipitation collectors sampled at 6-month intervals over a 2-year period. Additionally, we determined δ^2H and $\delta^{18}O$ values for groundwater samples across the study area. We then utilized these data to develop new conceptual models of groundwater flow and characterized groundwater flow paths in this complex and poorly understood hydrogeologic setting. The West Hawaiʻi LMWL indicates a primary source of oceanic moisture from the lee of the island, while the $\delta^{18}O$-elevation relationship resembles that determined for the trade-wind potion of the Hawaiʻi Volcano region. We developed updated conceptual models incorporating subsurface geological features on groundwater occurrence and flow in the West Hawaiʻi region which we utilized in conjunction with $\delta^{18}O$ values for groundwater samples to determine that groundwater flow paths in the West Hawaiʻi region generally originate at high elevations in the island's interior. This study demonstrates the utility of H and O isotopic composition of water as a tracer of groundwater flow in regions with poorly characterized hydrogeology and has important implications for future development and scientific investigation of water resources in West Hawaiʻi.

Introduction

The western, leeward portion of the island of Hawaiʻi, the youngest and largest of the Hawaiian archipelago, is largely devoid of surface water due to the permeability of its young, relatively unweathered volcanic terrain. As a result, groundwater constitutes this rapidly developing region's only reliable water supply while also serving as a vital nutrient delivery vector to coastal ecosystems via submarine groundwater discharge (SGD) (Johnson et al., 2008). Despite the economic and ecological importance of groundwater in West Hawaiʻi, the

hydrogeology of the region remains poorly understood, largely due to the lack of data on groundwater occurrence in its sparsely populated interior areas.

A local meteoric water line (LMWL) comprises a subset of the global meteoric water line (GMWL; Craig, 1961) and describes the relationship between δ^2H and $\delta^{18}O$ values in precipitation in a particular region. This relationship is controlled by both kinetic and equilibrium isotopic fractionation during evaporation and subsequent condensation of a water to form precipitation (Dansgaard, 1964). The progressive depletion of ^2H and ^{18}O in precipitation as a water vapor mass moves upslope is known as the altitude effect. In regions with steep relief such as West Hawai‘i, this effect results in large but consistent variations in δ^2H and $\delta^{18}O$ values in precipitation over small spatial scales, making these values especially useful as tracers of groundwater recharge elevation and flow paths given the conservative nature of these tracers in the subsurface.

Variations in δ^2H and $\delta^{18}O$ values in precipitation due to differences in elevation have been used previously in the Kilauea volcano region of Hawai‘i (Scholl et al., 1996), East Maui (Scholl et al., 2002), and West Hawai‘i (Tillman et al., 2014; Kelly and Glenn, 2015) in conjunction with groundwater δ^2H and $\delta^{18}O$ values to constrain groundwater recharge areas, indicate mixing, and delineate different groundwater systems. The insight gained by the previous studies on West Hawai‘i was limited, however, by a narrow spatial focus (Tillman et al., 2014) and a lack of locally obtained δ^2H and $\delta^{18}O$ values in precipitation (Kelly and Glenn, 2015). We build upon these works by (1) characterizing δ^2H and $\delta^{18}O$ values in precipitation and groundwater on a regional scale and (2) utilizing these values in conjunction with insight gained by previous investigations to develop new conceptual models of groundwater occurrence and flow throughout the study area to determine plausible groundwater flow paths based on these conceptual models.

Regional and Hydrogeologic Setting

Geology

The West Hawai‘i study area consists of the Hualālai volcano as well as portions of the larger Mauna Loa and Mauna Kea volcanoes (Figure 3.1). The Hualālai volcano contains a prominent rift zone trending northwest and southeast, respectively, from its main vents. The volcano’s structure consists of subsurface tholeiitic lavas (exposed only in boreholes and

submarine deposits) overlain by the Waa Waa Trachyte Member, emplaced approximately 114-92 ka, and the younger alkalic Hualālai volcanic series (Sherrod et al., 2007). Hualālai is unique among Hawaiian volcanoes in that its dense substructure, which is presumed to mark the eruptive pathways of the volcano's tholeiitic shield building stage, is displaced by 4 km from its surficial vents and rift zones (Kauahikaua et al., 2000; Flinders et al., 2013). Hualālai has also experienced large-scale mass wasting in the form of the North Kona Slump (>130 ka) which left a large offshore escarpment subsequently draped with younger lavas (Moore and Clague, 1992; Lipman and Coombs, 2006). The Hualālai volcano is surrounded by lavas of the much larger and more active Mauna Loa volcano. The subsurface contact between Hualālai and Mauna Loa lavas is not well characterized due to their simultaneous evolution. The older, dormant Mauna Kea volcano in the northeastern potion of the study area underlies portions of the Mauna Loa and Hualālai volcanoes. The Mauna Loa and Mauna Kea summits as well as the Humu'ula saddle between the summits are underlain by dense substructures presumed to mark these volcanoes' eruptive pathways (Flinders et al., 2013).

Groundwater

Groundwater in the West Hawai'i study area occurs as both a thin lens of basal groundwater near the coast and extending several km inland in some areas and as high-level groundwater further inland. The basal groundwater is characterized by low head levels (<2 m) due to the lack of confining coastal sediments and high hydraulic conductivities of the young lava flows. It also exhibits a strong response to tidal cycling (Oki, 1999), illustrating its hydraulic connectivity to the ocean. Groundwater also occurs at anomalously high head levels (~5-100 m) relative to the basal lens hydraulic gradient in numerous wells drilled further inland. The structures responsible for the presence of high-level groundwater in this area are not well characterized, but available drilling log, water level, and pump test data suggests that dense and impermeable flows or ash layers impounding water under artesian conditions and buried dikes impeding horizontal flow may be important factors (Oki, 1999; Bauer, 2003, Tillman et al., 2014). CFC age dating (Kelly and Glenn, 2015) of this high-level groundwater indicates that it contains a large fraction of "old" groundwater, recharged prior to 1940, while basal groundwater contains more "young" groundwater, recharged after 1940. Unpublished drilling log and depth profile data acquired from boreholes drilled through the basal lens in the portion of the aquifer

south of Hualālai's rift zone suggest that fresh water under artesian conditions, possibly related to the high-level water found further inland, underlies the basal lens in this area and is hydraulically connected to the ocean (Bowles, 2007; Nance, 2013). Geophysical survey and deep borehole data collected in the Humu'ula Saddle region show extensive perched and high-level groundwater, including groundwater under artesian conditions, with head levels in excess of 1000 m (Thomas et al., 2015). Izuka et al., (2016), proposed a low resolution conceptual model for groundwater occurrence and flow in the West Hawai'i region as part of a conceptual model for Hawai'i Island.

Climate and Land Use/Land Cover

The West Hawai'i study area is climatically diverse, with environments ranging from tropical rainforests to alpine deserts. Mean annual temperature varies from ~24˚C near the coast to ~4˚C at the summits of Mauna Loa and Mauna Kea (Giambelluca et al., 2014). The portion of the study area north of Hualālai's rift zone is relatively arid, with annual rainfall ranging from 200-800 mm, and originally consisted of dry scrubland vegetation at lower elevations (< 500 m), mesic forest at middle elevations (500-2000 m) and montane desert at high elevations (>2000 m). This area is lightly developed, with conservation land and forest reserves at higher elevations, current and former ranch land at middle elevations, and localized resort and golf course development along the coast. The portion of the study area south of Hualālai's rift zone contains the Kailua-Kona urban center and is considerably more developed than the Kīholo area. Relative to its higher elevations, the coastal portion of this region is arid, with annual rainfall ranging from 300-900 mm, and contains a wide variety of land use types including an airport, the Hawai'i Ocean Science and Technology Park administered by the Natural Energy Laboratory of Hawai'i Authority (NELHA), Kaloko-Honokōhau National Historical Park, the Kealakehe Wastewater Treatment Plant effluent disposal site, and the coastal and upland urban development of Kailua-Kona. The middle elevations of this area (roughly 400-1500 m) receive relatively high mean annual rainfall (1500-2000 mm) driven by the interaction of moisture-laden daytime sea breezes with the steep and high elevation western slope of the Hualālai and Mauna Loa volcanoes (Giambelluca et al., 2014). Land use at these middle elevations consists primarily of ranch land, coffee plantations, and light residential development. At elevations >1500 m, this region receives progressively less rainfall with increasing elevation and is dominated by

conservation and pasture lands with barren montane desert above 2000 m. A fog belt typically exists at middle elevations (975-2255 m) throughout the region and may contribute to aquifer recharge via fog drip (Giambelluca and Sanderson, 1993; Engott, 2011).

Methods

Sampling Methods

Precipitation collectors were placed at eight sites across the study area (Figure 3.1) covering a wide range of elevation and climate conditions. The design was based on that of Scholl et al. (1996) and consisted of a 5 gallon HDPE tank with a 76 or 110 mm diameter funnel affixed to the lid mounted on a wooden base with metal legs. Prior to deployment, a 1 cm layer of mineral oil was added to the collector to prevent evaporation of collected precipitation and the apparatus was wrapped in a black trash bag to prevent sun exposure. The collectors were sampled at roughly six-month intervals over a roughly two-year deployment period from October 2012 to December 2014. At each sampling event, the sample volume was measured and subsamples were collected in crimp-sealed 20 mL glass vials with butyl rubber septa for water isotope analysis. Volume weighted average (VWA) $\delta^{2}H$ and $\delta^{18}O$ values were computed for each station to account for variations in precipitation over the deployment period.

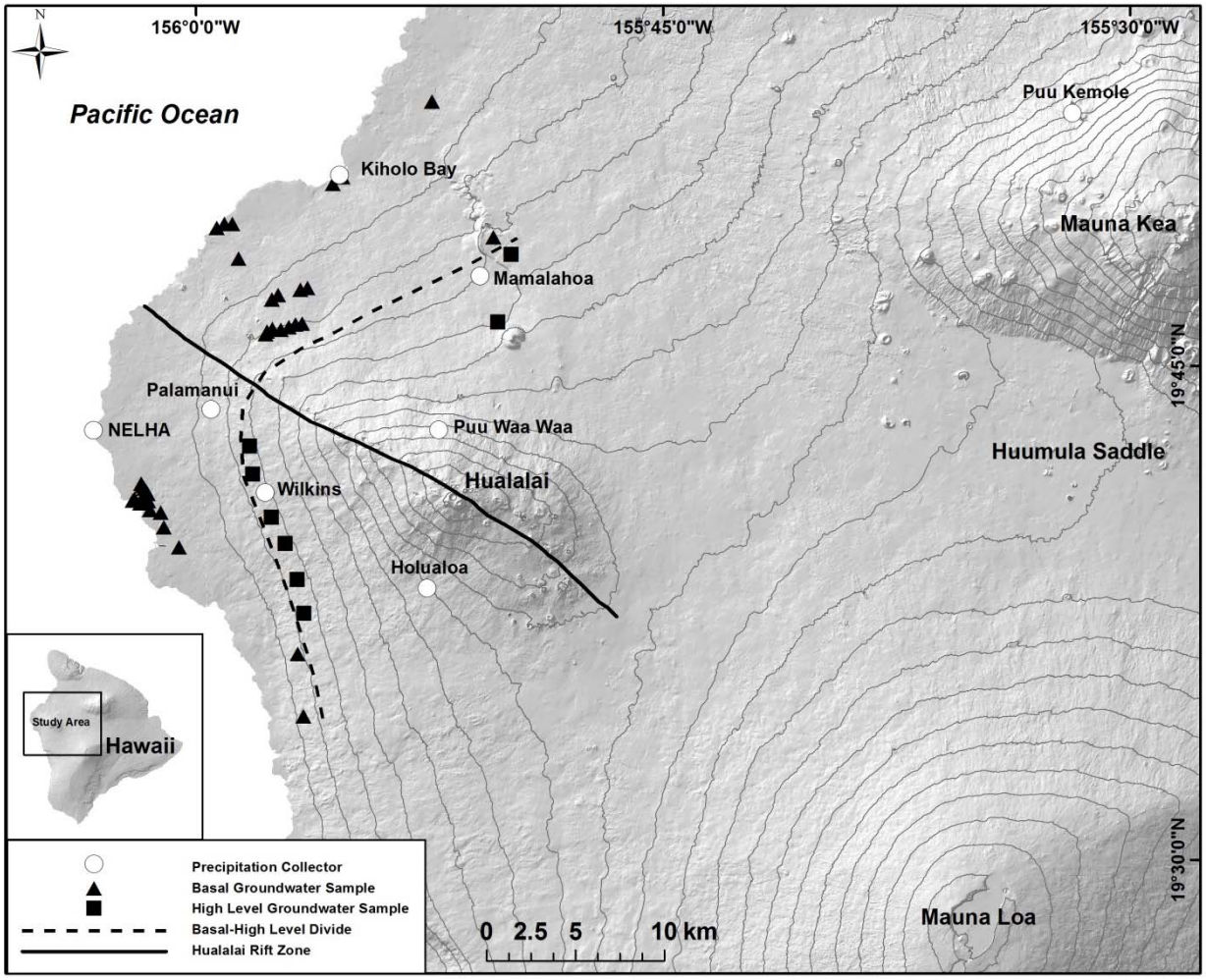

Figure 3.1. Location and sample map of the West Hawai‘i study area. Contour intervals are 200 m.

A total of 83 groundwater samples were collected from 42 separate locations (Figure 3.2) between March 2011 and October 2012. Sample locations included 29 production wells, 10 monitor wells, 2 lava tubes, and 1 coastal spring, and were divided into 11 groups (Figure 3.2) by geographic location. Wells were purged at least 3 borehole volumes before sample collection. Production wells were sampled using installed pump and sampling apparatus. Monitor wells and lava tubes were sampled using portable centrifugal pumps lowered to less than 3 m below the water table surface in order to obtain the freshest sample possible. The coastal spring sample was collected via piezometer using a peristaltic pump. All samples were collected in crimp sealed 20 mL glass vials with butyl rubber septa. Salinity measurements were taken at the time of collection using a YSI multi-parameter sonde.

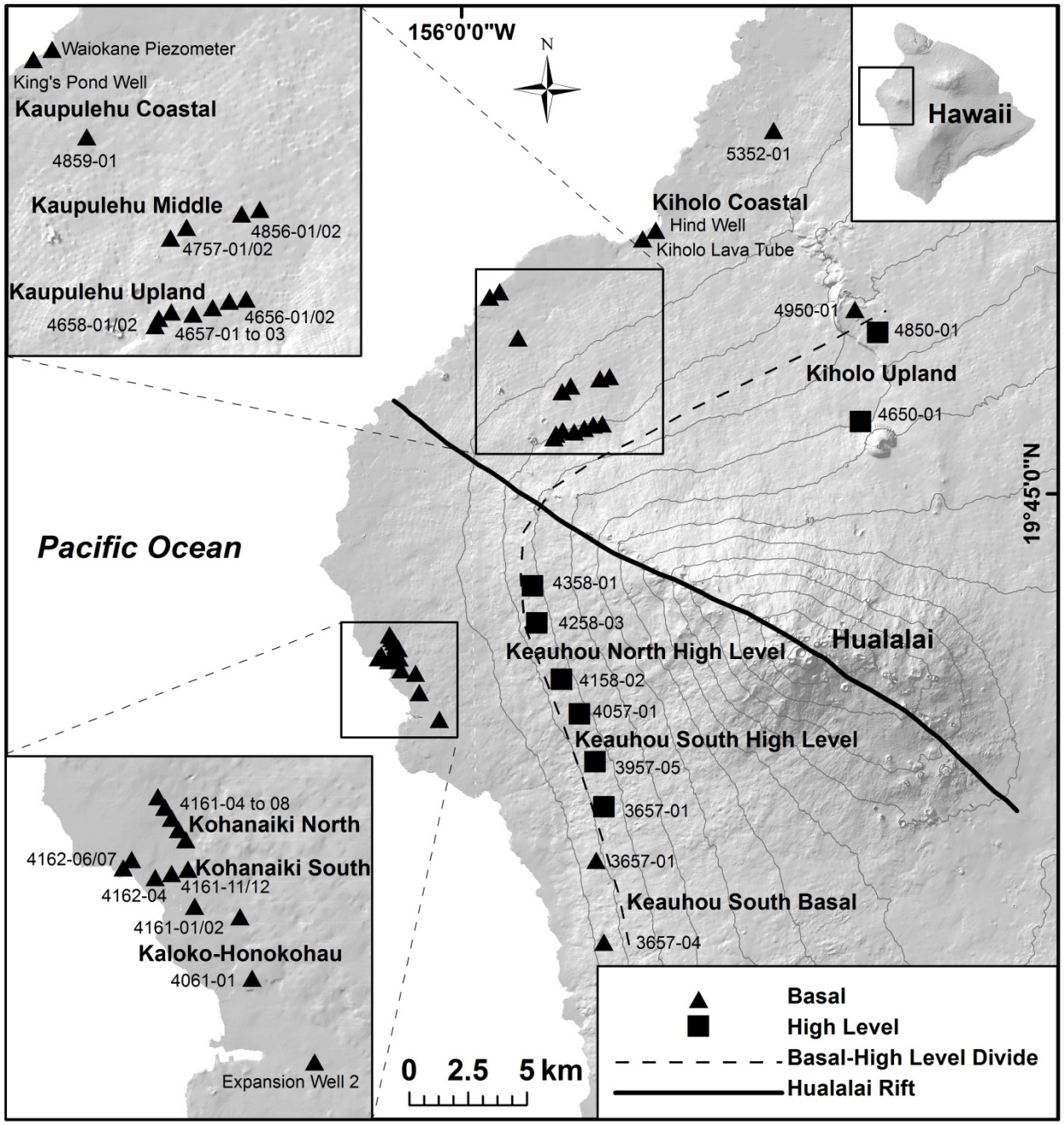

Figure 3.2. Groundwater sample locations with names and group designations. Contour intervals are 200 m.

Analytical Methods

Precipitation and groundwater samples were analyzed for $\delta^{18}O$ and $\delta^{2}H$ values of water at the University of Hawai‘i Stable Isotope Biogeochemistry Lab using an L1102-*i* Picarro cavity ring down mass spectrometer (Picarro, Inc., 2009). All results are expressed in permil (‰) notation relative to Vienna Standard Mean Ocean Water (VSMOW) on a normalized scale in

which the δ^2H and $\delta^{18}O$ values of standard light Arctic precipitation (SLAP) are -428 and -55.5‰, respectively. Samples were normalized to VSMOW using at least three laboratory reference materials that were extensively calibrated with NIST reference materials and bracketed the δ^2H and $\delta^{18}O$ values of the samples. Analytical precision (1σ) was determined by comparison of sample-duplicate pairs and was less than 0.1 and 0.7‰ for $\delta^{18}O$ and δ^2H values, respectively.

Salinity Correction of Groundwater Samples

Salinity values were used to correct the $\delta^{18}O$ and δ^2H values of groundwater samples for seawater content by mass balance. We assumed groundwater samples were a mixture of fresh meteoric water (salinity=0) and ocean water. Ocean water end-member salinity, $\delta^{18}O$, and δ^2H values were measured for 4 samples collected in October 2012 from seawater intake pipes at NELHA, located at Keahole Point on the westernmost tip of Hawai‘i (Table 3.1). The mean salinity, $\delta^{18}O$, and δ^2H values from the shallow seawater intake pipes (35.07, 0.22‰, and 2.58‰ , respectively) were used to correct samples collected north of Hualālai's rift zone, while the mean salinity, $\delta^{18}O$, and δ^2H values from both shallow and deep seawater intake pipes (34.54, -0.05‰, and 0.54‰, respectively) were used to correct samples collected south of Hualālai's rift zone to account for the presumed circulation of cold intermediate seawater through the aquifer in this region (Bowles, 2007; Hunt, 2014; Tillman et al., 2014).

Table 3.1. Seawater endmember sample data

Sample Location	Salinity	$\delta^{18}O$ (‰)	δ^2H (‰)
NELHA 24m Suction	35.07	0.24	2.62
NELHA 14m Suction	35.06	0.19	2.53
NELHA 900m Suction	33.93	-0.34	-1.77
NELHA 674m Suction	34.10	-0.29	-1.22
Shallow Seawater Average	**35.07**	**0.22**	**2.58**
Deep Seawater Average	**34.02**	**-0.32**	**-1.50**
Combined Average	**34.54**	**-0.05**	**0.54**

Integrated Recharge Flow Path Determination

Groundwater flow paths were determined for each groundwater sample group using a method modified after Scholl et al., (1996). We used $\delta^{18}O$ values instead of δ^2H values due to their having a more consistent relationship with elevation. The $\delta^{18}O$-elevation relationship determined below was assumed to apply to precipitation in the portion of the study area below

2000 m, while the Hawai‘i Volcano high elevation $\delta^{18}O$-elevation relationship (Scholl et al., 1996) was assumed to apply to precipitation in the portion of the study area above 2000 m. These relationships were applied to a digital elevation model (DEM) of the study area to produce a spatial coverage of $\delta^{18}O$ values. A recharge coverage was produced for the study area by subtracting the evapotranspiration (Giambelluca et al., 2014) from the rainfall (Gimabelluca et al., 2013). Runoff was not considered due to the lack of perennial streams in the region. Though evaporation of precipitation during the infiltration process undoubtedly occurs, resulting in relative isotopic enrichment of groundwater recharge, we assumed for the purposes of this study that rainfall isotopic composition was equivalent to recharge isotopic composition. We justified this assumption based on (1) exceptionally low evapotranspiration rates observed in dry barren areas with little or no soil, such as West Hawai‘i (Giambelluca et al., 2014) and (2) the likelihood of greater infiltration of isotopically depleted precipitation during intense storms (due to amount effect) and/or cooler weather (due to temperature effect, see below) relative to isotopically enriched precipitation during light rainfall events and/or warmer weather, which would act to offset evaporative enrichment of recharge relative to precipitation (Scholl et al., 1996). Viable groundwater flow path trajectories for each sample group were established by a preliminary analysis of potential trajectories combined with development of conceptual models for groundwater flow in different portions of the study area. To derive flow paths from the flow path trajectories, we used the following equation:

$$\delta^{18}O_{sample} = \frac{\sum_{int=1}^{n}(\delta^{18}O)n(R)n}{\sum_{int=1}^{n}(R)n} \quad (3.1)$$

where $\delta^{18}O(n)$ is the isotopic value of precipitation for the interval n and R(n) is the recharge volume for the interval n. Using intervals of 250 m to correspond to the pixel sizes of the $\delta^{18}O$ value and recharge coverage, we initiated the integrated recharge calculation at the sample group location and proceeded up the flow path trajectory until $\delta^{18}O$ values were matched. Flow path determinations for some portions of the study area required additional actions such as the addition of an indirect recharge component or the shielding of a portion of the flow path; these will be discussed in greater detail below.

Results

Precipitation

Volume weighted average (VWA) $\delta^{18}O$ and $\delta^{2}H$ values for the overall deployment period generally decreased with increasing elevation throughout the study area (Table 3.2). VWA $\delta^{18}O$ values ranged from -3.46‰ to -6.21‰ while VWA $\delta^{2}H$ values ranged from -9.6‰ to-33.1‰. Precipitation (measured in mm per deployment period) was uniformly low among all stations during the first deployment period (Figure 3.3) but increased to more typical levels in subsequent periods. $\delta^{18}O$ and $\delta^{2}H$ values from each station VWA $\delta^{18}O$ and $\delta^{2}H$ values were generally lower in winter measurement periods (10/2012-3/2013 and 11/2013-5/2014) than summer measurement periods (3/2013-11/2013 and 5/2014-12/2014).

Table 3.2. Precipitation Collector location and overall sample data

Station Information				October 2012 - December 2014 Totals		
Name	**Latitude**	**Longitude**	**Elevation (m)**	**Precipitation (mm)**	**VWA $\delta^{18}O$ (‰)**	**VWA $\delta^{2}H$ (‰)**
Kīholo Bay	19.85501	-155.92474	1	346	-3.64	-14.4
NELHA	19.72809	-156.05887	4	754	-3.48	-12.2
Palamanui	19.73753	-155.99583	263	1536	-3.52	-11.5
Wilkins	19.69495	-155.96759	578	2010	-3.46	-9.6
Mamalahoa	19.80267	-155.85064	603	1541	-3.88	-14.3
Holualoa	19.64507	-155.88199	1383	772	-4.90	-21.7
Puʻu Waʻa Waʻa	19.72511	-155.87415	1653	1320	-5.31	-24.3
Puʻu Kemole	19.87922	-155.53209	2220	1938	-6.21	-33.1

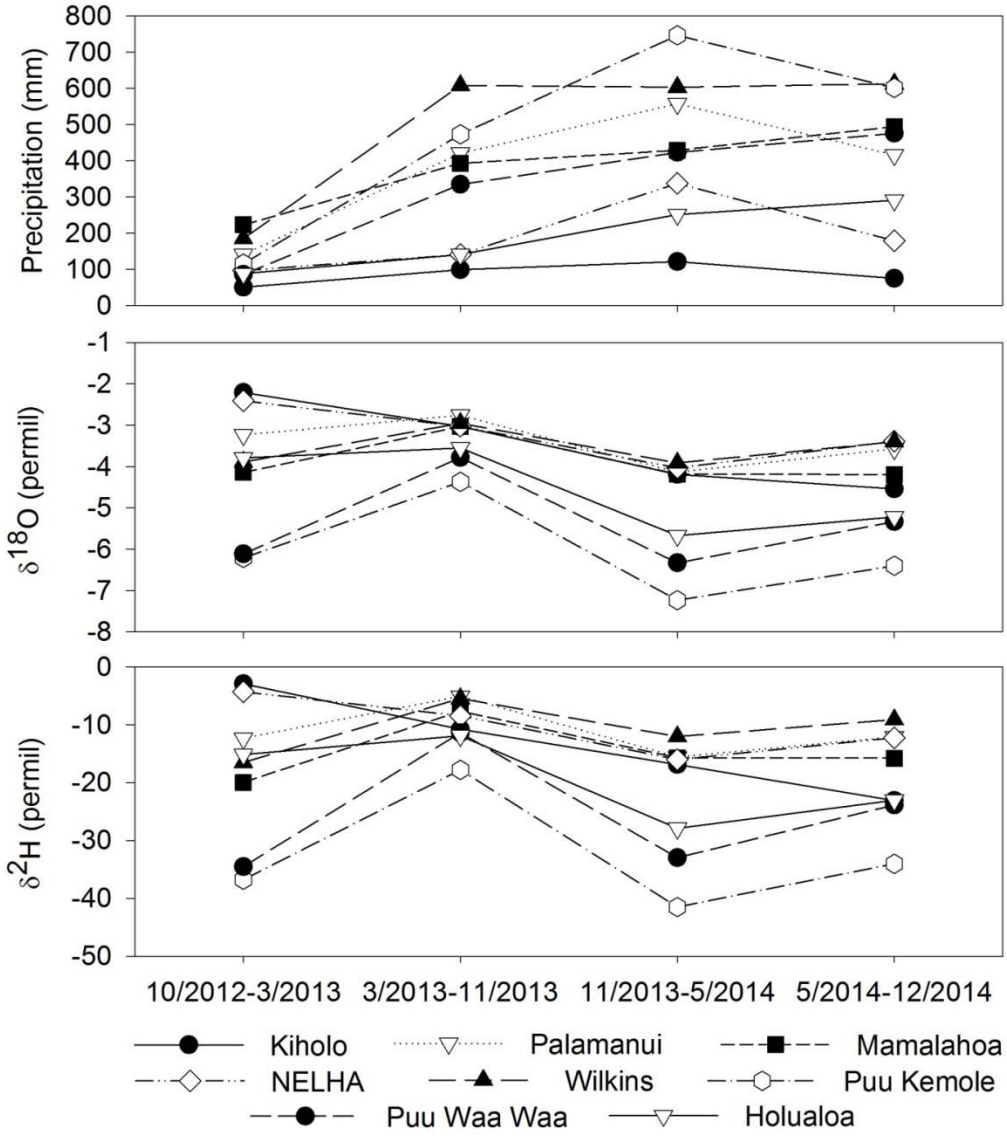

Figure 3.3. Temporal variation in precipitation depth, δ^2H, and $\delta^{18}O$ values.

Groundwater

Salinity-corrected groundwater $\delta^{18}O$ and δ^2H values were averaged for sample locations where multiple samples were collected. These average $\delta^{18}O$ and δ^2H values ranged from -4.12‰ to -8.31‰ and -18.4‰ to -56.1‰, respectively, across the study area (Table 3.3). The Kīholo Coastal and Upland sample groups had the lowest average $\delta^{18}O$ and δ^2H values, while the Kaloko-Honokōhau and Keauhou South Basal sample groups had the highest average $\delta^{18}O$ and δ^2H values. Unmixed groundwater $\delta^{18}O$ and δ^2H values showed little temporal variability for locations where multiple samples were collected over the 18-month sampling interval and are

similar to those reported for the same locations collected in 2008 by Kelly and Glenn (2015) and in 2012 and 2013 by Tillman et al. (2014).

Table 3.3. Groundwater sample data. $\delta^{18}O$ and $\delta^{2}H$ values are corrected for salinity.

Sample Location	Sample Type	Group	Latitude	Longitude	n	Salinity	$\delta^{18}O$ (‰)	$\delta^{2}H$ (‰)
Hind Well	Lava Tube	Kīholo Coastal	19.85400	-155.92307	2	2.07	-7.83	-50.1
Kīholo Lava Tube	Lava Tube	Kīholo Coastal	19.85073	-155.92847	2	1.82	-7.91	-51.0
5352-01	Production Well	Kīholo Coastal	19.89144	-155.87457	3	1.65	-8.31	-56.1
KĪHOLO COASTAL AVERAGE			**19.86539**	**-155.90870**		**1.85**	**-8.02**	**-52.4**
4950-01	Production Well	Kīholo Upland	19.82220	-155.84306	3	0.25	-8.28	-54.6
4850-01	Production Well	Kīholo Upland	19.81321	-155.83385	3	0.19	-7.94	-51.4
4650-01	Production Well	Kīholo Upland	19.77911	-155.84145	2	0.10	-8.15	-53.5
KĪHOLO UPLAND AVERAGE			**19.80484**	**-155.83945**		**0.18**	**-8.12**	**-53.2**
4859-01	Monitor Well	Kaʻūpūlehu Coastal	19.81362	-155.97974	1	2.06	-5.86	-32.1
Waiokane Piezometer	Spring	Kaʻūpūlehu Coastal	19.83146	-155.98682	1	8.64	-5.87	-31.6
King's Pond Well	Production Well	Kaʻūpūlehu Coastal	19.82946	-155.99089	2	19.22	-5.51	-30.0
KAʻŪPŪLEHU COASTAL AVERAGE			**19.82485**	**-155.98582**		**9.97**	**-5.75**	**-31.2**
4757-01	Production Well	Kaʻūpūlehu Middle	19.79276	-155.96220	3	1.39	-5.90	-32.6
4757-02	Production Well	Kaʻūpūlehu Middle	19.79489	-155.95872	3	0.67	-5.80	-31.7
4856-01	Production Well	Kaʻūpūlehu Middle	19.79742	-155.94684	2	0.81	-5.72	-31.6
4856-02	Production Well	Kaʻūpūlehu Middle	19.79825	-155.94293	3	1.06	-5.72	-31.9
KAʻŪPŪLEHU MIDDLE AVERAGE			**19.79583**	**-155.95267**		**0.98**	**-5.78**	**-31.9**
4658-01	Production Well	Kaʻūpūlehu Upland	19.77508	-155.96581	1	0.73	-5.66	-29.9
4658-02	Production Well	Kaʻūpūlehu Upland	19.77654	-155.96501	2	0.80	-5.50	-29.8
4657-01	Production Well	Kaʻūpūlehu Upland	19.77781	-155.96230	1	1.02	-5.78	-30.5
4657-02	Production Well	Kaʻūpūlehu Upland	19.77728	-155.95763	2	0.73	-5.55	-30.6
4657-03	Production Well	Kaʻūpūlehu Upland	19.77854	-155.95346	3	0.70	-5.63	-31.1
4656-01	Production Well	Kaʻūpūlehu Upland	19.77979	-155.94986	2	0.43	-5.91	-32.8
4656-02	Production Well	Kaʻūpūlehu Upland	19.78016	-155.94620	1	0.28	-5.90	-31.7
KAʻŪPŪLEHU UPLAND AVERAGE			**19.77789**	**-155.95718**		**0.67**	**-5.71**	**-30.9**
4161-04	Production Well	Kohanaiki North	19.70066	-156.03392	2	7.78	-6.61	-38.9
4161-05	Production Well	Kohanaiki North	19.69934	-156.03304	2	7.92	-6.55	-38.2
4161-06	Production Well	Kohanaiki North	19.69800	-156.03221	1	7.80	-6.21	-35.9
4161-07	Production Well	Kohanaiki North	19.69662	-156.03133	1	9.52	-6.15	-34.6
4161-08	Production Well	Kohanaiki North	19.69534	-156.03043	2	8.29	-5.86	-32.2
KOHANAIKI NORTH AVERAGE			**19.69799**	**-156.03219**		**8.26**	**-6.28**	**-35.9**
4162-06	Monitor Well	Kohanaiki South	19.69204	-156.03854	1	11.76	-6.13	-35.4
4162-07	Monitor Well	Kohanaiki South	19.69304	-156.03746	2	10.88	-5.99	-34.4
4162-04	Monitor Well	Kohanaiki South	19.69079	-156.03445	2	10.26	-5.68	-31.7
4161-11	Monitor Well	Kohanaiki South	19.69126	-156.03232	2	8.60	-5.58	-30.2
4161-12	Monitor Well	Kohanaiki South	19.69175	-156.03020	3	8.35	-5.66	-30.8
KOHANAIKI SOUTH AVERAGE			**19.69178**	**-156.03459**		**9.97**	**-5.81**	**-32.5**
4161-01	Monitor Well	Kaloko-Honokōhau	19.68722	-156.02944	1	6.09	-4.91	-23.8
4161-02	Monitor Well	Kaloko-Honokōhau	19.68583	-156.02361	1	4.93	-4.44	-21.3
4061-01	Monitor Well	Kaloko-Honokōhau	19.67833	-156.02222	1	11.10	-5.22	-27.1
Expansion Well 2	Monitor Well	Kaloko-Honokōhau	19.66799	-156.01433	3	5.29	-4.25	-22.6
KALOKO-HONOKŌHAU AVERAGE			**19.67984**	**-156.02240**		**6.85**	**-4.70**	**-23.7**
4158-02	Production Well	Keauhou North High Level	19.68240	-155.96442	3	0.10	-7.00	-43.0
4258-03	Production Well	Keauhou North High Level	19.70423	-155.97401	1	0.11	-7.14	-44.3
4358-01	Production Well	Keauhou North High Level	19.71846	-155.97554	3	0.13	-6.76	-41.2
KEAUHOU NORTH HIGH LEVEL AVERAGE			**19.70170**	**-155.97132**		**0.11**	**-6.97**	**-42.8**
4057-01	Production Well	Keauhou South High Level	19.66901	-155.95746	3	0.07	-5.61	-30.8
3957-05	Production Well	Keauhou South High Level	19.65059	-155.95142	1	0.07	-5.23	-26.4
3857-04	Production Well	Keauhou South High Level	19.63327	-155.94818	3	0.06	-5.30	-28.0
KEAUHOU SOUTH HIGH LEVEL AVERAGE			**19.65096**	**-155.95235**		**0.07**	**-5.38**	**-28.4**
3657-01	Production Well	Keauhou South Basal	19.61283	-155.95186	2	0.22	-4.12	-18.4
3557-04	Production Well	Keauhou South Basal	19.58138	-155.94926	1	0.36	-5.23	-28.3
KEAUHOU SOUTH BASAL AVERAGE			**19.59711**	**-155.95056**		**0.29**	**-4.68**	**-23.4**

Discussion

West Hawai‘i LMWL and $\delta^{18}O$-Elevation Relationship

The West Hawai‘i LMWL (Figure 3.4a) was determined by calculating the linear regression through the VWA $\delta^{18}O$ and $\delta^{2}H$ values from each precipitation collector (Table 3.2). This relationship ($\delta^{2}H=7.65\ \delta^{18}O+15.25$, $r^{2}=0.98$) is more similar to LMWLs determined for the Hawai‘i Volcano region (Scholl et al., 1996) and East Maui (Scholl et al., 2002) than the overall GMWL (Craig, 1961), reflecting the climatic similarities of these proximal locations. The data collected in this study are also consistent with the precipitation $\delta^{18}O$ and $\delta^{2}H$ values collected at five locations south of the Hualālai rift zone between September 2012 and March 2014 by Tillman et al., (2014). The increase in the $\delta^{2}H$ value of the y-intercept (Deuterium excess) of the West Hawai‘i LMWL relative to the Hawai‘i Volcano LMWL, East Maui LMWL, and GMWL is indicative of greater kinetic fractionation during the evaporation of the water vapor that subsequently contributes to precipitation in this region. This observation is suggests that water vapor that contributes to precipitation in West Hawai‘i is sourced primarily from the lee of the island, where lower atmospheric humidity would result in a higher humidity gradient across the air-sea interface, and, consequently, greater kinetic fractionation of the evaporated water mass leading to a larger Deuterium excess.

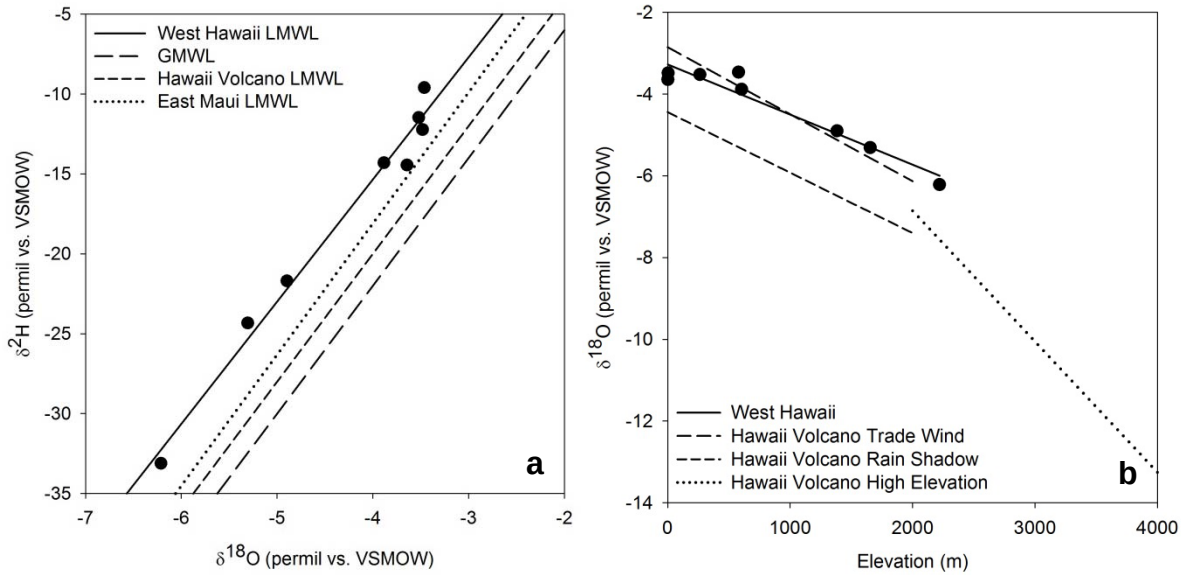

Figure 3.4(a-b). West Hawai‘i LMWL (a) and $\delta^{18}O$-elevation relationship (b). Best fit trend lines regions of Hawai‘i Volcano (Scholl et al., 1996) and East Maui (Scholl et al., 2002) are shown for reference.

Despite the leeward location of the West Hawai‘i study area, the $\delta^{18}O$-elevation relationship determined for the region ($\delta^{18}O$=-0.0012(elevation in meters)-3.27, r^2=0.93) is more similar to the $\delta^{18}O$-elevation relationship for the windward (trade wind) portion of the Hawai‘i Volcano region (Scholl et al., 1996) than the leeward (rain shadow) portion of the Hawai‘i Volcano region (Scholl et al., 1996) (Figure 3.4b). This finding is also consistent with precipitation in the West Hawai‘i region originating primarily as water vapor evaporating from the ocean to the lee (west) of the study area as opposed to water vapor entrained in the predominant easterly trade wind flow, which would tend produce lower $\delta^{18}O$ values in precipitation due to rainout during transit from the windward portion of the island. The interaction of the diurnal sea breezes common to the West Hawai‘i region with its steep topography is responsible for a large fraction of the region's precipitation, especially in the wetter areas (Giambelluca et al., 2013), and provides a plausible mechanism for the inland transport, condensation, and precipitation of water vapor originally evaporated from the ocean to the leeward of the study area.

Average Groundwater Recharge Elevations

Figure 3.5 illustrates that groundwater sample group average δ^2H and $\delta^{18}O$ values (Table 3.3) plot to slightly the right of the West Hawai‘i LMWL, indicating relative enrichment in groundwater ^{18}O. This deviation, which is more pronounced for groundwater with lower δ^2H and $\delta^{18}O$ values, may be the result of variability in precipitation δ^2H and $\delta^{18}O$ values during the two year measurement period relative to the long-term average, some degree of preferential evaporation of isotopically lighter water during the infiltration process, as discussed above, or a combination of these effects. Nevertheless, the similarity of the West Hawai‘i LMWL to the groundwater δ^2H vs. $\delta^{18}O$ relationship validates the use of the West Hawai‘i $\delta^{18}O$-elevation relationship as a proxy for determining average groundwater recharge elevations and flow paths.

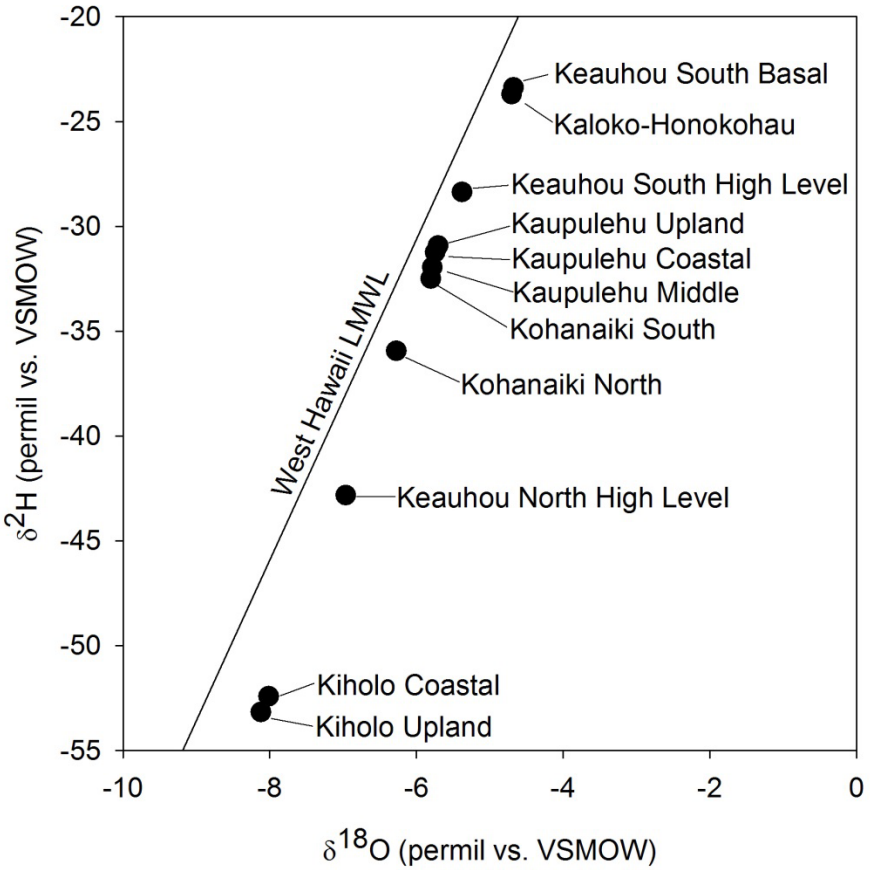

Figure 3.5. Groundwater sample group average δ^2H vs. $\delta^{18}O$ values plotted relative to West Hawai‘i LMWL.

Average groundwater recharge elevations (Figure 3.6) for the sample groups was determined by applying the West Hawai‘i $\delta^{18}O$-elevation relationship (Figure 3.4b) for average recharge elevations below 2000 m or the Hawai‘i Volcano high elevation $\delta^{18}O$-elevation relationship (Scholl et al., 1996) for average recharge elevations above 2000 m) to each sample group $\delta^{18}O$ value. The 2000 m elevation was chosen as a cutoff point for the use of the West Hawai‘i $\delta^{18}O$-elevation relationship because it is near the elevation of the highest precipitation collector used in this study and coincides with the top of the inversion layer, above which orographic precipitation is rare and infrequent winter cold fronts or subtropical low pressure systems known locally as “Kona storms” serve as the primary precipitation source (Scholl et al., 1996). Sample groups whose $\delta^{18}O$ values coincided with the discontinuity between the West Hawai‘i and Hawai‘i Volcano high elevation $\delta^{18}O$-elevation relationships (-5.67‰ to -6.83‰) were assigned an average recharge elevation of 2000 m. Projected in this way, average recharge elevations ranged from 1173 m (Keauhou South Basal) to 2405 m (Kīholo Upland). Though these average recharge elevations do not account for the spatial distribution of groundwater

recharge, they are indicative in many cases of groundwater flow paths extending well into the interior of Hawai‘i Island (cf. Figure 3.1) and are useful in constraining plausible flow path trajectories for the integrated analysis presented below.

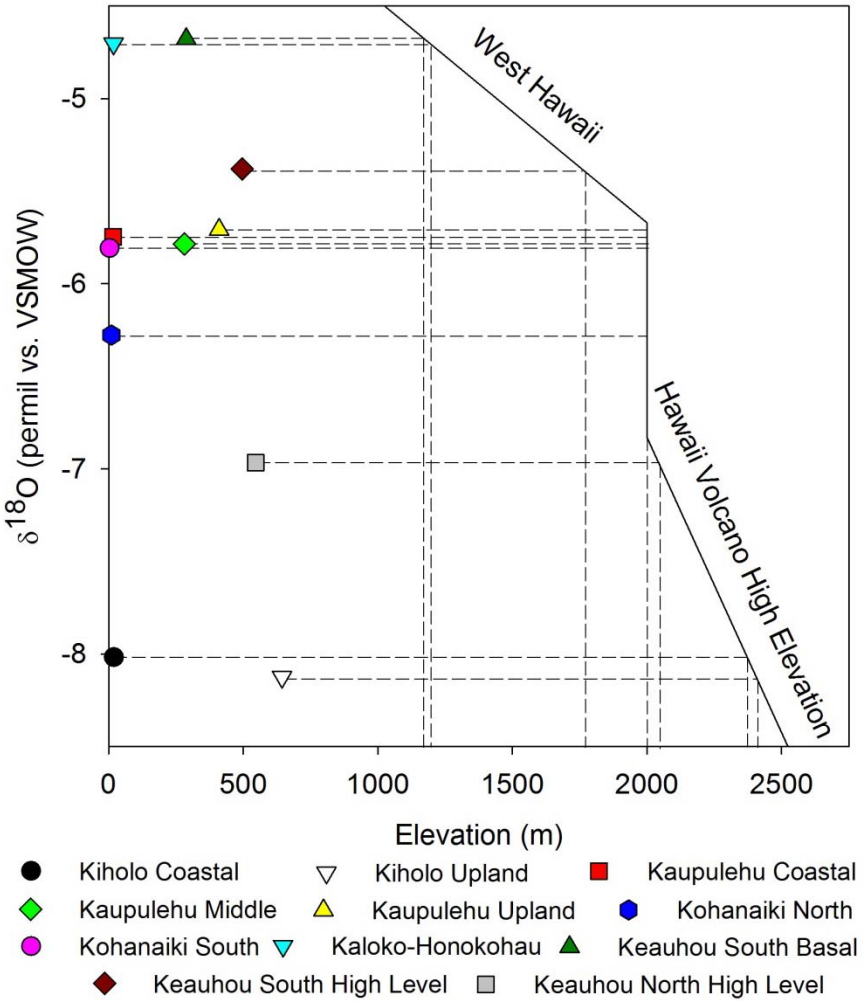

Figure 3.6. Average groundwater recharge elevations extrapolated using West Hawai‘i $\delta^{18}O$-elevation relationship for elevations less than 2000 m and Hawai‘i Volcano high elevation $\delta^{18}O$-elevation relationship (Scholl et al., 1996) for elevations above 2000 m.

Groundwater Conceptual Models and Flow Path Trajectories

Overview

A conceptual model of groundwater occurrence and flow is a necessary prerequisite to the development of groundwater flow paths by integrated analysis of $\delta^{18}O$ values in recharge. Previous studies utilizing water isotopes for flow path determination in Hawai‘i have used flow path trajectories generated from a pre-existing numerical groundwater model (Bishop et al., 2015) or flow paths trajectories perpendicular to elevation contours (Scholl et al., 1996; Scholl et

al., 2002; Kelly and Glenn, 2015). Since insufficient calibration data exists to create a meaningful numerical model of groundwater flow in the West Hawai‘i study area, we adopted the overall approach of assuming that groundwater in this region generally flows from high groundwater head level areas in the island’s interior towards the coast (Izuka et al., 2016). We carefully considered each portion of the study area separately to generate appropriate conceptual models (Figure 3.7) for generation of flow path trajectories in order to best account for the presence of the three prominent volcanic peaks in the study area (Hualālai, Mauna Loa, and Mauna Kea) complicating potential flow path trajectories (Table 3.4), spatially variable average recharge elevations (Figure 3.6), and observed hydrogeological phenomena including extensive bodies of confined and perched groundwater,.

Table 3.4. Summary of conceptual models used for developing flow path trajectories (Figure 3.7), flow path trajectories, shielding of flow paths, and indirect recharge contributions utilized in integrated recharge analysis of sample groups.

Sample Group	Conceptual Model	Flow Path Trajectory	Shielding	Indirect Recharge Contribution
Kīholo Coastal	Kīholo	Mauna Loa / Mauna Kea via Humu‘ula Saddle	No	Humu‘ula Saddle (-10.6 ‰)
Kīholo Upland	Kīholo	Mauna Loa / Mauna Kea via Humu‘ula Saddle	No	Humu‘ula Saddle (-10.6 ‰)
Ka‘ūpūlehu Coastal	Ka‘ūpūlehu	Mauna Loa	No	None
Ka‘ūpūlehu Middle	Ka‘ūpūlehu	Mauna Loa	No	None
Ka‘ūpūlehu Upland	Ka‘ūpūlehu	Mauna Loa	No	None
Kohanaiki North	Keauhou North	Hualālai	No	Keauhou North High Level (-6.97 ‰)
Kohanaiki South	Keauhou North	Hualālai	No	Keauhou North High Level (-6.97 ‰)
Kaloko-Honokōhau	Keauhou North	Hualālai	No	Keauhou North High Level (-6.97 ‰)
Keauhou North High Level	Keauhou North	Mauna Loa	Yes	None
Keauhou South High Level	Keauhou South	Mauna Loa	No	None
Keauhou South Basal	Keauhou South	Mauna Loa	No	None

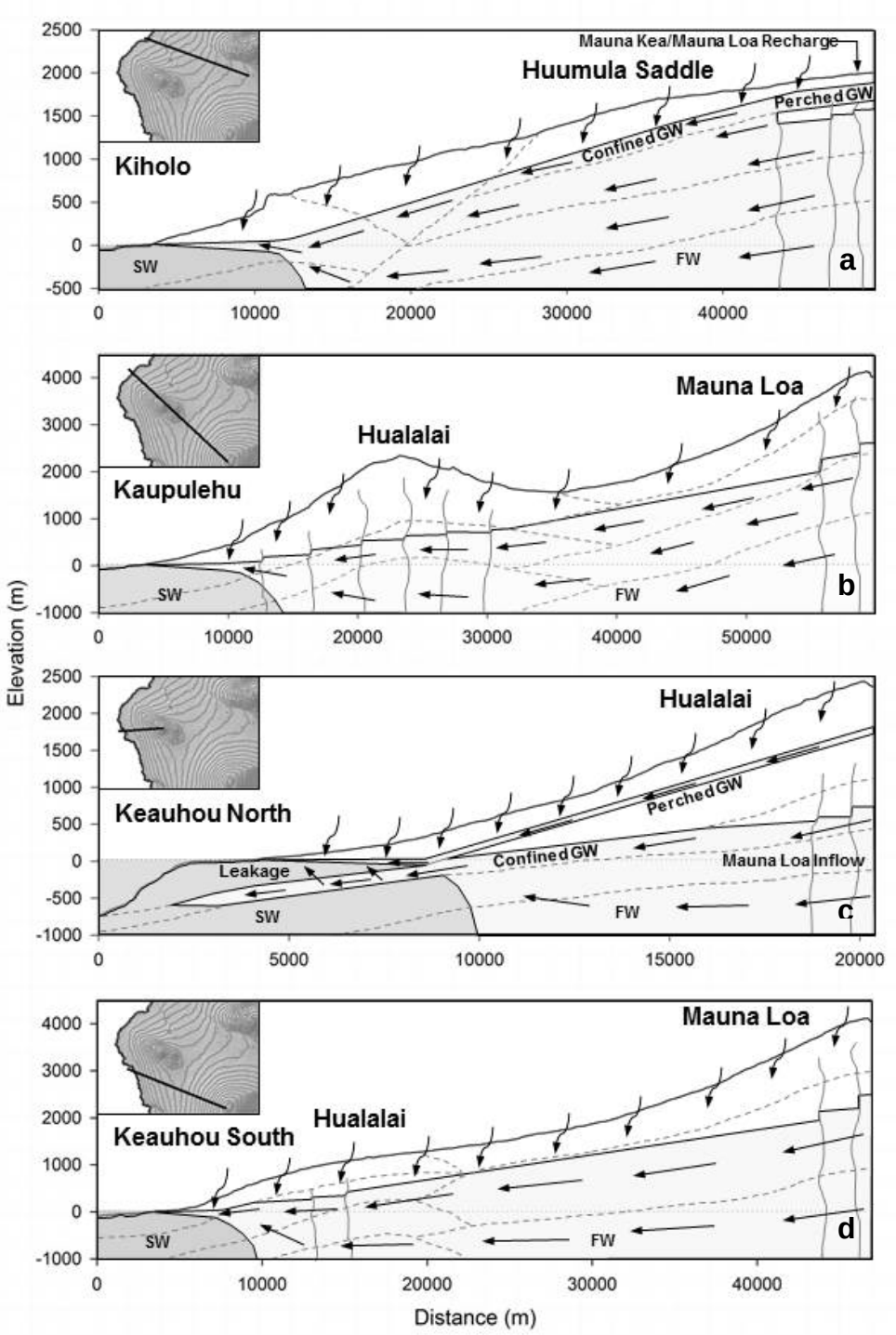

Figure 3.7(a-d). Conceptual hydrologic cross sections of Kīholo (a), Kaʻūpūlehu (b), Keauhou North (c), and Keauhou South (d) transects. Solid black lines define land surface, water table, and freshwater (FW)-seawater (SW) interface. Dashed gray lines are approximations of subsurface structure, while solid gray lines indicate dikes. Freshwater extent is light gray while seawater extent is dark gray. Straight arrows indicate groundwater flow direction in the saturated zone while curved arrows indicate recharge.

Kīholo Coastal and Upland Groundwater Sample Groups

The Kīholo Coastal and Upland sample groups had the lowest $\delta^{18}O$ values and thus the highest average recharge elevations of all the sample groups. The low $\delta^{18}O$ values found in groundwater in this portion of the study area cannot be accounted for by integrated recharge along a flow path trajectory toward the peak of Hualālai (Kelly and Glenn, 2015), suggesting that flow path trajectories toward the Mauna Kea or Mauna Loa peaks may be more appropriate. However, integrated recharge along straight line flow path trajectories from the sample group average locations toward either the Mauna Loa or Mauna Kea peaks were also unable to account for the low $\delta^{18}O$ values found in groundwater in this portion of the study area. As a result, we considered the Kīholo portion of the study area as a preferential drain for recharge falling on the upper elevations of Mauna Loa and Mauna Kea and designed flow path trajectories that connect the sample group locations to the 2000 m elevation of the Humu‘ula Saddle before branching toward the Mauna Loa and Mauna Kea peaks (Table 3.4). Figure 3.7a illustrates the conceptual model used for flow path trajectory development for the Kīholo Coastal and Upland sample groups. Integrated recharge analysis of these branching flow paths produced values close to, but slightly higher than observed sample group average $\delta^{18}O$ values. To account for the difference, we assumed that, in addition to direct recharge via precipitation, groundwater in the Kīholo area also contains a fraction of groundwater derived from the down-gradient flow of the large body of dike-confined low $\delta^{18}O$ value (-10.6‰) groundwater (Table 3.4, Figure 3.7a) found beneath perched groundwater formations in the Humu‘ula Saddle (Thomas et al., 2015). The fraction of this end-member required to match the integrated recharge analysis $\delta^{18}O$ value with the measured sample group average $\delta^{18}O$ value was calculated via a two-component end member mixing calculation.

Ka‘ūpūlehu Coastal, Middle, and Upland Sample Groups

The Ka‘ūpūlehu Coastal, Middle, and Upland sample groups had average $\delta^{18}O$ values within 0.1‰ of each other, suggesting similar provenance. Though these sample group locations fall near the northwest rift zone of the Hualālai, preliminary analysis showed that flow path trajectories toward the summit of the Hualālai yielded integrated recharge $\delta^{18}O$ values higher than observed sample group averages. As a result, we utilized flow path trajectories extending

from the sample group locations toward the summit of the much higher Mauna Loa (Table 3.4, Figure 3.7b).

Kohanaiki North and South, Kaloko-Honokōhau, and Keauhou North High Level Groundwater Sample Groups

Despite their geographical proximity (Figure 3.2), the Kohaniki North, Kohanaiki South, Kaloko-Honokōhau , and Keauhou North High Level sample groups had a large range of average $\delta^{18}O$ values (-4.70‰ to -6.97‰) (Table 3.3) and a correspondingly large range of recharge elevations (Figure 3.6). To account for the spatial heterogeneity of $\delta^{18}O$ values and the interconnectivity of high level and basal groundwater in this region (Oki et al., 1999; Tillman et al., 2014; Kelly and Glenn, 2015) we utilized the following principles for conceptualization (Figure 3.7c) for generation of flow path trajectories:

1) The flow path trajectories of the basal groundwater sample groups (Kohanaiki North, Kohanaiki South, and Kaloko-Honokōhau) extend toward the peak of Hualālai. Above the basal-high level groundwater divide, recharge along these trajectories is directed into the basal aquifer by perching formations overlying the high level aquifer (Paul Eyre, Hawai‘i Commission on Water Resource Management, personal communication). Additionally, the basal groundwater sample groups receive indirect recharge via leakage from the high level aquifer (Table 3.4, Figure 3.7c). The fraction of this -6.97‰ end-member required to match the integrated recharge analysis $\delta^{18}O$ value with the measured sample group average $\delta^{18}O$ value was calculated, as for the Kīholo Coastal and Upland sample groups above, via a two-component end member mixing.

2) The flow path trajectory of the Keauhou North High Level sample group extends toward the peak of Mauna Loa. In order to match the sample group average $\delta^{18}O$ value with the integrated recharge $\delta^{18}O$ value, the lower portion of the flow path is considered “shielded” from recharge by the perching formations directing this recharge to the basal aquifer (Table 3.4, Figure 3.7c).

Keauhou South Basal and High Level Sample Groups

The Keauhou South Basal and High Level sample groups had the highest and third-highest average $\delta^{18}O$ values, respectively. Though these sample groups are located on the southwest flanks of Hualālai, preliminary analysis showed that that flow path trajectories toward the summit of the Hualālai yielded integrated recharge $\delta^{18}O$ values higher than observed sample

group averages. As a result, we utilized flow path trajectories extending from the sample group locations toward the summit of the much higher Mauna Loa (Table 3.4, Figure 3.7d).

Groundwater Flow Paths

Overview

Groundwater flow paths for each of the sample groups described above are shown in Figure 3.8. These groundwater flow paths were determined by applying integrated recharge analysis to the flow path trajectories and special conditions (shielding and indirect recharge) where applicable generated via preliminary analysis (Table 3.4) and conceptual modeling (Figure 3.7). Due to the many unknowns regarding the subsurface geology and hydrogeology of much of the study area, these flow paths are best understood as plausible reconciliations of observed $\delta^{18}O$ values in precipitation and groundwater rather than precise vectors of actual groundwater travel. Nevertheless, they are useful tools for understanding the many variables controlling groundwater occurrence and transport in this poorly understood region, as discussed in greater detail below.

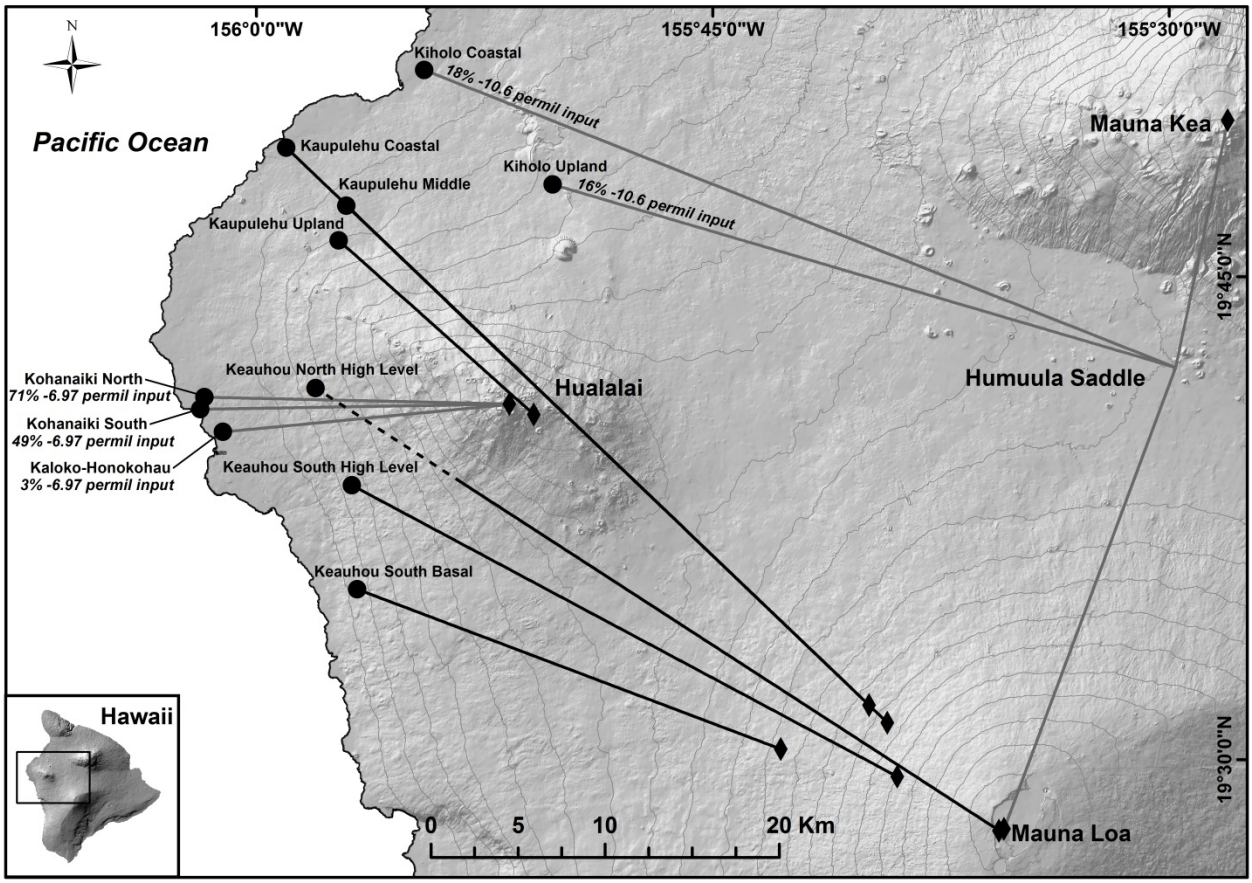

Figure 3.8. Sample group flow paths as defined by integrated recharge analysis of flow path trajectories. Flow path origins and endpoints are indicated by circles and diamonds, respectively. Direct recharge flow paths are in black while flow paths containing indirect recharge contributions are in gray and labeled with indirect recharge fraction. The shielded portion of the Keauhou North High Level flow path is indicated with a dashed line. Contour interval is 200 m.

Kīholo Coastal and Upland Sample Groups

Flow paths for the Kīholo Coastal and Kīholo Upland sample groups extend from the average group sample locations to the summits of Mauna Loa and Mauna Kea via the 2000 m elevation of Humu‘ula Saddle (Figure 3.8). The Kīholo Coastal and Kīholo Upland sample groups required 18% and 16% indirect recharge contributions from the -10.6‰ Humu‘ula Saddle groundwater end member, respectively, for integrated recharge $\delta^{18}O$ values along the flow paths to match observed sample group average values (Table 3.3). These findings support the interpretation of the Kīholo region as a preferential drain for modern recharge in the Humu‘ula Saddle region between the Hualālai, Mauna Loa, and Mauna Kea summits as well as older groundwater stored deep within the island’s interior slowly travelling seaward via confined aquifers (Thomas et al., 2015). The relatively large fractions of old (recharged prior to 1940),

CFC-free groundwater (37-53%) reported by Kelly and Glenn (2015) for coastal groundwater samples in the Kīholo region support this interpretation as well. The length and extent of the Kīholo Coastal and Kīholo Upland sample group flow paths suggest that recharge contributing to groundwater in this region occurs over large spatial and temporal scales and has important implications with respect to future investigations into or development of water resources in this region.

Ka‘ūpūlehu Coastal, Middle, and Upland Sample Groups

Flow paths for the Ka‘ūpūlehu Coastal, Middle, and Upland sample groups flow extend from the average sample group locations toward the Mauna Loa summit (Figure 3.8). The Ka‘ūpūlehu Coastal and Middle sample group flow paths end past the 2800 and 2600 m contours of Mauna Loa while the Ka‘ūpūlehu Upland sample group flow path ends near the Hualālai summit. This discrepancy in flow path end points between the Upper and Coastal/Middle sample groups despite their similar average $\delta^{18}O$ values is due to the greater fraction of high-elevation, low $\delta^{18}O$ value recharge required to balance out the low-elevation, high $\delta^{18}O$ value recharge along the lower portion of the flow paths of the Coastal/Middle sample groups. This phenomenon may be the result of geometry of the basal lens, which thins near the coast and would act to direct groundwater recharged at high elevation in the deeper portion of the lens closer to the surface of the water table near the coast. Unlike the Kīholo region flow paths, no indirect recharge contributions were required for Ka‘ūpūlehu flow path integrated recharge $\delta^{18}O$ values to match sample group average $\delta^{18}O$ values. The relatively low specific yields and vulnerability to salinization of groundwater wells in the Ka‘ūpūlehu region (Charles Dawrs, Hualālai Resort, personal communication) as well as their proximity to the northwest rift of the Hualālai volcano are indicative of dike intrusions impeding lateral groundwater flow. These dikes may also play a role in directing high-elevation recharge in the deeper portion of the aquifer towards the water table surface during down-gradient transit.

Kohanaiki North and South, Kaloko-Honokōhau , and Keauhou North High Level Sample Groups

Flow paths for the Kohanaiki North, Kohanaiki South, and Kaloko-Honokōhau sample groups extend to the Hualālai summit (Figure 3.8), with the assumption that perching formations direct recharge along the portions of these flow paths above the basal-high level divide directly

to the basal aquifer (Figure 3.7c). To match these sample groups' average $\delta^{18}O$ values with the integrated recharge flow path $\delta^{18}O$ values, we included indirect recharge via leakage from the high level aquifer, represented by the -6.97‰ Keauhou North High Level sample group average $\delta^{18}O$ value. Indirect recharge contributions from this source were 71%, 49%, and 3% for the Kohanaiki North, Kohanaiki South, and Kaloko-Honokōhau sample groups, respectively. These fractions of high-level groundwater contribution to the basal aquifer in this region are consistent with those determined by mixing analyses of basal groundwater samples by both Fackrell and Glenn (2014) and Tillman et al. (2014). The widely varying indirect recharge contributions between sample groups in this relatively small area is indicative of spatial heterogeneity in leakage from the high-level groundwater system to the basal groundwater system in this portion of the study area, with indirect recharge via leakage dominating to the north and direct recharge via precipitation on Hualālai's flanks dominating to the south. This finding has implications regarding the extent and permeability of the geologic structures controlling the distribution of high-level groundwater in this region. The Keauhou North High Level sample group flow path extends from the sample group average location to the Mauna Loa summit. The portion of the flow path from the sample group average location to the 1400 m elevation contour is considered shielded from direct recharge via precipitation by the same perching formations directing recharge toward the basal aquifer, resulting in the integrated recharge flow path $\delta^{18}O$ value for the non-shielded portion of the flow path matching the observed sample group average $\delta^{18}O$ value. The shielding of high level groundwater from local recharge in this portion of the study area is consistent with results from Bauer (2003) that indicated that the head level of a high level well in this region (4258-03) did not vary significantly in response to local precipitation as well as the results from Kelly and Glenn (2015) that showed large fractions of old (recharged prior to 1940), CFC-free groundwater (84-95%) in groundwater samples taken from wells in this region. Additionally, perched groundwater with $\delta^{18}O$ values consistent with local recharge has been observed flowing into a deep monitor well in this region (Paul Eyre, Hawai'i Commission on Water Resource Management, personal communication). The importance of Mauna Loa recharge as opposed to local recharge in supplying the high-level groundwater system in this portion of the study area has implications with regard to the evaluation of sustainable use and future exploration of this resource, which is heavily relied upon for drinking water.

Keauhou South Basal and High Level

Flow paths for the Keauhou South Basal and Keauhou South High Level sample groups extend from the sample group locations to elevations near 2200 m and 3200 m, respectively, on the western flanks of Mauna Loa (Figure 3.8). No indirect recharge contributions were required to match these sample groups' integrated recharge $\delta^{18}O$ values to match sample group average $\delta^{18}O$ values. Though the proximity of the perched groundwater discussed above (Figure 3.7c) to wells in this sample group suggest that some shielding of local recharge may be occurring in this portion of the study area, this phenomenon is not required to explain the $\delta^{18}O$ values observed and is not considered here due to lack of means to constrain its extent. While there is no long term groundwater head level data available for wells in the Keauhou South High Level sample group, three nearby high level groundwater wells located to the south of these wells exhibited head levels that responded to variability in local precipitation (Bauer, 2003). This suggests that the geological structures responsible for the occurrence of high level groundwater in this portion of the study area may be relatively permeable or have a geometry that allows for more infiltration of local recharge in contrast to those structures responsible for perching and impounding groundwater in vicinity of the Keauhou North High Level sample group wells. The extension of the Keauhou South Basal flow path to a point well above the basal-high level groundwater divide illustrates the interconnectivity of the basal and high level aquifers in this region.

Summary of Groundwater Flow Paths

Figure 3.9 provides a generalized summary of groundwater flow in West Hawai‘i based on the conceptual models shown in Figure 3.7 and calculated groundwater flow paths shown in Figure 3.8. These findings contrast markedly with traditional interpretations of West Hawai‘i's hydrogeology (e.g. Stearns and Macdonald, 1946), which generally do not consider the importance of structural controls other than vertical dikes on groundwater occurrence and flow as well as with more modern interpretations (e.g. Oki, 1999; Kelly and Glenn, 2015) which tend to focus on smaller areas and neglect the possibility of groundwater crossing lithological boundaries between volcanoes. While the summary of groundwater flow presented here is not entirely inconsistent with the Hawai‘i Island groundwater conceptual model of Izuka et al.,

(2016), it provides a more detailed delineation of probable groundwater flow directions and differs in interpretation of the areal extent of basal and perched groundwater bodies.

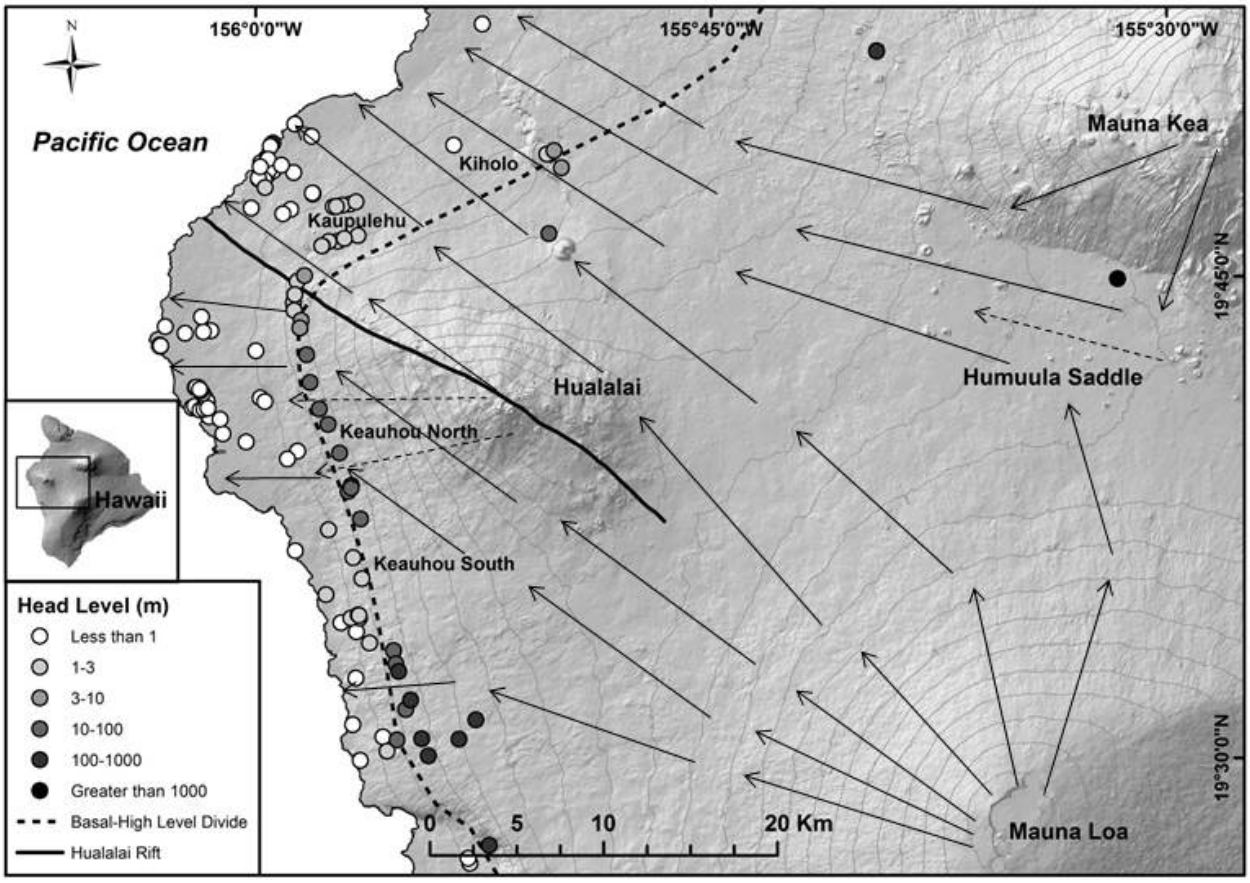

Figure 3.9. Generalized summary of West Hawai‘i groundwater flow based on calculated flow paths and conceptual models. Measured groundwater head levels (Hawai‘i Commission on Water Resource Management, 2008) are shown for reference. Flow of basal and high level groundwater is indicated by solid arrows while flow of perched groundwater is indicated by dashed arrows. Contour interval is 200 m.

Conclusions

We utilized a network of cumulative precipitation collectors to characterize the LMWL and $\delta^{18}O$-elevation relationship of the West Hawai‘i study area and then compared these results to groundwater $\delta^{18}O$ values measured throughout the study area to develop new conceptual models and groundwater flow paths consistent with observed hydrogeological phenomena. We determined that (1) the West Hawai‘i LMWL is consistent with a primary oceanic moisture source to the lee of Hawai‘i Island, while the West Hawai‘i $\delta^{18}O$-elevation relationship closely resembles that determined for the Hawai‘i Volcano Trade Wind region by Scholl et al., (1996), (2) dikes and low-permeability layers resulting in perched and confined groundwater in different portions of the study area necessitated the development of new conceptual models that can

reconcile $\delta^{18}O$ values observed in precipitation and groundwater, and (3) groundwater flow paths in West Hawai‘i tend to originate in the upper elevations of the Mauna Kea and Mauna Loa volcanoes as opposed to the much smaller Hualālai volcano, with long travel distances implying correspondingly long travel times These findings represent a significant step forward in scientific understanding of groundwater flow in the West Hawai‘i region and illustrate the utility of water isotope values as tracers of groundwater flow in high-relief regions as well as the importance of considering observed structural controls on groundwater flow when determining flow paths using the well-established integrated recharge method. Finally, these findings may serve to guide future efforts at better understanding and sustainably utilizing groundwater resources in this region. Further investigations into groundwater occurrence and flow in West Hawai‘i, integrating geophysical, geochemical, borehole drilling, and numerical modeling disciplines would be especially useful in evaluating the findings of this paper and working toward a more complete understanding of this complex system.

CHAPTER 4. NATURAL AND ANTHROPOGENIC CONTROLS ON GROUNDWATER NUTRIENT AND DISSOLVED INORGANIC CARBON CONCENTRATIONS: WEST HAWAI‘I, USA

Joseph K. Fackrell, Craig R. Glenn, Robert Whittier, and Brian N. Popp

Prepared for submission to *Applied Geochemistry*

Abstract

Groundwater in the western portion of the island of Hawai‘i serves as the region’s primary water supply and delivery mechanism of dissolved nutrients and inorganic carbon to the coastal ocean via submarine groundwater discharge (SGD). Despite the economic and ecological importance of groundwater in this region, the relationships between natural and anthropogenic terrestrial factors and groundwater nutrient and dissolved inorganic carbon (DIC) concentrations are poorly understood. We measure PO_4^{3-}, SiO_4^{4-}, NO_3^-, and DIC concentrations as well as $\delta^{15}N$ of NO_3^- and $\delta^{13}C$ of DIC values for groundwater samples collected throughout the West Hawai‘i study area. We then use the Spearman’s rank correlation test to aid in the assessment of the effects of land use/land cover, wastewater effluent discharge, and geothermal activity along flow paths determined for each groundwater sample (Chapter 3) on the measured parameters. We find that geothermal activity is significantly correlated to elevated groundwater SiO_4^{4-}, NO_3^-, and DIC concentrations and that wastewater effluent discharge as well as urban and park land use are significantly correlated to elevated groundwater NO_3^- concentrations. Additionally, land use and land cover types associated with greater precipitation and soil development are significantly correlated to elevated PO_4^{3-} concentrations.

Introduction

Understanding the relationship between natural and anthropogenic factors and groundwater nutrient and dissolved inorganic carbon (DIC) concentrations is important for determining sound water and land use policies in regions where groundwater is utilized as a resource as well as regions where groundwater discharges into rivers, lakes, or the ocean. Excessive concentrations of NO_3^- in drinking water pose a health risk (Ward et al., 2005), while high SiO_2 concentrations may cause scaling and damage to water filtration and delivery infrastructure (Ning, 2002). The loading of PO_4^{3-}, SiO_4^{4-}, and NO_3^- to rivers, lakes, and the ocean via groundwater base flow or submarine groundwater discharge (SGD) is frequently

implicated as a cause of harmful algae blooms, eutrophication, and resultant environmental degradation (e.g. Lapointe and Clark, 1992; McCook, 1999; Hwang et al., 2005; Lee et al., 2009). SGD containing high concentrations of DIC may affect the carbonate chemistry of coral reefs (Cyronak et al., 2013, 2014).

The process of linking terrestrial factors such as land use/land cover, wastewater effluent discharge, and geothermal activity with groundwater nutrient and DIC concentrations can be challenging due to the difficulty of constraining groundwater flow paths and recharge areas, lack of information regarding subsurface geology, and the complex and often non-conservative behavior of dissolved nutrients and DIC during infiltration and down-gradient transit. Commonly implicated sources of PO_4^{3-} and NO_3^- in groundwater include fertilized agriculture (e.g. Dubrovsky et al., 2010) and wastewater effluent (e.g. Lapointe et al., 1990; Richardson et al., 2015). $\delta^{15}N$ values of NO_3^- may be useful in differentiating different NO_3^- sources as well as identifying non-conservative behavior (e.g. Kendall, 1998). SiO_4^{4-} in groundwater is derived primarily from silicate rock weathering (e.g Schopka and Derry, 2012), and high SiO_2 concentrations are commonly associated with elevated geothermal heat flow (Swanberg et al., 1978). DIC in groundwater can originate from a variety of sources, including equilibration with CO_2 derived from decaying organic matter in the soil zone, respiration of organic C within the aquifer, and rock weathering (Clark and Fritz, 1997). As with SiO_4^{4-}, high DIC concentrations can also be associated with geothermal activity (e.g. Clark et al., 1982). $\delta^{13}C$ values of DIC may be useful in differentiating different DIC sources such as carbonate rock dissolution and oxidation of soil organic matter (Clark and Fritz, 1997).

In the western portion of the island of Hawai‘i, the youngest and largest island in the Hawai‘ian chain, groundwater serves as the primary source of water for agricultural, industrial, and domestic use as well as the primary vector of nutrient delivery to the coastal waters via SGD (e.g Johnson et al., 2008). However, the mechanisms controlling the highly variable groundwater nutrient and DIC concentrations in this region are poorly understood, and studies assessing the controls on nutrient and DIC variation in groundwater on similar high volcanic islands are relatively few (e.g. Knee et al., 2010; Bishop et al., 2015). Therefore, the purpose of this study is to systematically assess potential natural and anthropogenic controls on variation in groundwater nutrient and DIC concentrations in the West Hawai‘i region. We utilize Spearman’s rank correlation to assess the effects of land use/land cover, wastewater effluent

discharge, and geothermal activity along previously determined groundwater flow paths (Chapter 3) on groundwater nutrient and DIC concentrations as well as $\delta^{15}N$ values of NO_3^- and $\delta^{13}C$ values of DIC.

Methods

Setting and Background

The West Hawai‘i study area consists of the Hualālai volcano as well as portions of the larger Mauna Loa and Mauna Kea volcanoes. The Hualālai volcano is historically active, last erupting in 1802 from a prominent rift zone trending northwest from its main vents (Sherrod et al., 2007). Hualālai's northwest rift zone and summit have potential as a geothermal resource based on geochemical evidence (Thomas, 1986). The Hualālai volcano is surrounded by lavas of the much larger and more active Mauna Loa volcano, which last erupted in 1984 (Sherrod et al., 2007). The older, dormant Mauna Kea volcano is exposed in the northeastern portion of the study area and underlies portions of the Mauna Loa and Hualālai volcanoes. The surficial lavas found in the study area are primarily alkalic (Hualālai and Mauna Kea) and tholeiitic (Mauna Loa) and are geologically young, with the oldest lavas from Hualālai and Mauna Loa emplaced less than 50 kya and oldest lavas from Mauna Kea emplaced less than 300 kya (Sherrod et al., 2007).

The West Hawai‘i study area covers a wide variety of ecosystems and land use types. Climate ranges from humid and tropical at lower elevations to alpine desert on the upper elevations of Mauna Loa and Mauna Kea. The portion of the study area north of Hualālai's northwest rift is relatively arid and consists primarily of bare land, grassland, and scrubland. It is largely undeveloped, with some localized resort and golf course development along the coast and pasture at middle elevations. The portion of the study area south of Hualālai's northwest rift zone contains the Kailua-Kona urban center and is more developed at lower elevations than the portion of the study area north of Hualālai's northwest rift zone. Relative to its higher elevations, the coastal portion of this region is arid and contains a wide variety of land use, including an airport, an experimental industrial facility (NELHA), Kaloko-Honokōhau National Historical Park (KAHO), the Kealakehe Wastewater Treatment Plant effluent disposal site, and the urban and resort development of Kailua-Kona. The middle elevations of this area (roughly 400-1500 m) comprise Kona's famous "coffee belt" and receive relatively high rainfall driven by the

interaction of moisture-laden daytime sea breezes with the steep western slopes of the Hualālai and Mauna Loa volcanoes (Giambelluca et al., 2013). Land use at these middle elevations consists primarily of ranch land, coffee plantations, and light residential development. At elevations >1500 m, this region receives progressively less rainfall with increasing elevation and is dominated by scrubland and bare land. The majority of residences and businesses in the study area are not connected to sewer infrastructure and dispose of wastewater via on-site sewage disposal systems (OSDS) or underground injection (Whittier and El-Kadi, 2009).

Groundwater in the West Hawai‘i study area occurs as both a thin lens of basal groundwater under Ghyben-Herzberg conditions near the coast and extending several km inland in some areas and as high-level groundwater further inland. The basal groundwater is characterized by low head levels (<2 m) due to the lack of confining coastal sediments and high hydraulic conductivities of the young lava flows. It also exhibits a strong response to tidal cycling (Oki, 1999), illustrating its hydraulic connectivity to the ocean. The portion of the basal lens to the south of Hualālai's northwest rift zone exhibits anomalously low groundwater temperatures, suggesting that cold intermediate depth seawater intrudes the aquifer in this area through the steep offshore headwall of the North Kona slump (Bowles, 2007; Hunt, 2014). Groundwater also occurs at anomalously high head levels (~5-100 m) relative to the basal lens hydraulic gradient in numerous wells drilled further inland. The geologic structures responsible for the presence of high-level groundwater in this area are not well characterized, but available drilling log, water level, and pump test data suggests that dense and impermeable lava flows or ash layers impound water under artesian conditions and buried dikes impede horizontal flow (Oki, 1999; Bauer, 2003, Tillman et al., 2014). H and O isotopic composition of groundwater and precipitation in the region suggest that this high-level groundwater serves as a source of recharge to the basal aquifer (Fackrell and Glenn, 2014; Tillman et al., 2014). CFC age dating (Kelly and Glenn, 2015) of this high-level groundwater indicates that it contains a large fraction of "old" groundwater, recharged prior to 1940, while basal groundwater contains more "young" groundwater, recharged after 1940. Drilling log and depth profile data acquired from boreholes drilled through the basal lens in the portion of the aquifer south of Hualālai's rift zone suggest that fresh water under artesian conditions, possibly related to the high-level water found further inland, underlies the basal lens in this area and is hydraulically connected to the ocean (Bowles, 2007; Nance, 2013). Geophysical survey and deep borehole data collected in the Humu‘ula

Saddle region show extensive perched and high-level groundwater, including groundwater under artesian conditions, with head levels in excess of 1000 m (Thomas et al., 2015).

Numerous previous studies have shed light on nutrient concentrations in groundwater and the role of SGD in delivering dissolved nutrients to the ocean in West Hawai‘i. Kay et al. (1977) used water budget calculations combined with nutrient analyses of groundwater to estimate SGD-driven nutrient fluxes in the northern portion of the region. Dollar and Atkinson (1992) considered fertilizer application and leaching rates to demonstrate that fertilizer applied to two golf courses in the region could result in increased delivery of dissolved N and P species to the adjacent coastal ocean via SGD. More recent studies have used radiochemical tracers (e.g. Street et al., 2008; Peterson et al. 2007, 2009) and aerial thermal infrared imagery (Johnson et al., 2008) combined with nutrient analyses of groundwater and SGD to quantify the magnitude of SGD and its associated nutrient fluxes at various locations along the coast. An important outcome of these studies was identification of the high SGD rates and spatially variable nutrient concentrations in groundwater in this region. Knee et al. (2010) attempted to spatially link nutrient concentrations in SGD and up-gradient groundwater with land use at several West Hawai‘i locations, but were not able to establish conclusive relationships. Hunt (2014) used nutrient and wastewater indicator compound concentrations in coastal groundwater in the Kaloko-Honokōhau portion of the study area to implicate wastewater as a potential contributor.

Sampling Methods

Groundwater samples (83) were collected from 42 separate locations in March 2011, October 2011, March 2012, and October 2012 (Table 4.1, Figure 4.1). Sample locations included 29 production wells, 10 monitor wells, 2 lava tubes, and 1 coastal spring, and were divided into 4 regions and 11 sub-regions by geographic location for ease of referencing. Wells were purged at least 3 borehole volumes before sample collection. Production wells were sampled using installed pump and sampling apparatus. Monitor wells and lava tubes were sampled using portable centrifugal pumps lowered to less than 3 m below the water table surface. The coastal spring sample was collected via piezometer using a peristaltic pump. Samples for nutrients, DIC, and $\delta^{15}N$ of NO_3^- were collected in 500 mL HDPE bottles and chilled immediately. Nutrient and DIC samples were later subsampled and filtered through 0.45 μm cellulose acetate filters into 60 mL HDPE bottles and stored refrigerated (nutrients) or frozen

(DIC) prior to analysis. $\delta^{15}N$ of NO_3^- samples were subsampled unfiltered into 60 mL HDPE bottles and frozen prior to analysis. $\delta^{13}C$ of DIC samples were collected in crimp sealed 20 mL glass vials with butyl rubber septa and immediately poisoned with 0.5 mL of saturated $HgCl_2$ solution. These samples were stored at room temperature prior to analysis. Salinity measurements were taken at the time of collection using a YSI multi-parameter sonde.

Table 4.1. Groundwater sample information

Sample Name	Sample Type	Region	Subregion	Latitude	Longitude	n
Hind Well	Lava Tube	Kīholo	Kīholo Coastal	19.85400	-155.92307	2
Kīholo Lava Tube	Lava Tube			19.85073	-155.92847	2
5352-01	Production Well			19.89144	-155.87457	3
4950-01	Production Well		Kīholo Upland	19.82220	-155.84306	3
4850-01	Production Well			19.81321	-155.83385	3
4650-01	Production Well			19.77911	-155.84145	2
4859-01	Monitor Well	Kaʻūpūlehu	Kaʻūpūlehu Coastal	19.81362	-155.97974	1
Waiokane Piezometer	Spring			19.83146	-155.98682	1
King's Pond Well	Production Well			19.82946	-155.99089	2
4757-01	Production Well		Kaʻūpūlehu Middle	19.79276	-155.96220	3
4757-02	Production Well			19.79489	-155.95872	3
4856-01	Production Well			19.79742	-155.94684	2
4856-02	Production Well			19.79825	-155.94293	3
4658-01	Production Well		Kaʻūpūlehu Upland	19.77508	-155.96581	1
4658-02	Production Well			19.77654	-155.96501	2
4657-01	Production Well			19.77781	-155.96230	1
4657-02	Production Well			19.77728	-155.95763	2
4657-03	Production Well			19.77854	-155.95346	3
4656-01	Production Well			19.77979	-155.94986	2
4656-02	Production Well			19.78016	-155.94620	1
4161-04	Production Well	Keauhou Coastal	Kohanaiki North	19.70066	-156.03392	2
4161-05	Production Well			19.69934	-156.03304	2
4161-06	Production Well			19.69800	-156.03221	1
4161-07	Production Well			19.69662	-156.03133	1
4161-08	Production Well			19.69534	-156.03043	2
4162-06	Monitor Well		Kohanaiki South	19.69204	-156.03854	1
4162-07	Monitor Well			19.69304	-156.03746	2
4162-04	Monitor Well			19.69079	-156.03445	2
4161-11	Monitor Well			19.69126	-156.03232	2
4161-12	Monitor Well			19.69175	-156.03020	3
4161-01	Monitor Well		Kaloko-Honokōhau	19.68722	-156.02944	1
4161-02	Monitor Well			19.68583	-156.02361	1
4061-01	Monitor Well			19.67833	-156.02222	1
Expansion Well 2	Monitor Well			19.66799	-156.01433	3
4158-02	Production Well	Keauhou Upland	Keauhou North High Level	19.68240	-155.96442	3
4258-03	Production Well			19.70423	-155.97401	1
4358-01	Production Well			19.71846	-155.97554	3
3657-01	Production Well		Keauhou South Basal	19.61283	-155.95186	2
3557-04	Production Well			19.58138	-155.94926	1
4057-01	Production Well		Keauhou South High Level	19.66901	-155.95746	3
3957-05	Production Well			19.65059	-155.95142	1
3857-04	Production Well			19.63327	-155.94818	3

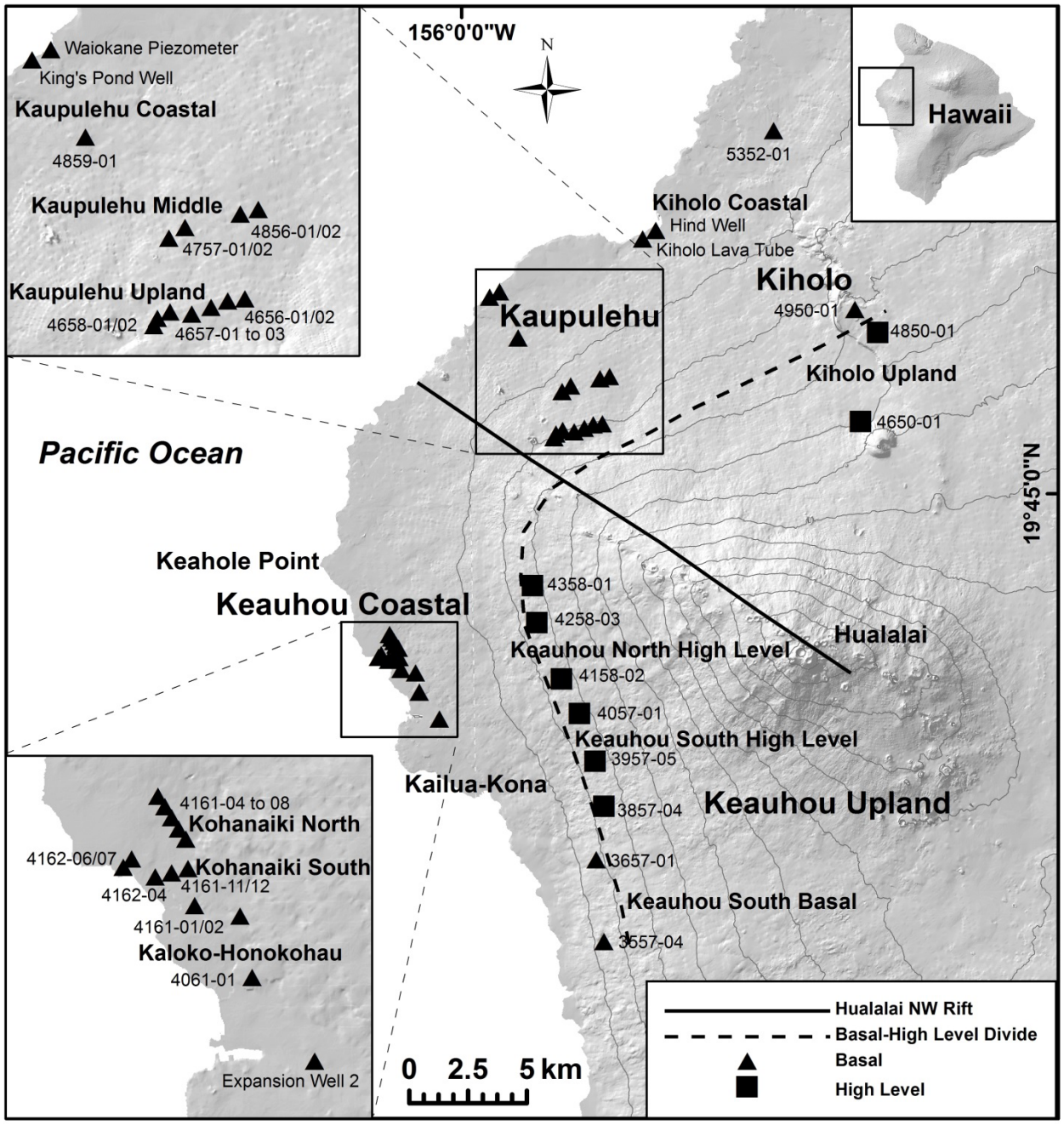

Figure 4.1. Groundwater sample locations with region and sub-region designations. Hualalai's northwest rift, basal-high level groundwater divide, and selected location names are shown for reference. Contour interval is 200 m.

Analytical Methods

PO_4^{3-}, SiO_4^{4-}, and NO_3^- samples collected in March 2011, October 2011, and March 2012 were shipped chilled to the University of Washington School of Oceanography Technical Services for analysis. PO_4^{3-}, SiO_2, and NO_3^- concentrations were measured using colorimetric procedures established by UNESCO (1994). PO_4^{3-}, SiO_4^{4-}, and NO_3^- samples collected in

October 2012 were transported chilled to the SOEST Lab for Analytical Biogeochemistry (SLAB) at the University of Hawai‘i at Mānoa. PO_4^{3-}, NO_3^-, and SiO_4^{4-} were measured at SLAB using the colorimetric methods of Murphy and Riley, (1962), Armstrong et al., (1967), and Grasshoff et al., (1983). All DIC samples were analyzed at the Water Resources Research Center Analytical Chemistry Laboratory at University of Hawai‘i at Mānoa using a Shimadzu TOC-V analyzer. DIC concentrations were determined by subtracting dissolved organic C (DOC) concentrations from total dissolved C (TDC) concentrations. All nutrient and DIC concentrations are expressed in micromoles per liter (μM). $\delta^{15}N$ of NO_3^- samples were analyzed at the Stable Isotope Biogeochemistry Lab and University of Hawai‘i at Mānoa using the denitrifier method (Sigman et al., 2001) coupled with the sulfamic acid method of NO_2^- removal during sample preparation (Granger et al., 2006). Samples were analyzed on Thermo Finnigan MAT 252 and 253 mass spectrometers using a continuous flow GC-interface. All results are expressed in per mil (‰) notation relative to AIR. $\delta^{15}N$ of NO_3^- values were normalized using the IAEA-N3 NO_3^- reference material assigned $\delta^{15}N$ of 4.7‰ VAIR (Bohlke and Coplen, 1995) as well as an internal laboratory reference material extensively calibrated using NIST and USGS isotope reference materials. $\delta^{13}C$ of DIC samples were analyzed at the University of Hawai‘i Stable Isotope Biogeochemistry laboratory with a ThermoFinnigan DeltaPlusV mass spectrometer coupled to a GasBench II peripheral using the method of Salata et al.(2000). Results are reported in units of ‰ relative to PDB and normalized to the NBS-18 and NBS-19 isotope reference materials using the accepted values of -5.04‰ VPDB and 1.95‰VPDB, respectively. Analytical uncertainty was quantified using the average standard deviation of sample/blind duplicate pairs. Average standard deviations for PO_4^{3-}, SiO_4^{4-}, and NO_3^- were 0.37, 32, and 2.6 μM, respectively (n=17). The average standard deviation for DIC was 28 μM (n=10), while average standard deviation for $\delta^{15}N$ of NO_3^- was 1.3‰ (n=26) and average standard deviation for $\delta^{13}C$ of DIC was 0.1‰ (n=11).

Salinity Unmixing of Groundwater Samples

Salinity was used to correct the nutrient and DIC concentrations as well as stable isotope values of groundwater samples for seawater content by mass balance. We assumed groundwater samples were a mixture of fresh recharge (salinity=0) and ocean water. Ocean water end-member salinity, nutrient, DIC, and stable isotope parameters were measured for 4 samples

collected in October 2012 from seawater intake pipes at the Natural Energy Laboratory of Hawai‘i Authority (NELHA), located at Keāhole Point on the westernmost tip of Hawai‘i (Table 4.2). The mean salinity, nutrient, and stable isotope parameters measured for the shallow seawater intake pipes were used to correct samples collected north of Hualālai’s rift zone, while the mean salinity, nutrient, and stable isotope parameters measured for both shallow and deep seawater intake pipes were used to correct samples collected south of Hualālai’s rift zone to account for the circulation of cold intermediate seawater through the aquifer in this region (Bowles, 2007; Hunt, 2014; Tillman et al., 2014).

Table 4.2. Seawater endmember parameters used in salinity unmixing of groundwater samples

Sample Name	Salinity	PO_4^{3-} (µM)	SiO_4^{4-} (µM)	NO_3^- (µM)	DIC (µM)	$\delta^{15}N$ of NO_3^- (‰)	$\delta^{13}C$ of DIC (‰)
NELHA 24m Suction	35.07	0.27	10	0.3	2172	0.00	0.99
NELHA 14m Suction	35.06	0.24	10	0.2	2191	0.00	1.32
NELHA 900m Suction	33.93	3.08	97	42.2	1978	5.44	0.21
NELHA 674m Suction	34.10	3.02	88	36.6	1962	7.13	0.18
Shallow Seawater Average	**35.07**	**0.26**	**10**	**0.3**	**2181**	**0.00**	**1.16**
Deep Seawater Average	**34.02**	**3.05**	**93**	**39.4**	**1970**	**6.29**	**0.20**
Combined Average	**34.54**	**1.65**	**51**	**19.8**	**2075**	**3.14**	**0.68**

Groundwater Flow Paths and Indirect Recharge Unmixing

Groundwater flow paths (Figure 4.2) for each groundwater sampling location were determined using the integrated recharge method, conceptual models, and salinity unmixed $\delta^{18}O$ values reported in Chapter 3 above. Several of the flow paths of samples in the Kīholo and Keauhou Coastal regions required a fraction of indirect recharge from deep groundwater bodies in addition to direct recharge via precipitation to match integrated recharge $\delta^{18}O$ values with observed groundwater $\delta^{18}O$ values (Table 4.3). We chose to correct the nutrient, DIC, and stable isotope parameters of applicable groundwater samples for indirect recharge contribution by mass balance in order to best assess the effects of land use/land cover, wastewater discharge, and geothermal activity on these parameters. Sample 4650-01, the furthest up-gradient of the Kīholo samples, was selected to represent the Humu‘ula Saddle deep groundwater end-member contributing indirect recharge to samples in this region. The mean of the Keauhou North High Level groundwater samples (4158-02, 4258-03, and 4358-01) were selected to represent the end-member contributing indirect recharge to the Keauhou Coastal samples.

Table 4.3. Indirect recharge fractions and unmixing endmembers for applicable groundwater sampling locations

Sample Name	Indirect Recharge Fraction	Endmember
Hind Well	0.18	Humu‘ula Saddle deep groundwater (Represented by 4650-01)
Kīholo Lava Tube	0.17	
5352-01	0.27	
4950-01	0.22	
4850-01	0.09	
4650-01	0.16	
4161-04	0.84	Keauhou North High Level groundwater (Mean of 4158-02, 4258-03, and 4358-01)
4161-05	0.82	
4161-06	0.69	
4161-07	0.65	
4161-08	0.54	
4162-06	0.64	
4162-07	0.59	
4162-04	0.44	
4161-11	0.41	
4161-12	0.42	
4161-01	0.13	
4061-01	0.25	

Potential Controls on Groundwater Nutrient and DIC Concentrations: Land Use/Land Cover, Wastewater Discharge, and Rift Zone Proximity

We chose to consider land use/land cover fractions along flow path, wastewater effluent-meteoric recharge ratios along flow path, and sample location proximity to Hualālai’s northwest rift zone as potential controls on nutrient and DIC concentrations in groundwater in the West Hawai‘i study area. Land use/land cover categories for the West Hawai‘i study were based on a 2005 NOAA land cover map (NOAA, 2012) for Hawai‘i containing 25 different land use categories. We reclassified these 25 categories into 8 (Undeveloped Bare, Undeveloped Grassland, Undeveloped Scrubland, Undeveloped Forest, Pasture, Cultivated, Park, and Urban) to best reflect variation in land use/land cover in the West Hawai‘i study area and simplify statistical analyses. The Park land use type refers specifically to non-agricultural developed open space, a land use category that in West Hawai‘i is dominated by golf courses. Wastewater effluent flow data for OSDS, injections wells, and Ka‘ūpūlehu WWTP were derived from Whittier and El Kadi, (2014), while effluent flow data for the Kealakehe WWTP was taken from Hunt (2014). Hualālai’s northwest rift zone was delineated by a spatial coverage of potential geothermal resources (State of Hawai‘i Office of Planning, 2008). Land use/land cover fractions along flow path were determined by dividing the length of each land use type transected by each

flow path by the total length of each flow path (Figure 4.2a). Wastewater effluent-meteoric recharge ratios were determined by dividing the volume of wastewater effluent flow (Figure 4.2b) by the volume of meteoric recharge (determined in Chapter 3 by subtracting evapotranspiration (Giambelluca et al., 2014) from rainfall (Giambelluca et al., 2013)) within a 500 m buffer of each flow path. The 500 m buffer distance was chosen to account for the potential of downgradient dispersion of wastewater effluent from its discharge points. Distance from Hualalai's northwest rift zone was calculated as the shortest straight line distance between each sample location and the rift zone axis (Figure 4.2b).

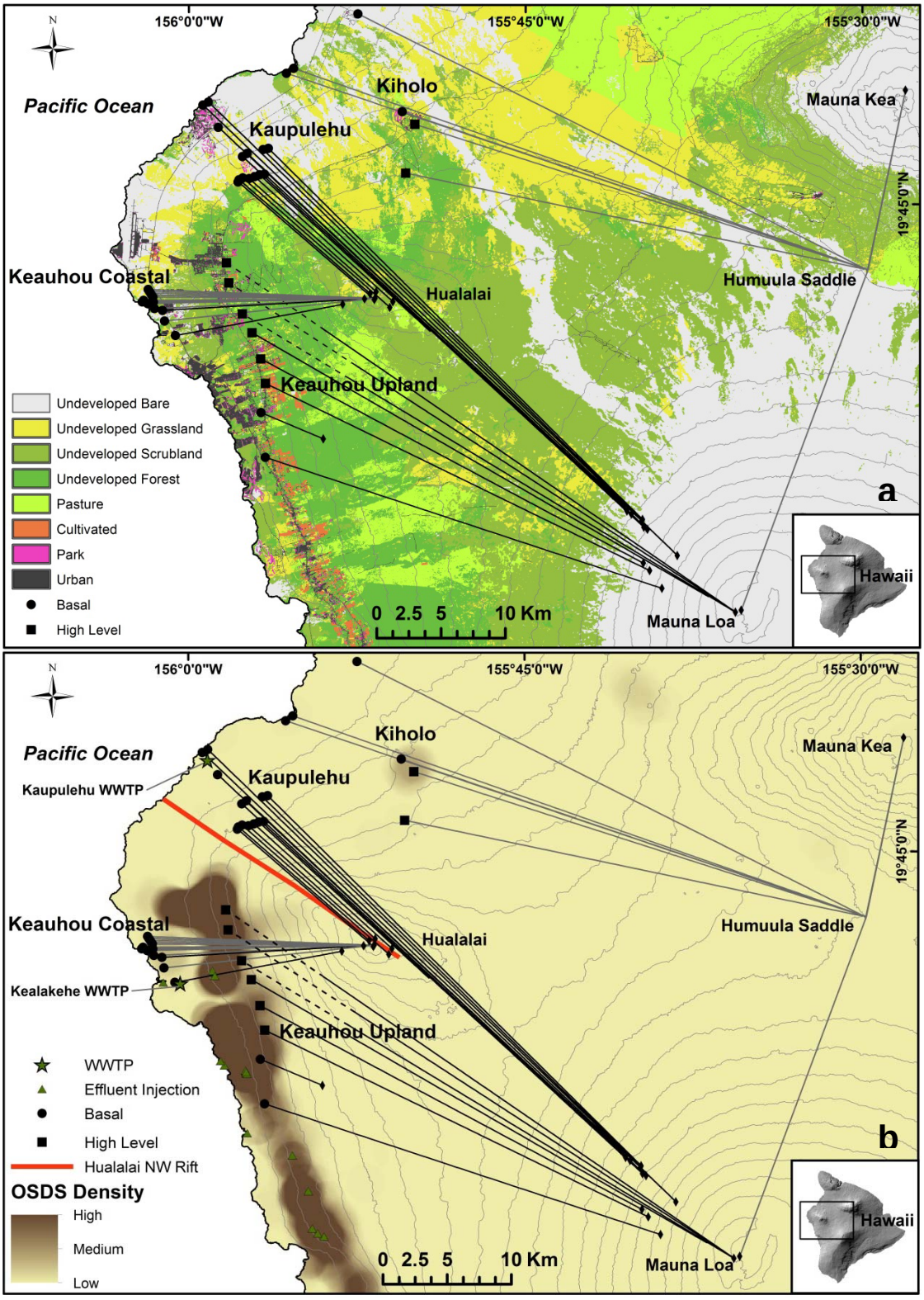

Figure 4.2(a-b). Groundwater flow paths relative to land use/land cover (a) and wastewater discharge and rift zone proximity (b). Flow path origins and endpoints are indicated by diamond symbols. Direct recharge flow paths are in black while flow paths containing indirect recharge contributions are in gray. The shielded portion of flow paths are indicated with dashed lines. Contour interval is 200 m.

Statistical Analysis

Parametric methods of statistical analysis are based on the assumption of normal data distribution. Normal distribution is not common in regional geochemical data (Reiman and Filzmoser, 1999) and our data set is no exception, as only one measured variable (SiO_4^{4-}) and one potential control variable (Undeveloped Scrubland) passed the Shapiro-Wilk normality test at 95% confidence ($P>0.05$). Consequently, we utilized the non-parametric Spearman rank correlation test, which does not rely on the assumption of normal data distribution, to evaluate correlation both between and among measured parameters and potential control variables. We report Spearman's rank correlation coefficient (ρ) for all relationships significant at 95% confidence ($P < 0.05$). The test was performed first on the entire data set, and subsequently on smaller subsets in order to examine the correlation among and between the measured parameters (PO_4^{3-}, SiO_4^{4-}, NO_3^-, $\delta^{15}N$ of NO_3^-, and $\delta^{13}C$ of DIC) and potential control variables (land use/land cover fractions, effluent-recharge ratio, and rift distance) in different portions of the study area.

Results

Measured Parameters: Groundwater Nutrients, DIC, and Stable Isotopes

Salinity and indirect recharge unmixed PO_4^{3-}, SiO_4^{4-}, NO_3^-, and DIC concentrations as well as $\delta^{15}N$ of NO_3^- and $\delta^{13}C$ of DIC values showed considerable variation between the four regions of the study area (Figure 4.3). Median PO_4^{3-} values ranged from 2.31 μM for the Kīholo region to 4.76 μM for the Ka‘ūpūlehu region. Median SiO_4^{4-} values ranged from 840 μM for the Keauhou Upland region to 1153 μM for the Ka‘ūpūlehu region. Median NO_3^- values ranged from 64.3 μM for the Kīholo region to 190.0 μM for the Ka‘ūpūlehu region. The Ka‘ūpūlehu and Keauhou Coastal regions had much larger ranges in PO_4^{3-}, SiO_4^{4-}, and NO_3^- concentrations than the Kīholo and Keauhou Upland regions. Median DIC concentrations ranged from 1103 μM for the Keauhou Upland region to 4494 μM for the Ka‘ūpūlehu region, which had a wide range of DIC concentrations distinctly elevated from the other three regions. Median $\delta^{15}N$ of NO_3^- values ranged from 3.84 ‰ for the Keauhou Upland region to 5.16 ‰ for the Keauhou Coastal region, with the Keauhou Coastal region having the widest range of $\delta^{15}N$ of NO_3^- values including several in excess of 10 ‰. Median $\delta^{13}C$ of DIC values ranged from -8.38 ‰ for the Keauhou Coastal region to -1.35 ‰ for the Kīholo region. As was the case with $\delta^{15}N$ of NO_3^-

values, the Keauhou Coastal region had the widest range of $\delta^{13}C$ of DIC values of all the study area regions.

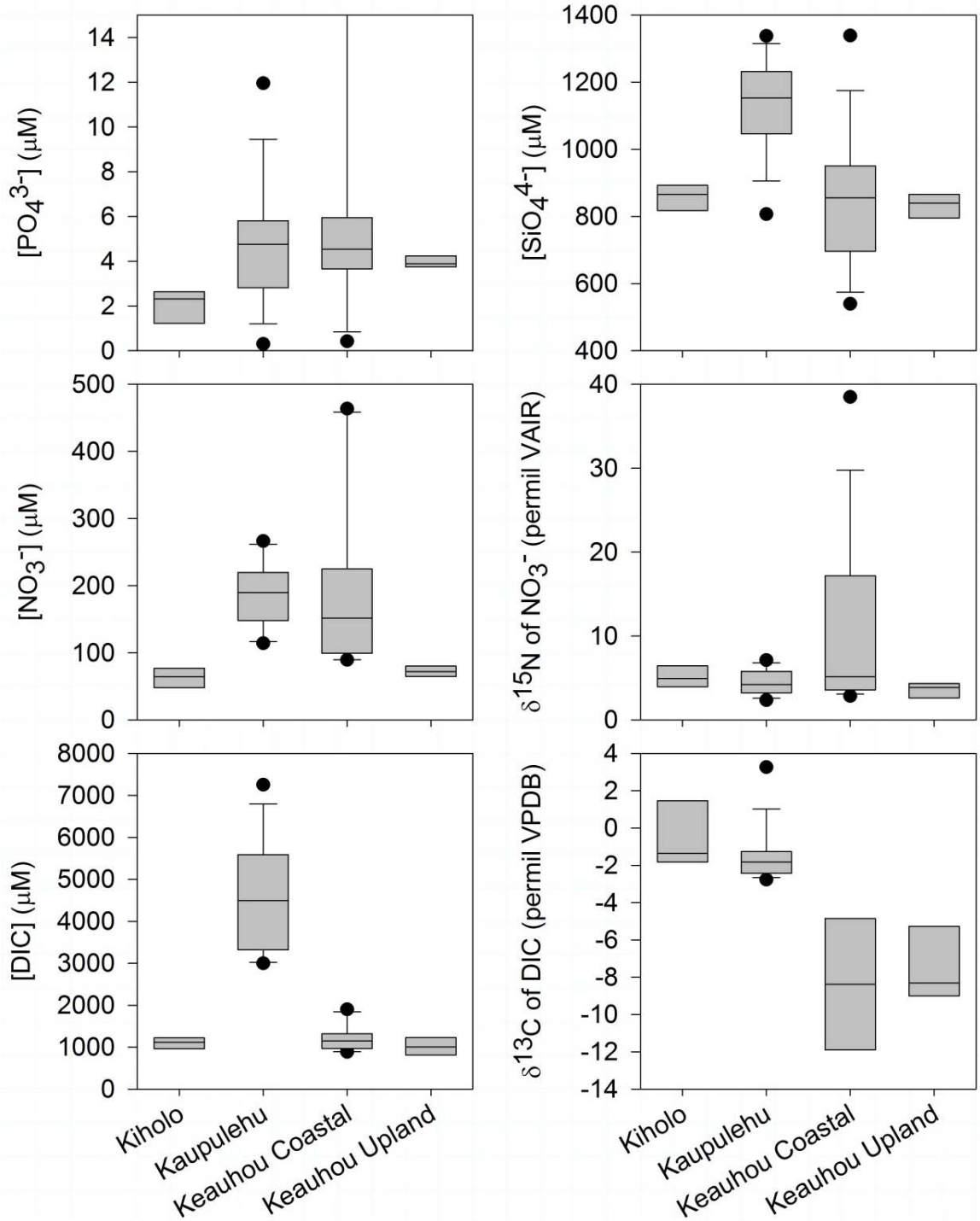

Figure 4.3. Box plots of salinity and indirect recharge unmixed groundwater nutrient, DIC, and stable isotope parameters grouped by region. The boundaries of the gray box represent the 25th and 75th percentiles, while the center line represents the median. For groups with n > 8, whiskers indicate the 10th and 90th percentiles and outliers are represented as points. For the Keauhou Coastal PO_4^{3-} plot, Expansion Well 2 ($[PO_4^{3-}]$ = 127.19 µM) is not pictured for clarity.

Potential Controls: Land Use/Land Cover

Groundwater flow paths for the four regions of the study area vary widely in fractions of land use/land cover categories transected (Figure 4.4). Groundwater flow paths from the Kīholo Region transected the largest fraction of undeveloped bare land of all the study area regions, with undeveloped grassland and undeveloped scrubland comprising most of the remainder of land use/land cover types transected by groundwater flow paths in this largely undeveloped portion of the study area. Groundwater flow paths from the Kaʻūpūlehu and Keauhou Upland regions transected primarily undeveloped scrubland, with lesser fractions of undeveloped forest, undeveloped grassland, undeveloped bare land, and pasture. Like the Kīholo region, these regions are largely undeveloped with the exception of pasture. Groundwater flow paths from the more developed Keauhou Coastal region transected the largest fractions of urban, park, and cultivated lands as well as the largest fraction of undeveloped forest.

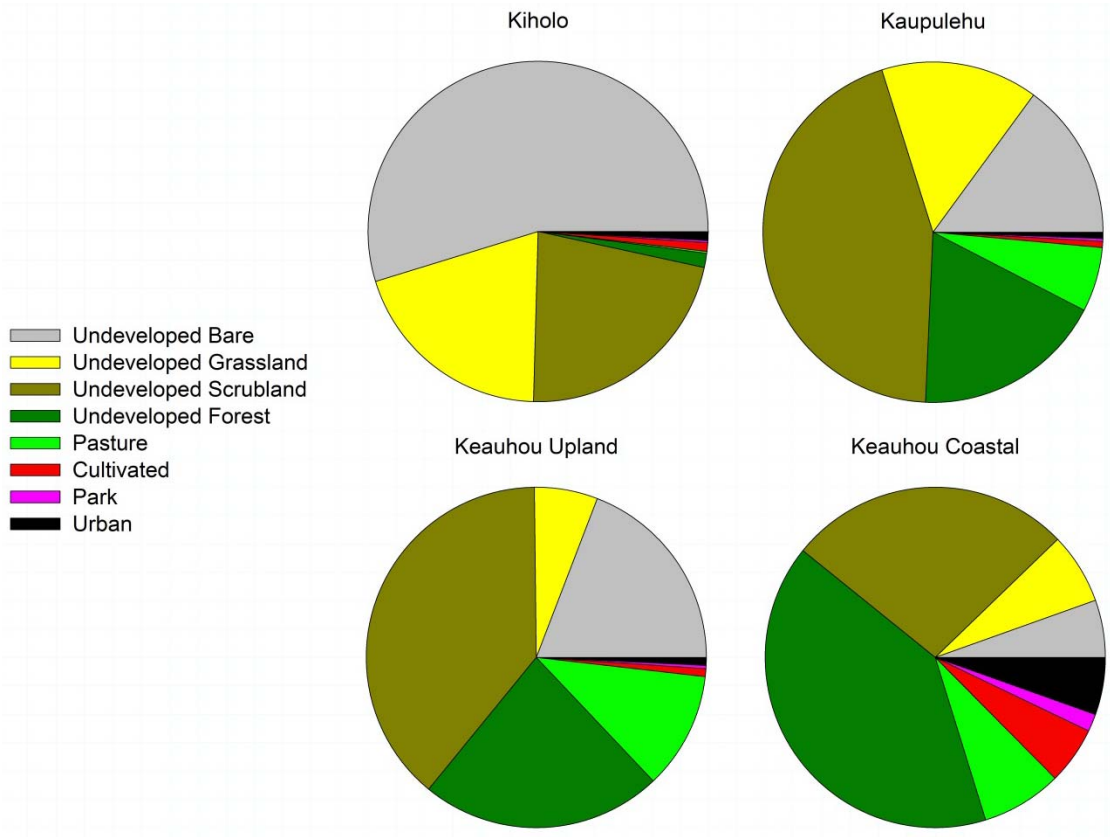

Figure 4.4. Mean land use/land cover fractions transected by groundwater flow paths for each study area region.

Potential Controls: Rift Zone Proximity and Wastewater Effluent

Sample location distances from Hualālai's northwest rift zone and wastewater effluent-meteoric recharge ratios along sample flow paths were assessed (Figure 4.5) in addition to land use/land cover due to their potential for explaining the variation in nutrient and DIC concentrations in groundwater. The Ka'ūpūlehu region samples had the closest median distance (2.86 km) to the Hualālai northwest rift zone by a wide margin relative to the next closest median distance of 8.07 km for the Keauhou Upland samples. The Keauhou Coastal region had the highest median wastewater/meteoric recharge ratio (0.104) of all the study area regions, while all other median ratios were less than 0.012. Two samples with wastewater treatment plants contributing effluent along their flow paths exhibited anomalous wastewater/meteoric recharge ratios relative to other samples in their region. These samples are King's Pond Well in the Ka'ūpūlehu region (wastewater/meteoric recharge ratio = 0.14), located downgradient of the Ka'ūpūlehu WWTP injection well, and Expansion Well 2 in the Keauhou Coastal region (wastewater/meteoric recharge ratio = 1.37), located downgradient of the Kealakehe WWTP disposal pit.

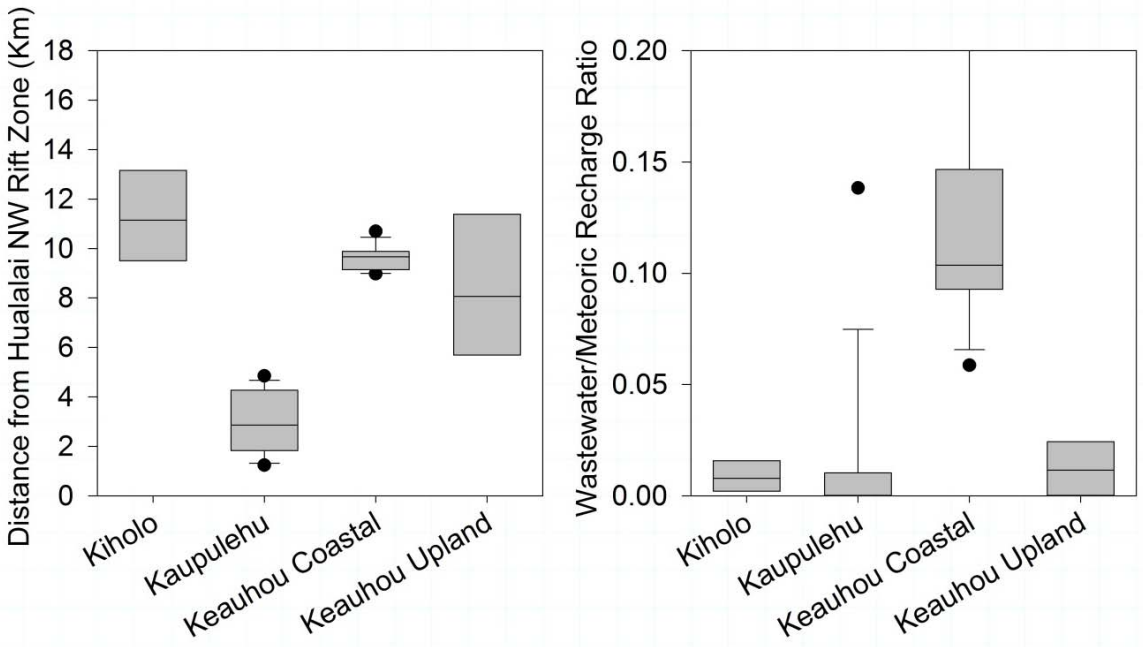

Figure 4.5. Box plots of sample location distance from the Hualālai northwest rift zone and wastewater/meteoric recharge ratio along flow path grouped by region. The boundaries of the gray box represent the 25th and 75th percentiles, while the center line represents the median. For groups with n > 8, whiskers indicate the 10th and 90th percentiles and outliers are represented as points. For the Keauhou Coastal Wastewater/Meteoric Recharge Ratio plot, Expansion Well 2 (1.34) is not pictured for clarity.

Spearman's Rank Correlations

Correlation Among Measured Parameters

Assessment of correlation among measured parameters (Table 4.4) can provide useful information for the determination of their controlling mechanisms. We found the strongest correlations between DIC and SiO_4^{4-} (ρ =0.67) and between DIC and NO_3^- (ρ =0.61). Other significant correlations exist between PO_4^{3-} and SiO_4^{4-} (ρ =0.42), SiO_4^{4-} and $\delta^{15}N$ of NO_3^- (ρ =-0.41), NO_3^- and SiO_4^{4-} (ρ =0.40), DIC and $\delta^{13}C$ of DIC (ρ =0.38), and PO_4^{3-} and $\delta^{13}C$ of DIC (ρ =-0.37).

Table 4.4. Significant Spearman's rank correlations among measured parameters ranked by magnitude of ρ.

Measured Parameter	Correlation 1	Correlation 2
PO_4^{3-}	SiO_4^{4-} (ρ =0.42, P<0.01, n=42)	$\delta^{13}C$ (ρ =-0.37, P=0.04, n=32)
SiO_4^{4-}	DIC (ρ =0.67, P<0.01, n=36)	$\delta^{15}N$ (ρ =-0.41, P<0.01, n=42)
NO_3^-	DIC (ρ =0.61, P<0.01, n=36)	SiO_4^{4-} (ρ =0.40, P<0.01, n=42)
DIC	$\delta^{13}C$ (ρ =0.38, P=0.03, n=32)	-

Correlation Among Potential Controls

Examination of correlation among the potential control variables (Table 4.5) is important for understanding whether the correlation between them and the measured parameters is potentially causal or coincidental. Due to the close associations between many of the land use types and the mutually exclusive nature of their distributions, several extremely strong correlations exist among them. The Urban-Park correlation (ρ =0.89) is the strongest among land use types. Other strong correlations among land use types include negative correlations between Undeveloped Forest and Undeveloped Bare (ρ =-0.87), Pasture and Undeveloped Grassland (ρ =-0.74), and Undeveloped Bare and Cultivated (ρ =-0.71). The strongest correlation for Rift Distance was with Undeveloped Scrubland (ρ =-0.74), while Effluent Recharge Ratio was strongly correlated with both Urban (ρ =0.87) and Park (ρ =0.85).

Table 4.5. Significant Spearman's rank correlations among potential controls ranked by magnitude of ρ. Potential Control abbreviations are as follows: Undeveloped Bare=UB, Undeveloped Grassland=UF, Undeveloped Scrubland=US, Undeveloped Forest=UF, Pasture=Pas, Cultivated=Cul, Park=Par, Urban=Urb, Rift Distance=RD, Effluent-Recharge Ratio=Eff.

Potential Control	Correlation 1	Correlation 2	Correlation 3	Correlation 4
Undeveloped Bare	Cul (ρ =-0.71, P<0.01)	Eff (ρ =-0.57, P<0.01)	Par (ρ =-0.50, P<0.01)	Pas (ρ =-0.37, P=0.02)
Undeveloped Grassland	UF (ρ =-0.58, P<0.01)	Cul (ρ =-0.45, P<0.01)	UB (ρ =0.32, P=0.04)	-
Undeveloped Scrubland	RD (ρ =-0.74, P<0.01)	Urb (ρ =-0.67, P<0.01)	Eff (ρ =-0.53, P<0.01)	-
Undeveloped Forest	UB(ρ =-0.87, P<0.01)	Eff (ρ =0.63, P<0.01)	Cul (ρ =0.63, P<0.01)	-
Pasture	UG (ρ =-0.75, P<0.01)	UF (ρ =0.42, P<0.01)	Cul (ρ =0.41, P<0.01)	-
Cultivated	Eff (ρ =0.67, P<0.01)	Par (ρ =0.47, P<0.01)	Urb (ρ =0.47, P<0.01)	-
Park	UF (ρ =0.66, P<0.01)	US (ρ =-0.49, P<0.01)	UG (ρ =-0.35, P=0.02)	-
Urban	Par (ρ =0.89, P<0.01)	UF (ρ =0.66, P<0.01)	UB (ρ =-0.51, P<0.01)	-
Rift Distance	Urb (ρ =0.52, P<0.01)	Eff (ρ =0.51, P<0.01)	Par(ρ =0.44, P<0.01)	-
Effluent-Recharge Ratio	Urb (ρ =0.87, P<0.01)	Par (ρ =0.85, P<0.01)	UG (ρ =-0.32, P=0.04)	-

Correlation Between Measured Parameters and Potential Controls

Correlation between the measured parameters and potential control variables, considered in conjunction with correlation among measured parameters and among potential controls, provides a means to evaluate the merits of the potential controls as causes of variation in the measured parameters (Table 4.6). The strongest correlations between measured parameters and potential controls are between DIC and Rift Distance (ρ =-0.79) and $\delta^{13}C$ of DIC and Undeveloped Grassland (ρ =0.77). The strongest correlations for the remaining measured parameters were between PO_4^{3-} and Undeveloped Grassland (ρ =-0.40), SiO_4^{4-} and Effluent Recharge Ratio (ρ =-0.53), NO_3^- and Undeveloped Bare (ρ =-0.49), and $\delta^{15}N$ of NO_3^- and Effluent Recharge Ratio (ρ =0.42).

Table 4.6. Significant Spearman's rank correlations between measured parameters and potential controls ranked by magnitude of ρ. Potential control abbreviations are per Table 4.5.

Measured Parameter	Correlation 1	Correlation 2	Correlation 3	Correlation 4	Correlation 5	Correlation 6	Correlation 7
PO_4^{3-} (n=42)	UG (ρ =-0.40, P<0.01)	UF (ρ =0.34, P=0.03)					
SiO_4^{4-} (n=42)	Eff (ρ =-0.53, P<0.01)	RD (ρ =-0.50, P<0.01)	Cul (ρ =-0.49, P<0.01)	US (ρ =0.45, P<0.01)	Urb (ρ =-0.45, P<0.01)	Par (ρ =-0.42, P<0.01)	
NO_3^- (n=42)	UB (ρ =-0.49, P<0.01)	UF (ρ =0.40, P<0.01)	RD (ρ =-0.39, P<0.01)				
DIC (n=36)	RD (ρ =-0.79, P<0.01)	US (ρ =0.54, P<0.01)	Eff (ρ =-0.43, P<0.01)	Urb (ρ =-0.37, P=0.03)	UG (ρ =0.35, P=0.04)	Par (ρ =-0.34, P=0.04)	Cul (ρ =-0.34, P=0.04)
$\delta^{15}N$ (n=42)	Eff (ρ =0.42, P<0.01)	Par (ρ =0.39, P=0.01)	Urb (ρ =0.37, P=0.02)				
$\delta^{13}C$ (n=32)	UG (ρ =0.77, P<0.01)	UF (ρ =-0.59, P<0.01)	Pas (ρ =-0.52, P<0.01)	Cul (ρ =-0.46, P<0.01)	Par (ρ =-0.44, P=0.01)	UB (ρ =0.42, P=0.02)	

Discussion

Assessment of Effects of Potential Controls on Measured Parameters

The assessment of the effects of the potential control variables on the measured parameters hinges upon distinguishing between correlations that may be causal and those that may be coincidental. In order to accomplish this, we consider regional distribution of the potential control variables and measured parameters as well as correlations among and between potential controls and measured parameters. In the following discussion, we first consider the entire data set and then progressively smaller subsets to best isolate and assess the effects of the potential controls on the measured parameters in the different regions of the study area,

Ka‘ūpūlehu Region: Geothermal Activity

Groundwater samples from the Ka‘ūpūlehu region had the highest median concentrations of PO_4^{3-}, SiO_4^{4-}, NO_3^- and DIC (Figure 4.3). These findings corroborate those of Swain (1973), who observed elevated NO_3^- and DIC concentrations in groundwater in this region, as well as those of Knee et al., (2010), who inferred high concentrations of PO_4^{3-}, SiO_4^{4-}, and NO_3^- in groundwater in this region through salinity unmixing of coastal water samples. The elevated values of these parameters in the Ka‘ūpūlehu region appear to be driving the significant correlations observed between SiO_4^{4-}, NO_3^- and DIC for the entire study area. The best candidate among the potential controls for explaining the elevated values of these parameters in the Ka‘ūpūlehu region is rift distance, which showed significant negative correlations with SiO_4^{4-}, NO_3^- and DIC for the entire data set (Table 4.6). The tendency of these parameters to increase with decreasing distance from Hualālai’s recently active northwest rift zone (Figure 4.6) suggests that geothermal activity may be responsible for this phenomenon. The lack of the anomalously high temperatures in groundwater in this region (Swain, 1973; Thomas, 1986) may be attributed to some combination of mixing with non-thermally affected groundwater and cooling during downgradient transit following geothermal heating.

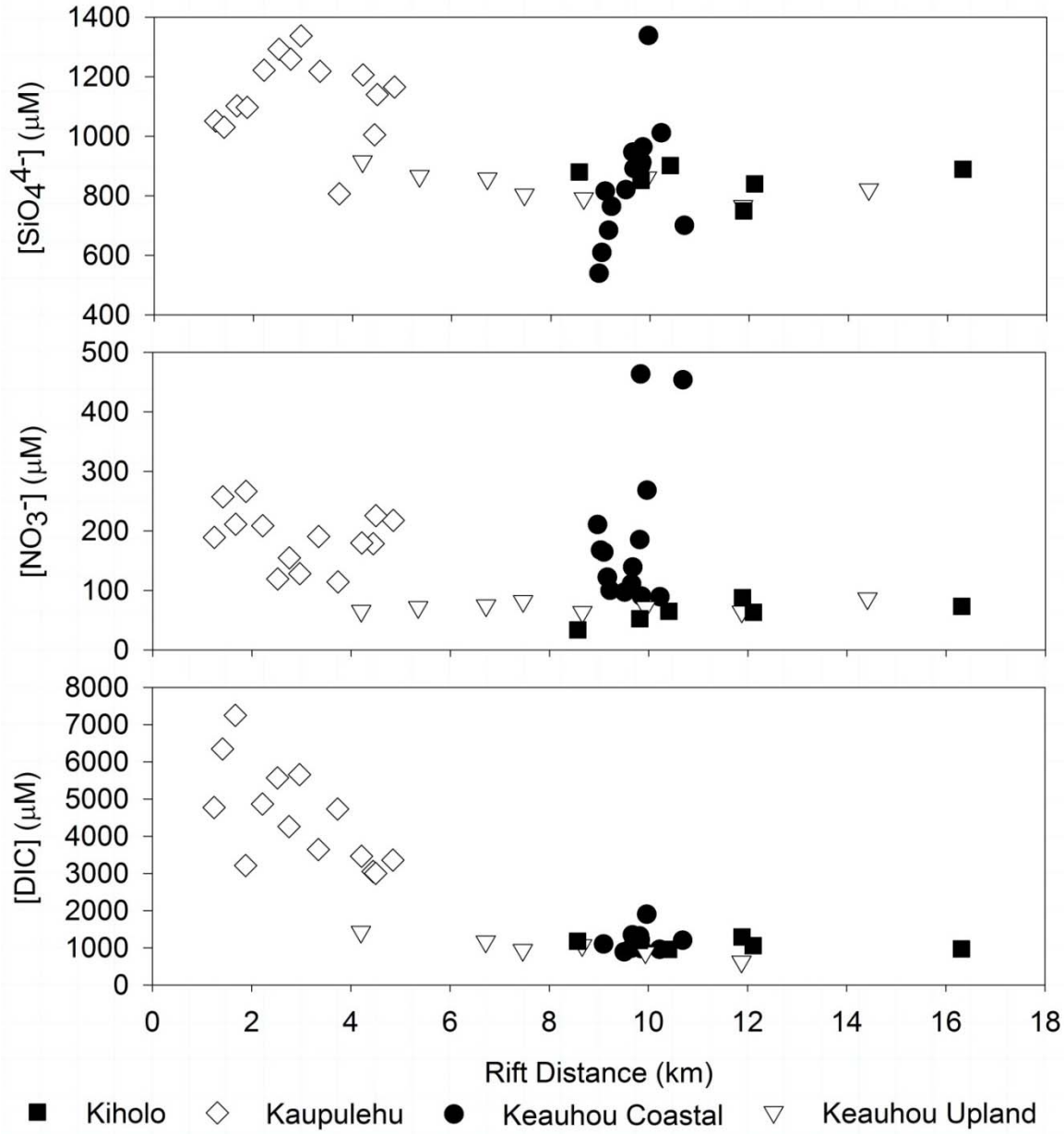

Figure 4.6. Relationship between groundwater sample SiO_4^{4-}, NO_3^- and DIC concentrations with rift distance by region.

Thermally affected groundwater is typically enriched in SiO_4^{4-} and DIC worldwide (e.g. Henley and Ellis, 1983) as well as specifically in Hawai‘i (e.g. Thomas, 1986) due to thermally enhanced dissolution of siliceous rocks (SiO_4^{4-}) and dissolution of magmatic CO_2 (DIC). The median $\delta^{13}C$ of DIC value for the Ka‘ūpūlehu region groundwater samples (-1.82‰) is relatively similar to the $\delta^{13}C$ values calculated for CO_2 in magma at the nearby Kilauea volcano (-3.4‰ - -3.6‰; Gerlach and Thomas, 1986). This finding supports the interpretation of a primarily magmatic origin for the elevated levels of DIC found in groundwater in the region.

While the effects of geothermal alteration on groundwater SiO_4^{4-} and DIC concentrations are well documented, the effects of geothermal alteration on groundwater PO_4^{3-} and especially NO_3^- concentrations are less characterized. Pringle and Triska (1991) observed that geothermally altered groundwater in Costa Rica was elevated in PO_4^{3-} but not NO_3^- relative to unaltered groundwater. Hoellein et al., (2012) observed significantly higher levels of PO_4^{3-} and NH_4^+ (but not NO_3^-) in geothermally impacted streams versus non-impacted streams in New Zealand. Similarly, Holloway et al., (2011) measured high levels of NH_4^+ but low levels of NO_3^- in several hot springs in the Yellowstone thermal system and undertook stable isotope measurements to characterize NH_4^+ source and fractionation processes.

Elevated PO_4^{3-} in geothermally altered groundwater results from thermally enhanced dissolution of PO_4^{3-} bearing minerals such as apatite. While the elevated PO_4^{3-} levels found in the Kaʻūpūlehu region groundwater may arise from geothermal alteration of P-bearing volcanic rock and/or interbedded paleosols, the similarity of PO_4^{3-} concentrations between this region and the Keauhou Coastal and Upland regions to the south as well as the lack of significant correlation between PO_4^{3-} concentration and rift distance across the study area complicate this assessment.

Elevated levels of N (typically observed as NH_4^+) in geothermally altered groundwater may be mantle-derived or arise from sedimentary or atmospheric sources (Sano et al., 2001). West Hawaiʻi groundwater is typically highly oxidizing and as a result dissolved inorganic N occurs predominantly as NO_3^- rather than NH_4^+ (e.g. Knee et al., 2010). We interpret the elevated levels of NO_3^- in groundwater in the Kaʻūpūlehu region as the result of oxidation of geothermally derived NH_4^+ occurring as geothermally altered groundwater mixes with the oxidizing surrounding groundwater and fresh recharge. The range of $\delta^{15}N$ of NO_3^- values in Kaʻūpūlehu groundwater samples (2.34‰ – 7.13‰) is generally consistent with a soil source (Kendall, 1998). This indicates that the elevated levels of NO_3^- in groundwater in this region may originate from the oxidation of NH_4^+ derived from geothermal alteration of N-bearing paleosols in the subsurface. The higher $\delta^{15}N$ of NO_3^- values observed may result from localized preferential volatilization and evasion of NH_3 containing ^{14}N, leaving the remaining pool of NH_4^+ (and thus ultimately NO_3^-) relatively enriched in ^{15}N (Holloway et al., 2011). Knee et al., (2010) presented evidence that elevated levels of NO_3^- in SGD in this region may be due to fertilizer leaching from golf courses based on spatial correlation with land use at the 5-km radius scale. While golf courses may contribute slightly to elevated NO_3^- in groundwater in the coastal

portion of this region, it appears that the primary cause of this phenomenon is geothermal alteration, as discussed above. We favor this interpretation because (1) high levels of NO_3^- in groundwater were observed in this region prior to golf course construction (Swain, 1973), (2) high levels of NO_3^- are observed in groundwater in this region up-gradient of any golf course development, and (3) no significant correlation was found between NO_3^- concentration and the Park land use type, which includes golf courses.

Keauhou Coastal Region: Wastewater Effluent and Fertilizer

As discussed above, the effects of geothermal alteration on the measured parameters in the Kaʻūpūlehu region exert a strong control on correlation observed among the measured parameters as well as between the measured parameters and potential controls. In order to best assess the relationships between the measured parameters and potential controls in the rest of the study area, we reassessed the Spearman's rank correlations among measured parameters and between measured parameters and potential controls (Table 4.7) after omitting the data from the Kaʻūpūlehu region.

Table 4.7. Significant Spearman's rank correlations between measured parameters and potential controls ranked by magnitude of ρ with the Kaʻūpūlehu region omitted. Potential control abbreviations are per Table 4.5.

Measured Parameter	Correlation 1	Correlation 2	Correlation 3	Correlation 4	Correlation 5
PO_4^{3-} (n=28)	UF (ρ =0.68, P<0.01)	UG(ρ =-0.63, P<0.01)	UB (ρ =-0.50, P=0.01)		
SiO_4^{4-} (n=28)	Cul (ρ =-0.48, P=0.01)				
NO_3^- (n=28)	Urb (ρ =0.78, P<0.01)	Eff (ρ =0.76, P<0.01)	Par (ρ =0.68, P<0.01)	UB (ρ =-0.64, P<0.01)	UF (ρ =0.60, P<0.01)
DIC (n=22)					
$\delta^{15}N$ (n=28)	Urb (ρ =0.45, P=0.02)	Eff (ρ =0.44, P=0.02)	Par (ρ =0.43, P=0.02)	UG (ρ =0.42, P=0.03)	
$\delta^{13}C$ (n=18)	UG (ρ =0.72, P<0.01)	UF (ρ =-0.66, P<0.01)	UB (ρ =-0.61, P=0.01)	Cul (ρ =-0.58, P=0.01)	Pas (ρ =-0.52, P=0.03)

Groundwater samples from the Keauhou Coastal region had the highest median $\delta^{15}N$ of NO_3^- value, lowest median $\delta^{13}C$ of DIC value of all the regions of the study area as well as the second highest median NO_3^- and PO_4^{3-} concentrations (Figure 4.3). These findings are generally consistent with those of Brock, (2010), Hunt, (2008; 2014), Knee et al., (2010), and Prouty et al., (2015) for groundwater samples collected in this region once seawater and indirect recharge unmixing calculations are taken into account. Keauhou Coastal groundwater samples also had

the widest range of values in every measured parameter except for DIC concentration. With Ka‘ūpūlehu region samples omitted, the only significant correlations among measured parameters were between $\delta^{15}N$ of NO_3^- and SiO_4^{4-} (ρ =-0.51) and $\delta^{13}C$ of DIC and PO_4^{3-} (ρ =-0.48). The elevated NO_3^- concentrations and $\delta^{15}N$ of NO_3^- values in Keauhou Coastal region groundwater samples together with the high effluent-recharge ratios (Figure 4.7) and high fractions of urban and park land use along groundwater flow paths in this region appear to be driving the significant positive correlations between these parameters and potential controls. Of these three potential controls, which are closely correlated with each other due to the tendency of park lands and effluent disposal sites to be co-located with urban development (Table 4.5), we assess effluent-recharge ratio as the potential control most likely to exert the greatest causal effect on both groundwater NO_3^- concentrations and $\delta^{15}N$ of NO_3^- values. This assessment is based on the typically high NO_3^- concentrations and $\delta^{15}N$ of NO_3^- values found in wastewater effluent relative to natural groundwater (e.g. Kendall, 1998). Urban and park land use is also associated with use of fertilizer, which may also contribute to the elevated NO_3^- concentrations of some of the groundwater samples observed in the Keauhou Coastal region.

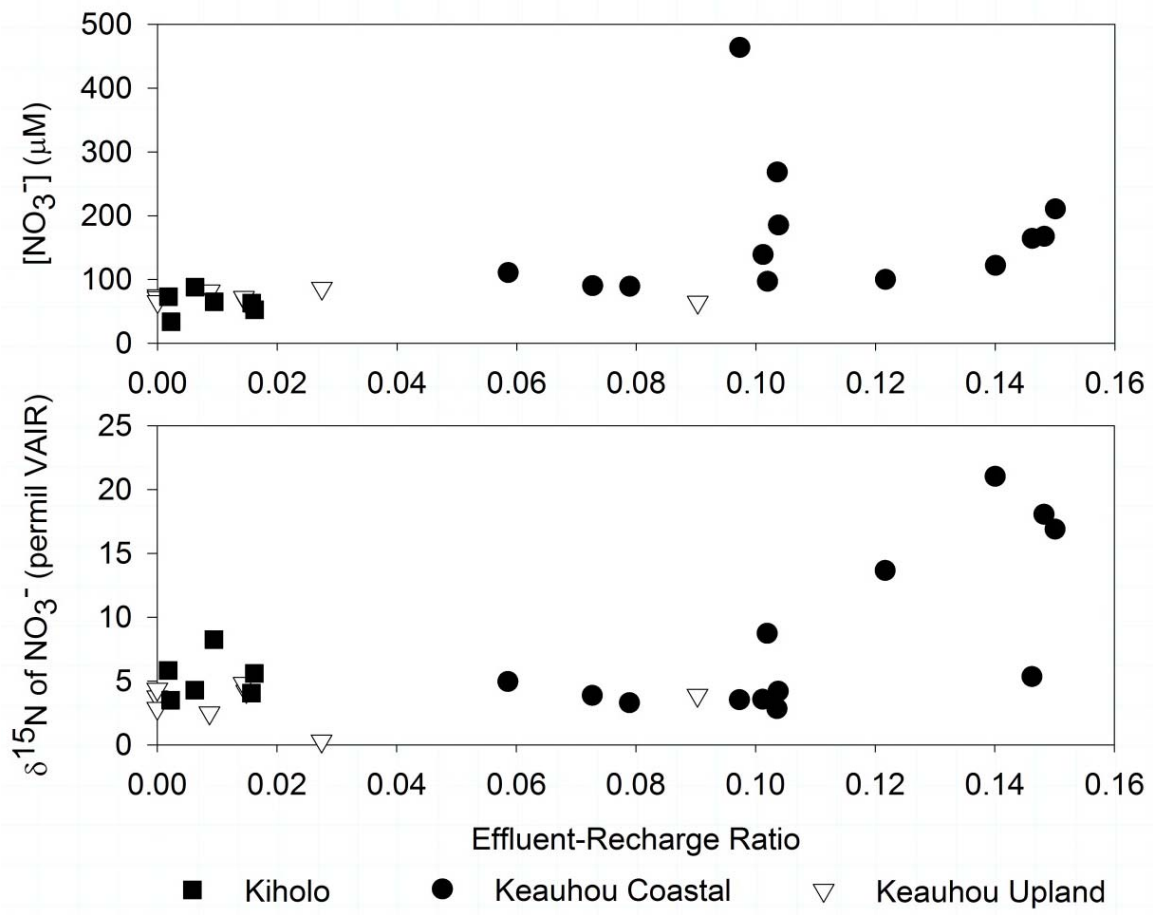

Figure 4.7. Relationship between groundwater sample NO_3^- concentrations and $\delta^{15}N$ of NO_3^- values with Effluent-Recharge ratio by region with the Ka‘ūpūlehu region samples omitted. Expansion Well 2 data ($[NO_3^-]$=453.8 μM, $\delta^{15}N$ of NO_3^-=38.5‰, effluent-recharge ratio =1.34) is omitted for clarity.

Wastewater effluent from OSDS and wastewater treatment plants has widely variable but typically elevated dissolved inorganic N concentrations relative to most natural groundwater (e.g. Whittier and El-Kadi, 2009). In oxidizing groundwater conditions, most dissolved inorganic N will occur as NO_3^-. Wastewater effluent has frequently been implicated as a source of NO_3^- to receiving groundwater worldwide (e.g. Wakida and Lerner, 2004) and in Hawai‘i specifically (Hunt and Rosa, 2009; Glenn et al., 2012; Bishop et al., 2015; Richardson et al., 2015). $\delta^{15}N$ values of wastewater NO_3^- sources (~10‰ - 20‰) are generally elevated with respect to $\delta^{15}N$ values of fertilizer NO_3^- sources (~-4‰ - 4‰) and can be used to distinguish between them (Kendall, 1998). The elevated levels of organic C typically found in wastewater effluent can foster heterotrophic respiration, which may lower dissolved oxygen levels to suboxic or anoxic conditions favorable for denitrification, which results in the preferential conversion of NO_3^- containing ^{14}N to N_2 gas and thus increasing the $\delta^{15}N$ value of remaining NO_3^- (e.g. Aravena and

Robertson, 1998). Wastewater effluent is also generally characterized by elevated levels of PO_4^{3-} relative to natural ground waters and is often cited as a source of PO_4^{3-} to groundwater (e.g. Lapointe, 1990; Glenn et al,. 2012). PO_4^{3-} is less mobile in the subsurface than NO_3^- due to its tendency to sorb to Fe and Al oxy-hydroxides under oxidizing conditions (Kehew, 2000). This lack of mobility may explain the lack of significant correlation observed between PO_4^{3-} concentration and effluent-recharge ratio.

Groundwater samples from the Keauhou Coastal region had the highest median $\delta^{15}N$ of NO_3^- value, lowest median $\delta^{13}C$ of DIC value of all the regions of the study area as well as the second highest median NO_3^- and PO_4^{3-} concentrations (Figure 4.3). These findings are generally consistent with those of Brock, (2010), Hunt, (2008; 2014), Knee et al., (2010), and Prouty et al., (2015) for groundwater samples collected in this region once seawater and indirect recharge unmixing calculations are taken into account. Keauhou Coastal groundwater samples also had the widest range of values in every measured parameter except for DIC concentration. With Kaʻūpūlehu region samples omitted, the only significant correlations among measured parameters were between $\delta^{15}N$ of NO_3^- and SiO_4^{4-} (ρ =-0.51) and $\delta^{13}C$ of DIC and PO_4^{3-} (ρ =-0.48). The elevated NO_3^- concentrations and $\delta^{15}N$ of NO_3^- values in Keauhou Coastal region groundwater samples together with the high effluent-recharge ratios (Figure 4.7) and high fractions of urban and park land use along groundwater flow paths in this region appear to be driving the significant positive correlations between these parameters and potential controls. Of these three potential controls, which are closely correlated with each other due to the tendency of park lands and effluent disposal sites to be co-located with urban development (Table 4.5), we assess effluent-recharge ratio as the potential control most likely to exert the greatest causal effect on both groundwater NO_3^- concentrations and $\delta^{15}N$ of NO_3^- values. This assessment is based on the typically high NO_3^- concentrations and $\delta^{15}N$ of NO_3^- values found in wastewater effluent relative to natural groundwater (e.g. Kendall, 1998). Urban and park land use is also associated with use of fertilizer, which may also contribute to the elevated NO_3^- concentrations of some of the groundwater samples observed in the Keauhou Coastal region.

Due to limited sewer infrastructure in the West Hawaiʻi study area, much of the wastewater generated is disposed of via OSDS or small-scale wastewater injection facilities (Whittier and El-Kadi, 2009). The majority of OSDS units in the study are located in the vicinity of the Kailua-Kona urban center, with many along the flow paths of groundwater samples in the

Keauhou Coastal region (Figure 4.2), contributing to the high effluent-recharge ratios which are significantly correlated to the elevated NO_3^- concentrations and $\delta^{15}N$ of NO_3^- values found in these samples relative to those in other regions of the study area. Additionally, the Kealakehe WWTP effluent disposal pit contributes 5700 m^3/day of treated effluent to the Expansion Well 2 flow path, resulting in an effluent-recharge ratio of 1.34, nearly an order of magnitude greater than the next highest ratio. Unsurprisingly, Expansion Well 2 had the second highest concentration of NO_3^- (453.8 μM) and highest concentration of PO_4^{3-} (127.19 μM) observed in the study area. The elevated $\delta^{15}N$ of NO_3^- value (38.5‰) for Expansion Well 2 is indicative of denitrification of the Kealakehe WWTP effluent endmember , which was found to have a $\delta^{15}N$ of NO_3^- value of 12‰ by Hunt, (2014), during infiltration and downgradient aquifer transit upon leaching to the water table.

Leachate from fertilized lands typically has elevated NO_3^- concentrations relative to most natural groundwater (e.g. Kendall, 1998). Fertilizer application is primarily associated with agricultural land use, but is also prevalent in urban and park land use settings for landscaping and golf course maintenance. Contribution of fertilizer leachate associated with the higher fractions of urban and park land use transecting groundwater flow paths in the Keauhou Coastal region relative to the other regions of the study area may be contributing to the significant correlations observed between these land use types and NO_3^- concentration. As discussed above, the differing ranges of $\delta^{15}N$ of NO_3^- values between fertilizer and wastewater effluent can aid in NO_3^- source identification. Well 4162-04, located at a plant nursery on a golf course under development at the time of the study, had the highest NO_3^- concentration observed in the study area (463.6 μM) and a $\delta^{15}N$ of NO_3^- value (3.54‰) more consistent with a fertilizer source than a wastewater effluent source. Brock (2010) and Hunt (2014) found intermittently elevated NO_3^- concentrations in groundwater at this location and attributed them to leaching of fertilizer applied during the golf course turf grow-in period.

Plotting $\delta^{15}N$ of NO_3^- value vs. $1/NO_3^-$ concentration is useful for assessing NO_3^- source contributions because mixing relationships are indicated by straight lines (Kendall, 1998). A plot of this type for the Kīholo, Keauhou Coastal, and Keauhou Upland region samples (Figure 4.8) indicates that both denitrified wastewater effluent (e.g. Expansion Well 2) and fertilizer leachate (e.g. 4162-04) contribute to the elevated NO_3^- concentrations observed in groundwater in the Keauhou Coastal region relative to the Kīholo and Keauhou Upland regions. These

findings add to the growing body of literature positively associating wastewater effluent (Richardson et al., 2015) and fertilizer leachate (Soicher and Peterson, 1997; Frans et al., 2012; Bishop et al., 2015) with elevated NO_3^- concentrations in Hawai‘ian groundwater on regional scales.

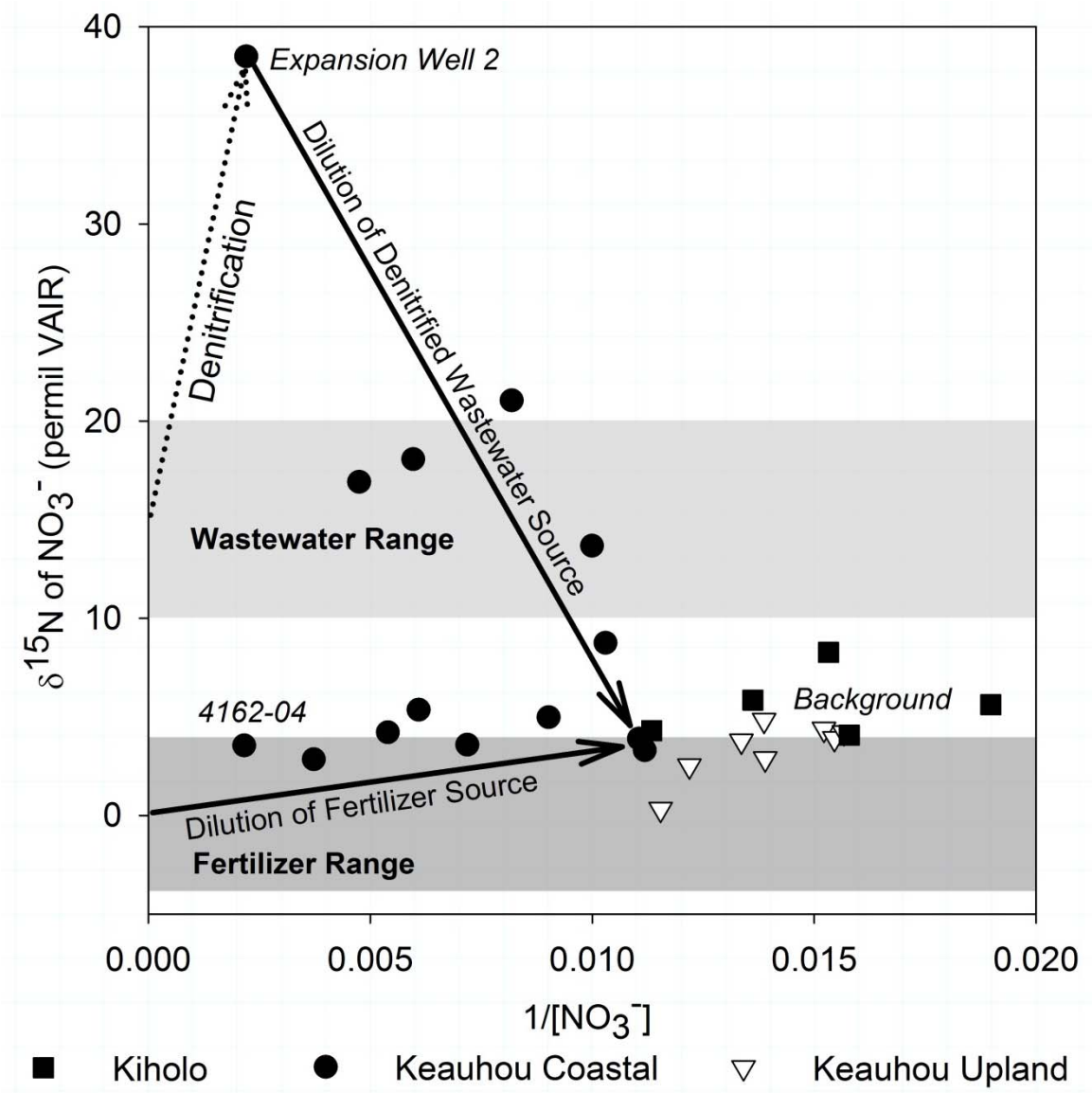

Figure 4.8. Plot of $\delta^{15}N$ of NO_3^- values vs. $1/NO_3^-$ concentration for Kīholo , Keauhou Coastal, and Keauhou Upland region samples. The Kīholo and Keauhou Upland region sample flow paths have low effluent-recharge ratios and fractions of urban and park land use and thus these samples are assumed to reflect a range of background values relatively unaffected by these potential controls. Solid arrows indicate dilution of hypothetical denitrified wastewater and fertilizer NO_3^- sources. The dotted arrow indicates the generalized effect of denitrification on a high NO_3^- concentration wastewater endmember with the caveat that a denitrification relationship would not be indicated by a straight line on this plot. Typical $\delta^{15}N$ of NO_3^- values for wastewater (light gray) and fertilizer (dark gray) NO_3^- sources (after Kendall, 1998) are shown for reference.

Kīholo and Keauhou Upland: Precipitation and Weathering

As discussed above, rift distance and the combination of effluent-recharge ratio with urban and park land use exert strong controls on measured parameters in the Kaʻūpūlehu and Keauhou Coastal regions, respectively. To best assess the effects of the potential controls on the measured parameters in the Kīholo and Keauhou Upland regions, we reassessed the Spearman's rank correlations among measured parameters and between measured parameters and potential controls (Table 4.8) after omitting the data from the Kaʻūpūlehu and Keauhou Coastal regions.

Table 4.8. Significant Spearman's rank correlations between measured parameters and potential controls ranked by magnitude of ρ with the Kaʻūpūlehu and Keauhou Coastal regions omitted. Potential control abbreviations are per Table 4.5.

Measured Parameter	Correlation 1	Correlation 2	Correlation 3	Correlation 4	Correlation 5
PO_4^{3-} (n=14)	Pas (ρ =0.88, P<0.01)	UB (ρ =-0.71, P<0.01)	UF (ρ =0.62, P=0.02)	UG (ρ =-0.60, P=0.02)	US (ρ =0.53, P=0.05)
SiO_4^{4-} (n=14)	Eff (ρ =-0.57, P=0.03)	Par (ρ =-0.53, P=0.05)			
NO_3^- (n=14)					
DIC (n=12)	Cul (ρ =-0.69, P=0.01)				
$\delta^{15}N$ (n=14)	UG (ρ =0.80, P<0.01)				
$\delta^{13}C$ (n=9)	UG (ρ =0.90, P<0.01)	Cul (ρ =-0.84, P=0.01)	UF (ρ =-0.82, P<0.01)	UB (ρ =0.78, P=0.01)	Pas (ρ =-0.70, P=0.03)

The Kīholo and Keauhou Upland region groundwater sample flow paths transect primarily undeveloped land. Measured parameters from these regions show little or no correlation with the rift distance and effluent-recharge ratio potential controls. As a result, consideration of the differences between these regions is useful for understanding the effects of the land use/land cover potential controls on the measured parameters. Groundwater samples from the Kīholo and Keauhou Upland regions were characterized by less variability in measured parameters than groundwater samples from the Kaʻūpūlehu and Keauhou Coastal regions. The primary contrasts between measured parameters among the Kīholo and Keauhou Upland regions were in PO_4^{3-} concentrations (medians of 2.32 μM vs. 3.89 μM, respectively), $\delta^{13}C$ of DIC values (medians of -1.36 ‰ vs. -8.31 ‰, respectively), and $\delta^{15}N$ of NO_3^- values (medians of 4.96 ‰ vs. 3.84 ‰, respectively) (Figure 4.3). The only significant correlation among the measured parameters for these regions was between PO_4^{3-} concentrations and $\delta^{13}C$ of DIC value (ρ =-0.72). Potentially causal relationships between measured parameters and individual potential controls are less apparent for the Kīholo and Keauhou Upland region groundwater

samples alone than with the other regions included. Rather, the correlations most likely to be causal occur between groups of land use types associated with the higher rainfall portions of the study area (undeveloped forest, cultivated, and pasture) and groups of land use types associated with arid portions of the study area (undeveloped grassland and undeveloped bare) with PO_4^{3-} concentrations, $\delta^{13}C$ of DIC values, and $\delta^{15}N$ of NO_3^- values (Figure 4.9). We conclude that the high fractions of land use/land cover types associated with high rainfall portions of the study area transected by groundwater flow paths in the Keauhou Upland region are the cause of the higher median PO_4^{3-} concentrations and lower median $\delta^{13}C$ of DIC and $\delta^{15}N$ of NO_3^- values observed here relative to the Kīholo region.

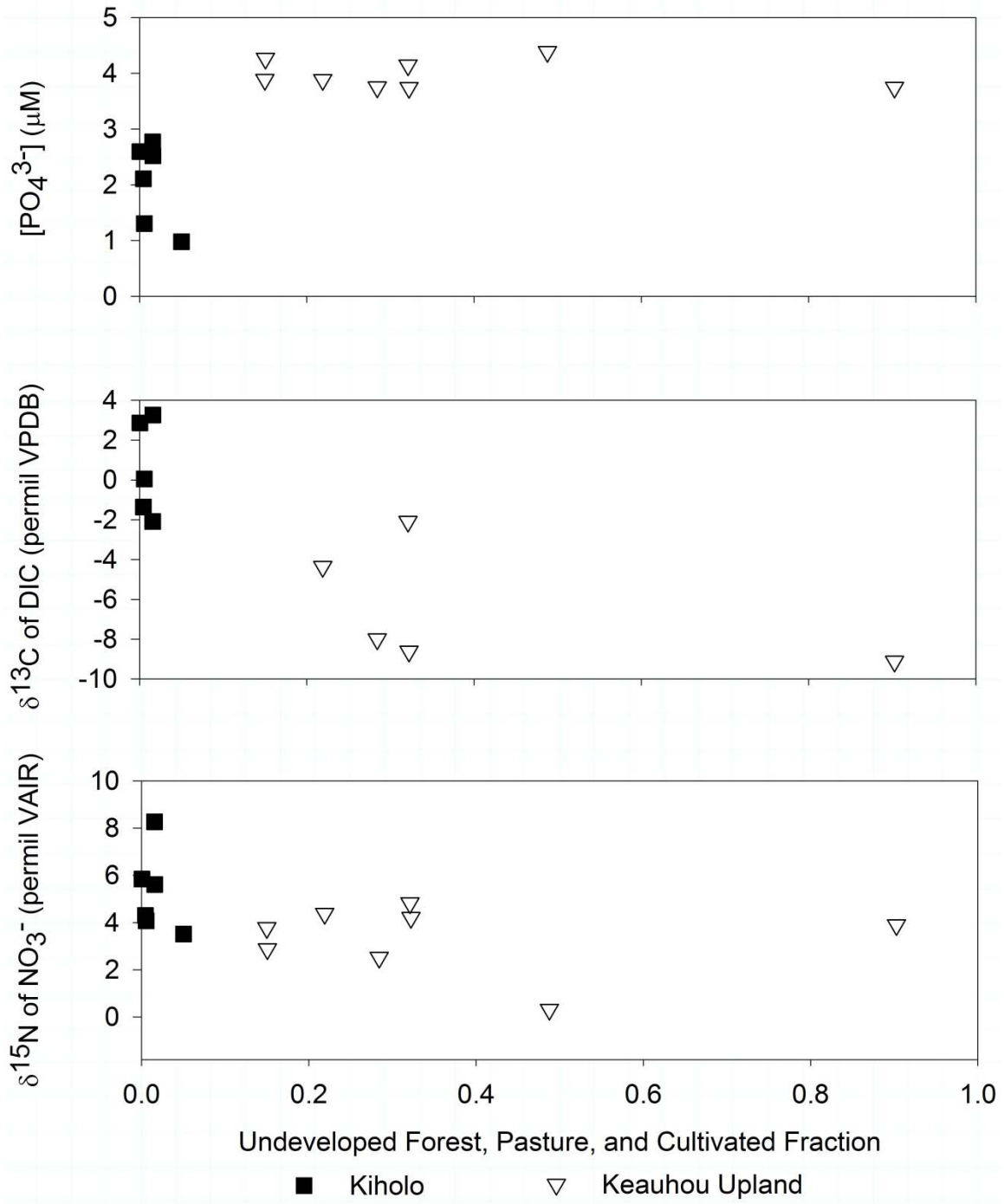

Figure 4.9. Relationship between Kīholo and Keauhou Upland groundwater sample PO_4^{3-} concentrations, $\delta^{13}C$ of DIC values, and $\delta^{15}N$ of NO_3^- values with Undeveloped Forest, Pasture, and Cultivated land fractions.

The Kīholo and Keauhou Upland region groundwater sample flow paths transect primarily undeveloped land. Measured parameters from these regions show little or no correlation with the rift distance and effluent-recharge ratio potential controls. As a result, consideration of the differences between these regions is useful for understanding the effects of

the land use/land cover potential controls on the measured parameters. Groundwater samples from the Kīholo and Keauhou Upland regions were characterized by less variability in measured parameters than groundwater samples from the Kaʻūpūlehu and Keauhou Coastal regions. The primary contrasts between measured parameters among the Kīholo and Keauhou Upland regions were in PO_4^{3-} concentrations (medians of 2.32 μM vs. 3.89 μM, respectively), $\delta^{13}C$ of DIC values (medians of -1.36 ‰ vs. -8.31 ‰, respectively), and $\delta^{15}N$ of NO_3^- values (medians of 4.96 ‰ vs. 3.84 ‰, respectively) (Figure 4.3). The only significant correlation among the measured parameters for these regions was between PO_4^{3-} concentrations and $\delta^{13}C$ of DIC value (ρ =-0.72). Potentially causal relationships between measured parameters and individual potential controls are less apparent for the Kīholo and Keauhou Upland region groundwater samples alone than with the other regions included. Rather, the correlations most likely to be causal occur between groups of land use types associated with the higher rainfall portions of the study area (undeveloped forest, cultivated, and pasture) and groups of land use types associated with arid portions of the study area (undeveloped grassland and undeveloped bare) with PO_4^{3-} concentrations, $\delta^{13}C$ of DIC values, and $\delta^{15}N$ of NO_3^- values (Figure 4.9). We conclude that the high fractions of land use/land cover types associated with high rainfall portions of the study area transected by groundwater flow paths in the Keauhou Upland region are the cause of the higher median PO_4^{3-} concentrations and lower median $\delta^{13}C$ of DIC and $\delta^{15}N$ of NO_3^- values observed here relative to the Kīholo region.

Rainfall exerts a strong control on soil development across the geologically young study area. The undeveloped bare land and grassland that dominate groundwater flow paths in the arid Kīholo region occur primarily on unweathered basalt, with little to no soil development, while the undeveloped forest, pasture, and cultivated lands that dominate groundwater flow paths the wetter middle elevations of the Keauhou Upland region occur primarily on more weathered, organic-rich Histosols and Andisols (Deenik and McClellan, 2007). Leaching of PO_4^{3-} from rock weathering is the dominant form of P loss from young (< 10 ky) soils in Hawai‘i (Vitousek, 2004). The increased precipitation-driven weathering along Keauhou Upland region flow paths relative to Kīholo region flow paths may be increasing leaching of PO_4^{3-}, resulting in higher PO_4^{3-} concentrations in groundwater in this region. Additionally, a study on pre-contact agricultural practices in the Kailua-Kona area (Lincoln et al., 2014) showed lower levels of

extractable P in soils receiving over 1300 mm/yr of precipitation, suggesting that these soils have leached more PO_4^{3-} to underlying groundwater than those in drier areas.

The contrasts in precipitation, land cover, and soil development between the Kīholo and Keauhou Upland regions is also likely responsible for the differences in $\delta^{13}C$ of DIC and $\delta^{15}N$ of NO_3^- values between them. DIC derived from oxidation of organic matter is typically characterized by lower $\delta^{13}C$ of DIC values (~-30 to -10‰) than DIC derived from other potential sources in the region such as atmospheric (~-7‰) or magmatic sources (~-3.5‰, as discussed above) (Clark and Fritz, 1997). The $\delta^{13}C$ of DIC values of Kīholo region samples are closest to those of a magmatic source, potentially related to contribution from the recently discovered geothermal resource in deep groundwater in the Humu‘ula Saddle (Thomas et al., 2015), while the $\delta^{13}C$ of DIC values of Keauhou Upland region samples are consistent with a mixture of DIC derived from oxidation of organic matter and a background magmatic source. This finding is consistent with the existence of better developed soils along groundwater flow paths in the Keauhou Upland region. Soils in arid climates are more likely to lose NH_4^+ through NH_3 volatilization than those in wetter climates as they are characterized by factors favoring NH_3 volatilization such as lower acidity (which reduces protonation of NH_3), lower humidity, and higher temperature (Kendall, 1998). Volatilization of NH_4^+ results in the preferential loss of NH_4^+ containing N-14, leaving the remaining NH_4^+ enriched in N-15. Subsequent oxidation and leaching of this N-15 enriched NH_4^+ results in elevated $\delta^{15}N$ of NO_3^- values in groundwater. The Kīholo region is generally hotter and less humid than the Keauhou Upland region (Giambelluca et al., 2013) and has generally less acidic soil (National Cooperative Soil Survey, 2013), factors that favor volatilization of NH_4^+. Thus, this phenomenon may explain the higher $\delta^{15}N$ of NO_3^- values found in groundwater in the Kīholo region relative to the Keauhou Upland region

Conclusions

We utilized the Spearmans rank correlation test to assess the effects of land use/land cover, geothermal activity, and wastewater effluent discharge along previously determined groundwater flow paths (Chapter 3) on groundwater nutrient concentrations, DIC concentrations, $\delta^{15}N$ of NO_3^- values, and $\delta^{13}C$ of DIC values. We found that (1) geothermal activity related to Hualālai's recently active northwest rift zone is responsible for the elevated SiO_4^{4-}, NO_3^-, and DIC concentrations in groundwater in the Ka‘ūpūlehu region, (2) both wastewater effluent and fertilizer associated with urban and park land use contribute to elevated NO_3^- concentrations in

groundwater in the Keauhou Coastal region, and (3) differences in land use/land cover associated with precipitation and soil development control differences in PO_4^{3-} concentration, $\delta^{13}C$ of DIC values, and $\delta^{15}N$ of NO_3^- values observed between the Kīholo and Keauhou Upland regions. These findings further illustrate the advantages of considering terrestrial controls along groundwater flow paths (e.g. Bishop et al., 2015) rather than within arbitrary buffer zones (e.g. Knee et al., 2010) when evaluating their effects on groundwater geochemical parameters on a regional scale in a complex hydrogeological environment. Additionally, these findings may aid policy makers in better understanding the potential effects of land use decisions on the sustainability of groundwater resources and the coastal environments they affect via SGD in West Hawai‘i and elsewhere. Further investigations into better constraining the mechanisms by which various natural and anthropogenic terrestrial factors influence groundwater geochemical parameters in this region and elsewhere would be beneficial in both evaluating the findings of this work and furthering scientific understanding of the complex relationships between terrestrial environments and underlying groundwater.

CHAPTER 5. CONCLUSIONS

Accomplishments and Scientific Advancements

This dissertation contains findings that are of practical use to regulators and policy makers in addition to findings of scientific interest to hydrogeologists and aqueous geochemists. In order to best pursue my objectives of (1) utilizing geochemical tracers to determine groundwater recharge areas, (2) assessing the origins of dissolved nutrients and DIC in groundwater, and (3) evaluating the biogeochemical reactions that may influence down-gradient geochemical evolution of groundwater prior to its discharge to the ocean in my two study sites, I developed new methods in addition to modifying existing methods as required.

Chapter 2 focused on the accomplishment of objective 3 for the LWRF wastewater effluent injection plume in West Maui. In order to best understand the biogeochemical reactions affecting N and C species concentrations in the effluent plume from injection to discharge, I devised the novel method of considering these processes as a set of reactions occurring in stepwise fashion with known stoichiometric ratios. This method was able to convincingly account for the differences in N and C species concentrations between the injected effluent and submarine spring discharge and also offered insight into the presence and extent of the different biogeochemical reactions occurring within the plume. Application of this method may be a useful approach for workers seeking to better understand the biogeochemistry of similar systems in the future. In Chapter 2, I also sought to better understand the temporal variability of N species concentrations in the discharge of the submarine springs fed by the LWRF wastewater effluent injection plume. To this end I compared long term N species monitoring data and treatment practices from LWRF with long term N species monitoring data from the submarine springs and determined that the chlorination of LWRF effluent for disinfection purposes in October 2011 was the most likely cause for the increase in submarine spring N species concentrations observed beginning in early 2013. This finding may be of great practical use to wastewater treatment plant operators and regulatory agencies seeking to minimize the N loading to the environment from underground wastewater injection sites.

Chapter 3 was intended to accomplish objective 1 for the West Hawai‘i region. While I utilized the established method of determining groundwater flow paths using integrated recharge analysis to match $\delta^{18}O$ values in precipitation with those in groundwater, I expanded upon this

method by carefully considering structural controls on groundwater recharge and flow in constraining flow path trajectories. This methodological expansion should be of use to future workers attempting to use water isotopes as tracers of groundwater recharge and flow in complex hydrogeological environments. My findings show that groundwater flow paths in the West Hawai‘i region generally originate at high elevations on the Mauna Kea and Mauna Loa volcanoes and, in most cases, contradict the region's current aquifer regulatory boundaries. Since these regulatory aquifer boundaries are used in calculating groundwater sustainable yield and in determining other water resource use policies, my findings may provide impetus for re-evaluating these boundaries and the sustainable yield calculations and other policies that stem from their use.

Chapter 4 utilized the groundwater flow paths for the West Hawai‘i region to accomplish objective 2. Since my data set did not meet the normality requirements for parametric statistical methods, I employed the novel method of utilizing the Spearman's rank correlation test to associate potential controls along groundwater flow paths with groundwater nutrient and DIC concentrations. Since this method establishes only significant correlation and not causation between variables, I had to carefully consider each significant correlation to assess whether it was potentially causal or coincidental using $\delta^{13}C$ of DIC and $\delta^{15}N$ of NO_3^- values as source tracers when applicable. This method, together with that of Chapter 3, provides a comprehensive blueprint for workers seeking to gain insight into relationships between natural and anthropogenic terrestrial factors and groundwater geochemistry in regions with poorly constrained hydrogeologic characteristics. The primary findings of Chapter 4 indicate that natural factors such as geothermal activity and soil development as well as anthropogenic factors such as wastewater effluent discharge and fertilizer application contribute to the variability in nutrient and DIC concentrations in groundwater in the West Hawai‘i region. These findings should be useful to policy makers responsible for making decisions regarding land and water use in West Hawai‘i and other similar environments.

Future Research

The findings of this dissertation open several new avenues for future research. In Chapter 2, I proposed that chlorination of injected LWRF wastewater effluent beginning in October 2011 was responsible for the increase in N species concentrations observed at the

downgradient submarine spring discharge locations in early 2013. Since chlorination of injected LWRF effluent ended in May 2014, continued monitoring of N species concentrations in the submarine spring discharge will be imperative to determining if and when pre-chlorination biogeochemical conditions favoring N-attenuation return. Additionally, studies focused on directly observing microbiology of the LWRF wastewater effluent plume would be useful in validating my findings, which were based on inferring biological processes from dissolved species concentrations alone.

In chapter 3 I propose new conceptual models for groundwater occurrence and flow in the West Hawai‘i region. Additional research into groundwater occurrence in this region employing both direct observation as well as geophysical survey techniques will be essential to validation and continued refinement of these conceptual models. While numerical simulation of groundwater flow has previously only been accomplished for small sections of the West Hawai‘i region, my new conceptual models provide a basis for expanding these models over the entire region. These conceptual models also have implications regarding the volumetric distribution of SGD emanating both along the coastline and potentially at locations further offshore. Additional research into locating and quantifying SGD along the West Hawai‘i coastline and at greater depths offshore on a regional scale would be of great use in validating and refining my conceptual models as well as working towards a balanced water budget for the region.

In chapter 4 I associate natural and anthropogenic factors with variations in groundwater nutrient and DIC concentrations in the West Hawai‘i region. This approach can be used flexibly and has great potential to be applied using other potentially controlling factors and geochemical parameters in West Hawai‘i as well as other regions where groundwater flow paths can be approximated. Additionally, further work into the exact mechanisms by which these natural and anthropogenic factors affect the geochemistry of groundwater recharge in the soil and unsaturated zones would be useful in validating and refining my findings.

APPENDIX 1. WEST MAUI DATA

Table A1.1. Weekly LWRF Effluent N species concentrations from 1/2005-5/2013 in units of μM. Empty fields indicate parameter not measured or below detection limit.

Date	NH_4^+	DON	$NO_3^- + NO_2^-$	TN
01/03/05	80	125	327	532
01/10/05	15	136	409	559
01/18/05	70	107	337	514
01/24/05	45	90	400	535
02/01/05	50	100	400	550
02/07/05		90	264	354
02/15/05	80	90	299	469
02/22/05	147	108	187	442
02/28/05	118	92	331	541
03/07/05	65	92	314	471
03/14/05	63	127	366	556
03/21/05	75	95	339	509
03/28/05	100	296	341	737
04/04/05	60	120	357	537
04/11/05	85	97	379	561
04/18/05	60	97	325	482
04/25/05	83	90	243	416
05/02/05	50	61		111
05/09/05	90	136	299	524
05/16/05	45	95	392	532
05/23/05	145	130	344	619
05/31/05	65	120	291	476
06/06/05	30	130	326	486
06/13/05	123	67	301	491
06/20/05	99	68	279	446
06/28/05	75	85	305	465
07/05/05	60	90	234	384
07/11/05	55	95	119	269
07/18/05		90	316	406
07/25/05	105	93	163	361
08/01/05	75	150	219	444
08/09/05	120	75	149	344
08/15/05	110	70	268	448
08/22/05	382	143	149	674
08/25/05		103		103

Table A1.1 (Cont.)

Date	NH_4^+	DON	$NO_3^- + NO_2^-$	TN
08/29/05		140	501	641
09/06/05		90	451	541
09/13/05		100	491	591
09/19/05	30	115	309	454
09/26/05	30	115	411	556
10/03/05	45	120	353	518
10/10/05	60	60	424	544
10/17/05	35	105	346	486
10/24/05		90	451	541
10/31/05	10	123	206	339
11/07/05	20	81	459	560
11/14/05	40	85	340	465
11/21/05	10	135	425	570
11/28/05		80	328	408
12/05/05	23	67	447	537
12/13/05	60	90	325	475
12/19/05	50	115	279	444
12/27/05	245	90	209	544
01/03/06	87	113	269	469
01/09/06	40	107	339	486
01/17/06		120	396	516
01/23/06	70	100	244	414
01/30/06	45	112	389	546
02/06/06	85	112	421	618
02/13/06	125	125	301	551
02/20/06	185	95	289	569
02/28/06	60	105		165
03/06/06	80	110	436	626
03/13/06	70	130	416	616
03/20/06	110	146	358	614
03/28/06	97	128		225
04/03/06	100	135	176	411
04/10/06	130	120	253	503
04/17/06	100	150	255	505
04/24/06	130	121	300	551
05/01/06	127	148	256	531
05/08/06	50	105	356	511
05/15/06	25	100	352	477
05/22/06	110	190	202	502

Table A1.1 (Cont.)

Date	NH_4^+	DON	$NO_3^- + NO_2^-$	TN
05/30/06		120	394	514
06/05/06		80	424	504
06/13/06	117	80	369	566
06/20/06	200	115	229	544
06/27/06	85	68	554	707
07/04/06	510	100	163	773
07/07/06	117	118	489	724
07/11/06	140	90	327	557
07/19/06	240	100	288	628
07/26/06	140	90	201	431
08/01/06	103	74	329	506
08/08/06	20	70	266	356
08/15/06		80	426	506
08/23/06		55	346	401
08/30/06		100	310	410
09/05/06	60	85	234	379
09/12/06		80	247	327
09/20/06		100	247	347
09/26/06		90	316	406
10/03/06		75	392	467
10/10/06		50	493	543
10/19/06		75	436	511
10/24/06		65	441	506
11/03/06		75	347	422
11/08/06		80	378	458
11/14/06		110	374	484
11/21/06		45	485	530
11/28/06		90	725	815
12/05/06		65	632	697
12/12/06		80	401	481
12/20/06	25	120	579	724
12/27/06	30	105	373	508
01/02/07	20	50	478	548
01/10/07		85	530	615
01/16/07	20	60	523	603
01/23/07		65	606	671
01/30/07	15	115	582	712
02/06/07		45	591	636
02/14/07	55	135	656	846

Table A1.1 (Cont.)

Date	NH_4^+	DON	$NO_3^- + NO_2^-$	TN
02/23/07		97	488	585
02/27/07		100	484	584
03/06/07		80	394	474
03/13/07		60	425	485
03/21/07	10	60	380	450
03/27/07		85	460	545
04/03/07	10	80	373	463
04/10/07		105	342	447
04/17/07		85	415	500
04/24/07		115	291	406
05/01/07		85	259	344
05/08/07		70	223	293
05/15/07		72	232	304
05/23/07	10	37	0	47
05/29/07		35	158	193
06/06/07		80	211	291
06/12/07		100	247	347
06/19/07	15	80	307	402
06/26/07		83	316	399
07/03/07		87	351	439
07/11/07		90	343	433
07/17/07		113	366	479
07/24/07	10	110	347	467
07/31/07		97	389	486
08/07/07		115	366	481
08/14/07		100	351	451
08/21/07		110	387	497
08/31/07		80	306	386
09/04/07		60	349	409
09/11/07		70	394	464
09/18/07		90		90
09/25/07		80	259	339
10/03/07		70	256	326
10/09/07		80	242	322
10/16/07		110	236	346
10/24/07	5	85	334	424
10/30/07	63	107	351	521
11/07/07		90	367	457
11/13/07	40	90	401	531

Table A1.1 (Cont.)

Date	NH_4^+	DON	$NO_3^- + NO_2^-$	TN
11/20/07	50	75		125
11/28/07	63	92	320	475
12/04/07	10	90	194	294
12/11/07	5	152	341	499
12/18/07	395	73	163	631
12/25/07	635	80	155	870
01/07/08	95	120	257	472
01/14/08	150	120	241	511
01/22/08	47	108	173	328
01/29/08	30	30		60
02/04/08	155	125		280
02/11/08	73	107	316	496
02/19/08	297	83	186	566
02/25/08	40	105	166	311
03/03/08		125	194	319
03/11/08		110	224	334
03/17/08	50	175	64	289
03/24/08	215	110	175	500
03/31/08	80	125	166	371
04/07/08	100	116	142	358
04/14/08	85	155	186	426
04/22/08	30	185	279	494
04/28/08	95	110	256	461
05/06/08	45	90	292	427
05/12/08	120	100	231	451
05/19/08	240	70	240	550
05/27/08	400	75	224	699
06/03/08	145	240	297	682
06/09/08	372	171	277	820
06/16/08	542	123	205	870
06/23/08	380	95	269	744
06/30/08	217	73	287	577
07/07/08	200	95	239	534
07/14/08	105	110	226	441
07/21/08	145	95	219	459
07/28/08	140	150	228	518
08/04/08	140	115	174	429
08/11/08	170	150	141	461
08/18/08	235	140	141	516

Table A1.1 (Cont.)

Date	NH_4^+	DON	$NO_3^- + NO_2^-$	TN
08/25/08	70	110	213	393
09/02/08	10	120	233	363
09/09/08	7	143	276	426
09/15/08	85	70	172	327
09/22/08	60	213	156	429
09/29/08	40	85	145	270
10/06/08	90	55		145
10/13/08	80	95	213	388
10/20/08	90	75	199	364
10/28/08	340	105	182	627
11/03/08	55	120	185	360
11/10/08	80	65		145
11/17/08	60	85	234	379
11/24/08	145	60	226	431
12/01/08	65	60	286	411
12/09/08	85	125	276	486
12/16/08	25	45	260	330
12/22/08	96	140	190	426
01/05/09	140	90	194	424
01/12/09	210	65	201	476
01/19/09	170	100	209	479
01/26/09	250	25	182	457
02/02/09	210	115	209	534
02/10/09	205	145	179	529
02/17/09	156	104	181	441
02/23/09	135	88	179	402
03/03/09	65	108	275	448
03/09/09	80	80	204	364
03/17/09	25	70	229	324
03/23/09	135	70	189	394
03/30/09	117	76	216	409
04/06/09	155	75	217	447
04/13/09	180	155	170	505
04/20/09	55	95	184	334
04/27/09	20	65	214	299
05/05/09	120	60	231	411
05/11/09		75	164	239
05/18/09		80	135	215
05/26/09	80	100	128	308

Table A1.1 (Cont.)

Date	NH_4^+	DON	$NO_3^- + NO_2^-$	TN
06/02/09		75	119	194
06/09/09		55	119	174
06/16/09		80	85	165
06/23/09		60	101	161
06/30/09		65	140	205
07/01/09		65	140	205
07/06/09	15	60	206	281
07/13/09		80	126	206
07/20/09	75	160	381	616
07/27/09		80	211	291
08/03/09		80	151	231
08/10/09	110	85	263	458
08/17/09		70	217	287
08/24/09		95	163	258
08/31/09		60	270	330
09/08/09		85	194	279
09/14/09		60	210	270
09/21/09		55	253	308
09/28/09		95	340	435
10/06/09		105	507	612
10/12/09	20	60	48	128
10/20/09		65	80	145
10/26/09		70	147	217
11/05/09		57	204	261
11/09/09		60	170	230
11/16/09		60	134	194
11/23/09		70	139	209
11/30/09		70	136	206
12/07/09		100	112	212
12/14/09		75	91	166
12/21/09	75	70	94	239
12/28/09	171	100	101	373
01/04/10	179	136	89	404
01/11/10	66	86	86	238
01/19/10	75	115	96	286
01/26/10	100	90	135	325
02/01/10	95	100	109	304
02/08/10	90	66	117	273
02/16/10		110	137	247

Table A1.1 (Cont.)

Date	NH_4^+	DON	$NO_3^- + NO_2^-$	TN
02/22/10	140	70	167	377
03/01/10	30	80	109	219
03/08/10	100	90	173	363
03/16/10	110	75	196	381
03/23/10	465	145	114	724
03/29/10	415	90	114	619
04/05/10	1215	145	100	1460
04/12/10	1485	725	79	2289
04/19/10	165	125	186	476
04/26/10		90	475	565
05/03/10	20	90	582	692
05/10/10		80		80
05/17/10	10	90	336	436
05/24/10	85	65	454	604
05/31/10	65	70	479	614
06/08/10	105	35	420	560
06/14/10	185	75	353	613
06/21/10	385	70	200	655
06/28/10	525	105	245	875
07/05/10	120	110	436	666
07/12/10	50	155	434	639
07/19/10	40	55	261	356
07/26/10	45	85	260	390
08/02/10	35	85	244	364
08/09/10	425	95	99	619
08/16/10	320	105	391	816
08/23/10	65	95	627	787
08/31/10		130	654	784
09/07/10	65	85	667	817
09/13/10	25	55	527	607
09/20/10	605	160	125	890
09/27/10	925	160	107	1192
10/05/10	830	135	125	1090
10/11/10	1080	140	232	1452
10/18/10	1220	110	268	1598
10/25/10	1130	125	129	1384
11/01/10	690	105	293	1088
11/08/10	270	150	282	702
11/15/10	265	90	407	762

Table A1.1 (Cont.)

Date	NH_4^+	DON	$NO_3^- + NO_2^-$	TN
11/22/10	160	85	404	649
11/29/10	135	100	461	696
12/06/10	50	106	393	549
12/13/10	120	120	459	699
12/20/10	20	85	132	237
12/27/10	890	85	143	1118
01/03/11	17	80	154	251
01/10/11		80	243	323
01/17/11	40	60	257	357
01/24/11		50	96	146
01/31/11		50	239	289
02/07/11		95	325	420
02/14/11	160	160	325	645
02/22/11	210	120	336	666
02/28/11		65	293	358
03/07/11	10	80	464	554
03/14/11	7	98	379	484
03/21/11	60	70	311	441
03/28/11	15	70	443	528
04/04/11	165	65	182	412
04/11/11	75	70	239	384
04/18/11	35	80	271	386
04/25/11	30	65	225	320
05/02/11		70	211	281
05/09/11		55	461	516
05/16/11	20	60	217	297
05/23/11	40	60	182	282
05/31/11	35	65	171	271
06/06/11	15	50	286	351
06/14/11	65	80	264	409
06/21/11	280	135	161	576
06/28/11	280	85	168	533
07/05/11	240	110	271	621
07/12/11	90	65	221	376
07/18/11	95	90	325	510
07/27/11	185	130	221	536
08/02/11	115	85	364	564
08/09/11	180	155	346	681
08/16/11	50	115	407	572

Table A1.1 (Cont.)

Date	NH_4^+	DON	$NO_3^- + NO_2^-$	TN
08/23/11	95	125	368	588
08/30/11	120	95	261	476
09/06/11	120	115	432	667
09/16/11	80	155	196	431
09/20/11	75	95	329	499
09/27/11	75	135	196	406
10/04/11	100	110	507	717
10/11/11	140	120	379	639
10/18/11	90	95	404	589
10/25/11	270	80	257	607
11/01/11	230	95	436	761
11/08/11	225	90	286	601
11/15/11	550	145	75	770
11/22/11	115	150	157	422
11/29/11	205	180	182	567
12/06/11	85	115	218	418
12/13/11	55	145	257	457
12/20/11	165	145	143	453
12/27/11	435	120	96	651
01/03/12	140	170	114	424
01/10/12	0	135	261	396
01/17/12	45	130	250	425
01/23/12	45	145	236	426
01/31/12	55	140	116	311
02/06/12	45	135	94	274
02/13/12	35	165	99	299
02/21/12	65	105	114	284
02/27/12	50	135	76	261
03/06/12	55	95	70	220
03/14/12	75	100	45	220
03/19/12	385	90	18	493
03/27/12	150	100	71	321
04/03/12	880	135	0	1015
04/10/12	70	165	71	306
04/17/12	60	170	20	250
04/24/12	215	120	0	335
05/01/12	300	110	29	439
05/08/12	400	120	29	549
05/15/12	405	120	33	558

Table A1.1 (Cont.)

Date	NH_4^+	DON	$NO_3^- + NO_2^-$	TN
05/22/12	135	115	0	250
05/29/12	95	130	17	242
06/05/12	90	100	19	209
06/12/12	30	205	133	368
06/19/12	50	210	109	369
06/26/12	40	170	105	315
07/03/12	75	150	257	482
07/10/12	60	115	124	299
07/17/12	100	150	116	366
07/24/12	140	100	205	445
07/31/12	90	150	136	376
08/07/12	120	125	47	292
08/14/12	60	125	119	304
08/21/12	100	120	129	349
08/28/12	0	110	149	259
09/04/12	30	140	213	383
09/11/12	0	160	136	296
09/18/12	0	170	407	577
09/25/12	20	145	211	376
10/02/12	10	110	304	424
10/09/12	30	135	283	448
10/16/12	30	125	266	421
10/23/12	35	155	355	545
10/30/12	25	130		
11/06/12	35	35		
11/13/12	10	85	321	416
11/20/12	40	45	296	381
11/27/12	30	50	223	303
12/04/12	15	100	593	708
12/11/12	10	25	561	596
12/18/12	10	5	529	544
12/27/12	30	20	336	386
01/03/13	55	5	386	446
01/08/13	10	15	357	382
01/15/13	40	30	414	484
01/22/13	140	55	371	566
01/29/13	40	35	343	418
02/05/13	45	20	629	694
02/12/13	50	10	486	546

Table A1.1 (Cont.)

Date	NH_4^+	DON	$NO_3^- + NO_2^-$	TN
02/19/13	20	10	389	419
02/26/13	35	35		
03/05/13	15	45	197	257
03/12/13	5	10	274	289
03/19/13	20	10	62	92
03/25/13	20	25	340	385
04/02/13	25	90	287	402
04/09/13	80	20	321	421
04/16/13	15	10	279	304
04/23/13	30	20	304	354
04/30/13	35	5	340	380
05/07/13	10	30	206	246
05/14/13	15	5		

Table A1.2. LWRF TRC concentrations in mg/L from 10/2011 to 7/2014.

Date	TRC
10/01/11	0.03
10/02/11	0.03
10/03/11	0.00
10/04/11	0.00
10/05/11	0.10
10/06/11	0.04
10/07/11	0.05
10/08/11	0.03
10/09/11	0.03
10/10/11	0.00
10/11/11	0.00
10/12/11	0.02
10/13/11	0.02
10/14/11	0.02
10/15/11	0.03
10/16/11	0.01
10/17/11	0.00
10/18/11	0.00
10/19/11	0.04
10/20/11	0.01
10/21/11	0.68
10/22/11	1.54

Table A1.2 (Cont.)

Date	TRC
10/23/11	1.09
10/24/11	0.30
10/25/11	0.43
10/26/11	0.55
10/27/11	0.03
10/28/11	0.96
10/29/11	1.07
10/30/11	2.08
10/31/11	0.10
11/01/11	0.60
11/02/11	0.78
11/03/11	1.14
11/04/11	0.60
11/05/11	1.64
11/06/11	1.98
11/07/11	0.63
11/08/11	0.40
11/09/11	0.40
11/10/11	1.42
11/11/11	2.30
11/12/11	5.05
11/13/11	1.50
11/14/11	1.25
11/15/11	1.67
11/16/11	0.71
11/17/11	1.22
11/18/11	1.46
11/19/11	2.68
11/20/11	1.89
11/21/11	1.40
11/22/11	1.20
11/23/11	1.09
11/24/11	2.20
11/25/11	1.90
11/26/11	3.02
11/27/11	2.64
11/28/11	1.14
11/29/11	1.72
11/30/11	0.00

Table A1.2 (Cont.)

Date	TRC
12/02/11	1.52
12/05/11	1.03
12/06/11	
12/07/11	1.06
12/09/11	0.94
12/12/11	0.97
12/14/11	0.79
12/16/11	1.13
12/19/11	1.96
12/21/11	2.64
12/23/11	3.12
12/28/11	0.62
12/30/11	0.80
01/04/12	1.73
01/06/12	0.54
01/11/12	0.23
01/13/12	0.55
01/18/12	0.77
01/20/12	0.51
01/23/12	0.36
01/25/12	0.37
01/27/12	0.33
01/30/12	0.39
02/01/12	0.50
02/03/12	0.72
02/06/12	1.15
02/08/12	0.83
02/10/12	2.43
02/13/12	2.32
02/15/12	0.85
02/17/12	0.33
02/20/12	1.70
02/22/12	0.86
02/24/12	2.16
02/27/12	2.68
03/02/12	2.66
03/05/12	1.81
03/07/12	1.07
03/09/12	3.68

Table A1.2 (Cont.)

Date	TRC
03/12/12	2.86
03/14/12	1.17
03/16/12	5.70
03/19/12	5.68
03/21/12	3.66
03/23/12	6.80
03/26/12	3.42
03/28/12	6.12
03/30/12	6.29
04/02/12	4.92
04/04/12	5.32
04/06/12	4.12
04/09/12	0.48
04/11/12	2.11
04/13/12	1.98
04/16/12	2.17
04/18/12	1.31
04/20/12	0.71
04/23/12	4.30
04/25/12	4.68
04/27/12	3.48
04/30/12	2.20
05/02/12	2.02
05/04/12	4.83
05/07/12	4.56
05/08/12	3.86
05/09/12	1.22
05/11/12	4.34
05/14/12	4.32
05/16/12	1.35
05/18/12	4.44
05/21/12	1.64
05/23/12	5.31
05/25/12	1.53
05/28/12	1.88
05/30/12	1.27
06/01/12	3.74
06/04/12	6.33
06/06/12	1.66

Table A1.2 (Cont.)

Date	TRC
06/08/12	4.24
06/11/12	3.52
06/13/12	0.78
06/15/12	3.54
06/18/12	1.65
06/19/12	0.88
06/20/12	1.23
06/22/12	3.72
06/25/12	1.14
06/27/12	1.87
06/29/12	1.56
07/02/12	2.94
07/04/12	4.80
07/06/12	5.58
07/09/12	4.04
07/11/12	1.20
07/13/12	3.77
07/16/12	3.16
07/18/12	0.89
07/20/12	3.04
07/23/12	0.86
07/25/12	2.50
07/27/12	1.01
07/30/12	2.03
08/01/12	2.54
08/03/12	7.70
08/06/12	2.13
08/08/12	1.01
08/10/12	1.14
08/13/12	1.82
08/15/12	0.89
08/17/12	1.35
08/20/12	2.68
08/22/12	3.28
08/24/12	7.80
08/27/12	7.70
08/29/12	3.60
08/31/12	5.05
09/03/12	>22.20

Table A1.2 (Cont.)

Date	TRC
09/05/12	3.20
09/07/12	>22.00
09/10/12	2.88
09/12/12	0.45
09/14/12	1.02
09/17/12	1.14
09/19/12	0.98
09/21/12	1.85
09/24/12	1.46
09/26/12	0.95
09/28/12	2.06
10/01/12	8.60
10/03/12	0.65
10/05/12	1.17
10/08/12	0.95
10/10/12	0.59
10/12/12	1.15
10/15/12	1.39
10/17/12	0.90
10/19/12	0.61
10/22/12	0.68
10/24/12	0.93
10/26/12	1.35
10/29/12	0.77
10/31/12	0.74
11/02/12	1.57
11/05/12	1.50
11/7/112	0.67
11/09/12	1.09
11/14/12	1.02
11/16/12	1.79
11/19/12	0.79
11/21/12	0.57
11/23/12	3.38
11/26/12	2.22
11/28/12	0.53
11/30/12	3.68
12/03/12	3.24
12/05/12	0.96

Table A1.2 (Cont.)

Date	TRC
12/07/12	0.78
12/10/12	4.22
12/12/12	5.44
12/14/12	1.74
12/17/12	3.10
12/19/12	1.80
12/21/12	5.94
12/24/12	1.58
12/26/12	2.14
12/28/12	8.00
12/31/12	8.00
01/02/13	5.00
01/04/13	4.15
01/07/13	1.95
01/09/13	0.92
01/11/13	1.09
01/14/13	2.66
01/16/13	1.04
01/18/13	4.40
01/21/13	4.80
01/23/13	2.26
01/25/13	6.16
01/28/13	3.24
01/30/13	0.89
02/01/13	0.93
02/04/13	1.00
02/06/13	0.60
02/08/13	1.69
02/11/13	1.15
02/13/13	0.54
02/15/13	0.80
02/18/13	0.58
02/20/13	1.06
02/22/13	1.26
02/25/13	3.04
02/27/13	1.19
03/01/13	1.13
03/04/13	0.96
03/06/13	0.48

Table A1.2 (Cont.)

Date	TRC
03/08/13	0.75
03/11/13	0.99
03/13/13	0.48
03/15/13	0.03
03/18/13	0.89
03/20/13	0.80
03/22/13	1.06
03/25/13	0.74
03/27/13	0.80
03/29/13	0.86
04/01/13	1.14
04/03/13	0.66
04/05/13	0.60
04/08/13	0.37
04/10/13	0.96
04/12/13	1.73
04/15/13	0.89
04/17/13	0.89
04/19/13	
04/22/13	3.12
04/24/13	1.97
04/26/13	0.61
04/29/13	2.20
05/01/13	2.00
05/03/13	2.50
05/06/13	0.75
05/08/13	0.39
05/10/13	1.99
05/13/13	1.40
05/15/13	0.76
05/17/13	1.22
05/20/13	1.21
05/22/13	8.64
05/24/13	2.06
05/27/13	43.80
05/29/13	5.85
05/31/13	11.50
06/03/13	9.20
06/05/13	2.20

Table A1.2 (Cont.)

Date	TRC
06/07/13	7.25
06/10/13	11.20
06/12/13	1.72
06/14/13	11.50
06/17/13	2.06
06/19/13	2.34
06/20/13	1.42
06/24/13	1.38
06/26/13	3.42
06/28/13	0.84
07/01/13	1.48
07/03/13	1.63
07/05/13	3.30
07/08/13	0.73
07/10/13	0.45
07/12/13	0.54
07/15/13	1.49
07/17/13	0.24
07/19/13	1.11
07/22/13	1.48
07/24/13	2.05
07/26/13	1.18
07/29/13	1.22
07/31/13	0.81
08/02/13	0.71
08/05/13	0.02
08/07/13	0.03
08/09/13	2.80
08/12/13	0.51
08/14/13	0.04
08/16/13	0.16
08/19/13	
08/21/13	
08/23/13	
08/26/13	0.05
08/28/13	0.02
08/30/13	0.03
09/02/13	0.05
09/04/13	0.28

Table A1.2 (Cont.)

Date	TRC
09/06/13	1.08
09/09/13	1.56
09/11/13	0.73
09/13/13	0.09
09/16/13	9.20
09/18/13	0.63
09/20/13	1.77
09/23/13	0.16
09/25/13	0.39
09/27/13	0.45
09/30/13	0.66
10/02/13	4.14
10/04/13	0.88
10/07/13	2.40
10/09/13	0.68
10/11/13	1.14
10/14/13	0.74
10/16/13	
10/18/13	1.77
10/21/13	1.41
10/23/13	0.76
10/25/13	0.21
10/28/13	0.29
10/30/13	1.01
11/01/13	0.84
11/04/13	0.84
11/06/13	0.75
11/08/13	0.93
11/11/13	3.08
11/13/13	0.41
11/15/13	0.92
11/18/13	2.54
11/20/13	2.78
11/22/13	2.18
11/25/13	2.60
11/27/13	0.79
11/29/13	1.68
12/02/13	0.68
12/04/13	

Table A1.2 (Cont.)

Date	TRC
12/06/13	1.75
12/09/13	1.64
12/11/13	1.20
12/13/13	2.60
12/16/13	3.56
12/18/13	1.38
12/19/13	0.77
12/23/13	0.75
12/24/13	2.16
12/25/13	3.62
12/26/13	1.80
12/27/13	4.08
12/28/13	3.60
12/29/13	4.12
12/30/13	3.60
12/31/13	2.32
01/01/14	2.44
01/02/14	1.72
01/03/14	1.84
01/04/14	1.21
01/05/14	1.47
01/06/14	1.21
01/07/14	0.60
01/08/14	0.60
01/09/14	0.68
01/10/14	0.67
01/11/14	1.26
01/12/14	0.43
01/13/14	2.18
01/14/14	0.26
01/15/14	0.20
01/16/14	0.81
01/17/14	0.78
01/18/14	1.77
01/19/14	2.68
01/20/14	0.03
01/21/14	0.03
01/22/14	0.57
01/23/14	0.61

Table A1.2 (Cont.)

Date	TRC
01/24/14	0.06
01/25/14	2.34
01/26/14	0.03
01/27/14	0.03
01/28/14	0.76
01/29/14	0.68
01/30/14	0.50
01/31/14	0.30
02/01/14	3.42
02/02/14	3.56
02/03/14	2.58
02/04/14	2.58
02/05/14	1.80
02/06/14	3.16
02/07/14	2.58
02/08/14	2.42
02/09/14	3.28
02/10/14	3.18
02/11/14	1.87
02/12/14	1.53
02/13/14	0.81
02/14/14	0.50
02/15/14	0.46
02/16/14	0.44
02/17/14	0.50
02/18/14	0.44
02/19/14	0.51
02/20/14	0.74
02/21/14	0.38
02/22/14	0.61
02/23/14	0.52
02/24/14	0.50
02/25/14	0.61
02/26/14	0.64
02/27/14	0.81
02/28/14	0.89
03/01/14	0.92
03/02/14	1.36
03/03/14	0.62

Table A1.2 (Cont.)

Date	TRC
03/04/14	0.70
03/05/14	0.70
03/06/14	0.96
03/07/14	2.50
03/08/14	1.46
03/09/14	1.52
03/10/14	0.13
03/11/14	0.53
03/12/14	0.95
03/13/14	0.51
03/14/14	0.95
03/15/14	0.16
03/16/14	0.19
03/17/14	0.36
03/18/14	
03/19/14	
03/20/14	
03/21/14	
03/22/14	0.57
03/23/14	0.22
03/24/14	0.51
03/25/14	0.60
03/26/14	0.54
03/27/14	0.89
03/28/14	
03/29/14	
03/30/14	
03/31/14	
04/01/14	1.42
04/02/14	0.39
04/03/14	0.73
04/04/14	0.50
04/05/14	1.11
04/06/14	1.07
04/07/14	0.51
04/08/14	0.42
04/09/14	0.53
04/10/14	0.41
04/11/14	0.69

Table A1.2 (Cont.)

Date	TRC
04/12/14	0.74
04/13/14	1.63
04/14/14	1.89
04/15/14	1.23
04/16/14	0.30
04/17/14	0.36
04/18/14	0.53
04/19/14	0.46
04/20/14	0.48
04/21/14	0.28
04/22/14	0.45
04/23/14	0.32
04/24/14	0.31
04/25/14	
04/26/14	
04/27/14	0.67
04/28/14	0.40
04/29/14	0.30
04/30/14	0.28
05/01/14	0.23
05/02/14	0.37
05/03/14	0.38
05/04/14	0.48
05/05/14	0.46
05/06/14	0.23
05/07/14	0.57
05/08/14	0.47
05/09/14	0.78
05/10/14	0.34
05/11/14	0.44
05/12/14	0.39
05/13/14	
05/14/14	0.65
05/15/14	0.52
05/16/14	
05/17/14	0.33
05/18/14	0.51
05/19/14	0.28
05/20/14	0.38

Table A1.2 (Cont.)

Date	TRC
05/21/14	0.31
05/22/14	0.08
05/23/14	0.34
05/24/14	0.07
05/25/14	0.28
05/26/14	0.66
05/27/14	0.12
05/28/14	0.37
05/29/14	0.03
05/30/14	0.40
05/31/14	0.87
06/01/14	0.98
06/02/14	0.70
06/03/14	0.35
06/04/14	0.35
06/05/14	0.03
06/06/14	0.60
06/07/14	0.02
06/08/14	0.04
06/09/14	0.04
06/10/14	0.02
06/11/14	0.03
06/12/14	0.02
06/13/14	0.03
06/14/14	0.03
06/15/14	0.03
06/16/14	0.02
06/17/14	0.03
06/18/14	0.05
06/19/14	0.02
06/20/14	0.04
06/21/14	0.03
06/22/14	0.04
06/23/14	0.04
06/24/14	0.00
06/25/14	0.03
06/26/14	0.03
06/27/14	
06/28/14	0.02

Table A1.2 (Cont.)

Date	TRC
06/29/14	0.04
06/30/14	0.02
07/01/14	0.04
07/02/14	0.04
07/03/14	0.04
07/04/14	0.03
07/05/14	0.02
07/06/14	0.04
07/07/14	0.04
07/08/14	0.02
07/09/14	0.03
07/10/14	0.02
07/11/14	0.03
07/12/14	0.04
07/13/14	0.04
07/14/14	0.03
07/15/14	0.03
07/16/14	0.03
07/17/14	0.08
07/18/14	0.02
07/19/14	0.02
07/20/14	0.04
07/21/14	0.07
07/22/14	0.02
07/23/14	0.04
07/24/14	0.10
07/25/14	0.07
07/26/14	0.03
07/27/14	0.03
07/28/14	0.03
07/29/14	0.03
07/30/14	0.04
07/31/14	0.05

Table A1.3. LWRF monthly average injection flow rates from 1/2011 to 7/2014 in MGD.

Date	Well 1	Well 2	Well 3	Well 4
01/01/11	0.18	2.90	0.89	0.66
02/01/11	0.24	1.85	1.14	0.87
03/01/11	0.22	2.06	0.89	0.80
04/01/11	0.22	1.63	0.88	0.82
05/01/11	0.21	1.04	1.05	0.83
06/01/11	0.20	0.70	1.18	1.03
07/01/11	0.19	0.41	1.36	1.15
08/01/11	0.20	0.62	1.22	1.13
09/01/11	0.13	0.25	1.23	1.07
10/01/11	0.17	0.50	1.25	1.12
11/01/11	0.16	0.63	1.32	1.37
12/01/11	0.13	0.67	1.13	1.30
01/01/12	0.13	0.75	1.25	1.51
02/01/12	0.08	0.18	1.59	1.53
03/01/12	0.07	0.06	1.90	1.39
04/01/12	0.04	0.01	1.81	1.16
05/01/12	0.03	0.01	1.80	1.19
06/01/12	0.08	0.02	1.94	1.33
07/01/12	0.03	0.03	2.00	1.16
08/01/12	0.02	0.00	1.93	1.12
09/01/12	0.05	0.02	0.96	1.02
10/01/12	0.05	0.03	1.93	0.93
11/01/12	0.07	0.06	1.99	0.86
12/01/12	0.13	0.11	0.76	1.10
01/01/13	0.13	0.75	1.25	1.51
02/01/13	0.20	0.20	0.00	1.81
03/01/13	0.18	0.13	1.92	1.27
04/01/13	0.15	0.12	2.19	0.43
05/01/13	0.14	0.07	2.43	0.19
06/01/13	0.09	0.07	2.43	0.19
07/01/13	0.14	0.09	1.88	0.99
08/01/13	0.23	0.62	1.92	1.64
09/01/13	0.17	0.03	1.92	0.86
10/01/13	0.12	0.17	0.06	2.44
11/01/13	0.21	0.29	0.00	2.71
12/01/13	0.32	0.52	0.75	1.80
01/01/14	0.50	1.69	0.02	2.27
02/01/14	0.56	1.52	0.01	2.37

Table A1.3 (Cont.)

Date	Well 1	Well 2	Well 3	Well 4
03/01/14	0.52	1.00	0.79	1.97
04/01/14	0.52	0.20	1.74	1.03
05/01/14	0.46	0.20	1.62	0.79
06/01/14	0.66	0.96	0.54	1.08
07/01/14	0.67	1.67	0.02	1.16

Table A1.4. HDOH submarine spring sample basic water quality parameters from 2/2012 to 2/2014. NS= North Seep and SS=South Seep. Missing values indicates parameter not measured.

Date	Time	Location	Temperature (˚C)	Salinity (PSU)	pH	DO (mg/L)
02/27/12	9:45	NSA	27.02	4.33	7.77	5.38
02/27/12	10:15	NSB	26.99	4.06	7.68	3.89
02/27/12	10:35	NSC	28.45	4.20	7.76	4.85
02/27/12	11:49	SSA	28.75	2.88	7.75	5.01
02/27/12	12:35	SSB	28.14	11.56	7.71	4.45
02/27/12	13:02	SSC	29.77	3.25	7.71	4.10
03/27/12	9:20	NSA	25.70	4.28	7.63	5.85
03/27/12	10:42	SSA	25.79	2.94	7.55	6.00
03/27/12	11:27	SSB	27.47	12.93	7.51	5.99
03/27/12	11:55	SSC	27.07	3.22	7.58	5.17
04/16/12	9:06	NSA	26.09	4.08	7.84	4.87
04/16/12	10:54	SSA	27.44	2.98	7.77	6.94
04/16/12	11:35	SSB	27.95	12.02	7.80	6.08
04/16/12	12:02	SSC	27.15	3.26	7.80	4.71
05/07/12	9:24	NSA	28.03	4.34	7.52	5.96
05/07/12	10:02	NSB	28.95	4.25	7.75	5.87
05/07/12	11:06	SSA	27.50	3.14	7.60	2.73
05/07/12	11:30	SSB	28.45	11.11	7.61	6.20
05/07/12	12:02	SSC	27.77	6.13	7.67	5.88
06/18/12	9:16	NSA	27.96	25.39	7.95	6.46
06/18/12	9:56	NSB	29.91	4.56	7.82	5.89
06/18/12	11:15	SSA	29.22	3.24	7.64	5.18
06/18/12	12:01	SSB	30.15	7.20	7.61	5.13
07/23/12	9:03	NSA	28.90	4.70	7.59	
07/23/12	9:39	NSB	29.00	6.50	7.53	
07/23/12	10:50	SSA	31.90	3.20	7.63	
07/23/12	11:23	SSB	31.90	3.60	7.63	
07/23/12	11:51	SSC	32.60	3.50	7.59	
08/21/12	9:20	NSA	29.30	4.50	7.67	

Table A1.4 (Cont.)

Date	Time	Location	Temperature (˚C)	Salinity (PSU)	pH	DO (mg/L)
08/21/12	10:39	SSA	31.40	3.20	7.42	
08/21/12	11:09	SSB	33.00	3.70	7.49	
08/21/12	11:46	SSC	34.50	3.50	7.55	
09/12/12	9:12	NSA	27.81	4.56	7.52	4.94
09/12/12	10:45	SSA	30.45	3.16	7.52	4.22
09/12/12	11:17	SSB	32.02	3.67	7.50	4.25
09/12/12	11:47	SSC	33.35	3.41	7.53	4.77
10/22/12	9:21	NSA	27.86	4.97	7.41	4.22
10/22/12	9:51	NSB	28.98	7.33	7.49	5.58
10/22/12	11:10	SSA	28.52	5.26	7.55	2.95
10/22/12	11:40	SSB	29.57	3.71	7.52	4.10
10/22/12	12:08	SSC	30.09	3.55	7.55	3.25
11/27/12	10:16	SSA	26.57	3.26	7.63	5.83
11/27/12	10:58	SSB	27.82	4.36	7.70	6.50
11/27/12	11:38	SSC	28.32	3.44	7.68	6.59
12/10/12	9:39	NSA	26.18	10.51	7.48	4.26
12/10/12	11:10	SSA	28.39	3.19	7.68	3.71
12/10/12	11:35	SSB	27.85	3.63	7.68	2.19
12/10/12	12:00	SSC	28.79	3.42	7.59	3.67
02/11/13	9:32	NSA	24.16	4.97	7.68	7.55
02/11/13	11:04	SSA	27.42	3.45	7.79	7.14
02/11/13	11:46	SSB	28.92	3.77	7.80	7.05
02/11/13	12:25	SSC	28.39	10.47	7.74	7.01
02/25/13	9:20	NSA	27.34	4.70	7.57	7.18
02/25/13	9:56	NSB	27.19	4.60	7.96	7.11
02/25/13	11:36	SSA	29.56	3.35	7.60	6.38
02/25/13	12:02	SSB	28.48	3.71	7.65	6.10
03/27/13	9:09	NSA	26.64	4.75	7.53	6.13
03/27/13	9:37	NSB	26.63	5.16	7.53	5.16
03/27/13	10:40	SSA	27.30	3.34	7.50	6.29
03/27/13	11:09	SSB	28.24	3.71	7.52	6.17
03/27/13	11:37	SSC	26.71	10.45	7.50	6.34
04/24/13	9:21	NSA	25.92	19.88	7.34	5.60
04/24/13	9:50	NSB	30.73	4.89	7.57	5.00
04/24/13	10:56	SSA	29.61	3.41	7.48	4.39
04/24/13	11:24	SSB	31.75	3.80	7.51	4.90
04/24/13	11:57	SSC	29.14	20.25	7.44	6.14
06/05/13	10:08	SSA	31.12	19.88	7.48	6.02

Table A1.4 (Cont.)

Date	Time	Location	Temperature (˚C)	Salinity (PSU)	pH	DO (mg/L)
06/05/13	10:35	SSB	30.54	3.99	7.66	5.94
06/05/13	11:02	SSC	32.40	28.43	7.79	5.75
06/17/13	9:11	NSA	30.20	4.93	7.40	5.06
06/17/13	9:58	NSC	32.24	20.25	7.42	5.07
06/17/13	11:00	SSA	31.46	3.95	7.59	4.35
06/17/13	11:23	SSB	32.08	21.57	7.44	5.26
06/17/13	11:45	SSC	31.83	15.72	7.55	5.65
07/24/13	9:18	NSA	29.02	5.11	7.33	5.76
07/24/13	9:43	NSB	30.24	4.90	7.36	6.04
07/24/13	10:42	SSA	30.30	4.19	7.79	4.74
07/24/13	11:08	SSB	30.54	8.47	7.79	5.17
07/24/13	11:33	SSC	31.28	3.99	7.78	4.68
08/19/13	9:10	NSA	27.73	5.15	7.77	6.63
08/19/13	9:55	NSB	29.98	5.42	8.00	5.66
08/19/13	10:52	SSA	31.14	3.72	7.64	4.04
08/19/13	11:15	SSB	31.82	19.55	7.56	5.27
08/19/13	11:41	SSC	29.51	4.58	7.85	4.38
10/09/13	9:41	NSA	29.27	5.00	7.75	3.55
10/09/13	10:06	NSB	30.62	4.60	7.74	3.02
10/09/13	11:04	SSA	31.13	5.04	7.52	3.28
10/09/13	11:41	SSB	30.77	22.73	7.68	4.43
10/21/13	9:22	NSA	27.97	4.98	7.74	4.79
10/21/13	9:50	NSB	28.54	4.94	7.65	6.72
10/21/13	10:50	SSA	29.13	11.97	7.62	6.44
10/21/13	11:17	SSB	30.23	7.12	7.68	6.52
10/21/13	11:45	SSC	30.32	4.27	7.75	6.70
11/04/13	9:16	NSA	27.79	4.65	7.94	5.77
11/04/13	9:44	NSB	28.17	5.07	7.85	5.75
11/04/13	10:51	SSA	29.53	22.76	7.90	5.29
11/04/13	11:15	SSB	30.27	8.40	7.72	4.66
11/04/13	11:40	SSC	31.38	3.88	7.73	5.45
12/04/13	9:31	NSA	27.52	4.51	8.14	7.01
12/04/13	10:19	NSB	29.12	13.34	7.98	6.05
12/04/13	11:14	SSA	29.45	6.43	7.79	4.88
12/04/13	11:38	SSB	29.77	5.12	7.84	4.49
12/04/13	12:04	SSC	28.17	12.61	7.85	5.40
02/10/14	9:24	NSA	25.19	4.69	7.95	4.31
02/10/14	9:52	NSB	26.26	4.61	7.69	4.38

Table A1.4 (Cont.)

Date	Time	Location	Temperature (˚C)	Salinity (PSU)	pH	DO (mg/L)
02/10/14	10:55	SSA	27.17	3.50	7.69	4.50
02/10/14	11:20	SSB	27.58	3.60	7.71	4.72
02/10/14	11:48	SSC	28.45	5.49	7.87	5.09
02/24/14	9:20	NSA	25.44	4.56	7.99	4.53
02/24/14	9:44	NSB	26.74	6.30	8.03	4.55
02/24/14	10:44	SSA	27.03	3.55	7.78	5.24
02/24/14	11:01	SSB	27.62	3.66	7.78	5.38
02/24/14	11:26	SSC	28.02	7.68	7.95	5.66

Table A1.5. HDOH submarine spring sample N species concentrations from 2/2012 to 2/2014. NS= North Seep and SS=South Seep. Missing values indicates parameter not measured

Date	Time	Location	NH_4^+	DON	$NO_3^- + NO_2^-$	TN
02/27/12	9:45	NSA	0.1	19.8	4.0	23.9
02/27/12	10:15	NSB	0.1	18.8	3.5	22.4
02/27/12	10:35	NSC	0.1	20.6	3.0	23.8
02/27/12	11:49	SSA	0.1	11.9	1.5	13.6
02/27/12	12:35	SSB	0.3	11.9	1.2	13.4
02/27/12	13:02	SSC	0.1	24.4	1.4	25.9
03/27/12	9:20	NSA	0.4		2.8	
03/27/12	10:42	SSA	0.1		0.9	
03/27/12	11:27	SSB	0.1		1.3	
03/27/12	11:55	SSC	0.1		1.6	
04/16/12	9:06	NSA	0.3	10.9	0.1	11.2
04/16/12	10:54	SSA	0.1	5.7	0.1	6.0
04/16/12	11:35	SSB	0.2	3.9	0.1	4.2
04/16/12	12:02	SSC	0.1	14.1	0.4	14.6
05/07/12	9:24	NSA	0.2	4.0	0.9	5.1
05/07/12	10:02	NSB	0.2	4.4	0.2	4.9
05/07/12	11:06	SSA	0.2	4.9	0.7	5.9
05/07/12	11:30	SSB	0.2	3.2	0.9	4.3
05/07/12	12:02	SSC	0.4	3.7	0.4	4.4
06/18/12	9:16	NSA	0.4	2.3	0.2	2.9
06/18/12	9:56	NSB	0.1	3.0	0.1	3.2
06/18/12	11:15	SSA	0.3	5.9	0.1	6.3
06/18/12	12:01	SSB	0.1	3.6	0.1	3.9
07/23/12	9:03	NSA	0.1	3.1	0.4	3.6
07/23/12	9:39	NSB	0.1	3.0	0.1	3.2
07/23/12	10:50	SSA	0.3	3.0	0.1	3.4

Table A1.5 (Cont.)

Date	Time	Location	NH_4^+	DON	$NO_3^- + NO_2^-$	TN
07/23/12	11:23	SSB	0.1	4.1	0.1	4.4
07/23/12	11:51	SSC	0.2	4.7	0.1	5.0
08/21/12	9:20	NSA	0.1	5.4	0.1	5.6
08/21/12	10:39	SSA	0.3	8.4	0.1	8.8
08/21/12	11:09	SSB	0.1	6.6	0.1	6.9
08/21/12	11:46	SSC	0.1	6.7	0.1	6.9
09/12/12	9:12	NSA	0.1	5.9	0.1	6.1
09/12/12	10:45	SSA	0.4	6.9	0.1	7.4
09/12/12	11:17	SSB	0.3	6.4	0.1	6.7
09/12/12	11:47	SSC	0.4	6.3	0.1	6.7
10/22/12	9:21	NSA	0.1	6.6	0.1	6.8
10/22/12	9:51	NSB	0.1	6.3	0.1	6.5
10/22/12	11:10	SSA	0.4	9.3	0.1	9.8
10/22/12	11:40	SSB	0.4	9.1	0.1	9.6
10/22/12	12:08	SSC	0.4	7.4	0.1	7.9
11/27/12	10:16	SSA	0.5	8.3	0.1	8.9
11/27/12	10:58	SSB	0.2	6.1	0.1	6.4
11/27/12	11:38	SSC	0.4	9.4	0.1	9.8
12/10/12	9:39	NSA	0.3	3.0	0.1	3.4
12/10/12	11:10	SSA	0.8	4.0	0.1	4.9
12/10/12	11:35	SSB	0.6	3.1	0.1	3.8
12/10/12	12:00	SSC	0.6	4.1	0.1	4.9
02/11/13	9:32	NSA	0.1	4.9	3.9	9.0
02/11/13	11:04	SSA		8.0	0.1	8.1
02/11/13	11:46	SSB		7.5	0.1	7.6
02/11/13	12:25	SSC		7.4	0.4	7.8
02/25/13	9:20	NSA		6.4	6.0	12.4
02/25/13	9:56	NSB		5.6	6.9	12.6
02/25/13	11:36	SSA		8.0	0.3	8.3
02/25/13	12:02	SSB		6.5	0.5	7.0
03/27/13	9:09	NSA	0.1	14.9	31.7	46.7
03/27/13	9:37	NSB	0.1	18.5	28.6	47.3
03/27/13	10:40	SSA	0.1	4.1	17.6	21.9
03/27/13	11:09	SSB	0.1	2.0	13.3	15.4
03/27/13	11:37	SSC	0.1	3.0	7.9	11.0
04/24/13	9:21	NSA	0.1	3.5	28.6	32.3
04/24/13	9:50	NSB	0.5	21.3	53.9	75.7
04/24/13	10:56	SSA	0.1	13.5	46.6	60.3

Table A1.5 (Cont.)

Date	Time	Location	NH_4^+	DON	$NO_3^- + NO_2^-$	TN
04/24/13	11:24	SSB	0.1	17.4	36.4	53.9
04/24/13	11:57	SSC	0.1	3.8	16.5	20.4
06/05/13	10:08	SSA	0.5	8.3	18.0	26.8
06/05/13	10:35	SSB	0.4	47.9	39.6	87.9
06/05/13	11:02	SSC	0.3		12.4	10.7
06/17/13	9:11	NSA	0.2	40.9	58.9	100.0
06/17/13	9:58	NSC	0.3		58.9	58.0
06/17/13	11:00	SSA	0.2	62.2	55.4	117.9
06/17/13	11:23	SSB	0.1	15.8	19.1	35.1
06/17/13	11:45	SSC	0.5	8.1	25.5	34.1
07/24/13	9:18	NSA	0.4	88.2	85.0	173.6
07/24/13	9:43	NSB	0.1	74.1	124.3	198.6
07/24/13	10:42	SSA	0.2	59.8	115.7	175.7
07/24/13	11:08	SSB	0.6	106.5	76.4	183.6
07/24/13	11:33	SSC	0.1	71.3	81.4	152.9
08/19/13	9:10	NSA	0.3		59.4	
08/19/13	9:55	NSB	0.2		41.0	
08/19/13	10:52	SSA	0.2		40.6	
08/19/13	11:15	SSB	0.4		24.0	
08/19/13	11:41	SSC	0.2		39.6	
10/21/13	9:22	NSA	0.3			
10/21/13	9:50	NSB	0.1			
10/21/13	10:50	SSA	0.1			
10/21/13	11:17	SSB	0.1			
10/21/13	11:45	SSC	0.1			
11/04/13	9:16	NSA	0.1		130.7	
11/04/13	9:44	NSB	0.1		136.4	
11/04/13	10:51	SSA	0.2		67.1	
11/04/13	11:15	SSB	0.1		114.3	
11/04/13	11:40	SSC	0.1		161.4	
12/04/13	9:31	NSA	0.1	50.6	59.3	110.0
12/04/13	10:19	NSB	0.1	103.4	139.3	242.9
12/04/13	11:14	SSA	0.1	172.0	187.1	359.3
12/04/13	11:38	SSB	0.1	142.7	201.4	344.3
12/04/13	12:04	SSC	0.1	135.6	116.4	252.1
02/10/14	9:24	NSA	0.2	136.2	182.9	319.3
02/10/14	9:52	NSB	0.4	103.2	180.0	283.6
02/10/14	10:55	SSA	0.3	98.3	190.0	288.6

Table A1.5 (Cont.)

Date	Time	Location	NH_4^+	DON	$NO_3^- + NO_2^-$	TN
02/10/14	11:20	SSB	0.4	97.5	191.4	289.3
02/10/14	11:48	SSC	0.3	74.7	173.6	248.6
02/24/14	9:20	NSA	0.1	45.4	404.3	449.8
02/24/14	9:44	NSB	0.1	61.4	293.6	355.1
02/24/14	10:44	SSA	0.2	144.6	252.9	397.7
02/24/14	11:01	SSB	0.2	71.4	156.4	228.0
02/24/14	11:26	SSC	0.1	44.9	170.7	215.8

APPENDIX 2. WEST HAWAIʻI DATA

Table A2.1. Cumulative precipitation collector precipitation depth, d18O, and d2H values by measurement period.

Station Name	Period	Depth (mm)	$\delta^{18}O$ (‰)	$\delta^{2}H$ (‰)
Kīholo Bay	10/2012-3/2013	51	-2.21	-2.93
	3/2013-11/2013	99	-3.03	-10.79
	11/2013-5/2014	121	-4.19	-16.88
	5/2014-12/2014	75	-4.54	-23.11
Palamanui	10/2012-3/2013	141	-3.23	-12.37
	3/2013-11/2013	421	-2.76	-5.08
	11/2013-5/2014	558	-4.13	-15.58
	5/2014-12/2014	417	-3.57	-12.1
Mamalahoa	10/2012-3/2013	223	-4.14	-19.96
	3/2013-11/2013	394	-3.03	-7.68
	11/2013-5/2014	429	-4.18	-15.71
	5/2014-12/2014	495	-4.19	-15.78
NELHA	10/2012-3/2013	97	-2.41	-4.34
	3/2013-11/2013	141	-3.02	-8.45
	11/2013-5/2014	338	-4.03	-16.03
	5/2014-12/2014	179	-3.39	-12.27
Wilkins	10/2012-3/2013	185	-3.89	-16.54
	3/2013-11/2013	608	-2.95	-5.49
	11/2013-5/2014	604	-3.91	-12.06
	5/2014-12/2014	613	-3.4	-9.13
Puʻu Kemole	10/2012-3/2013	116	-6.21	-36.79
	3/2013-11/2013	474	-4.37	-17.8
	11/2013-5/2014	747	-7.23	-41.5
	5/2014-12/2014	602	-6.4	-34.04
Puʻu Waʻa Waʻa	10/2012-3/2013	86	-6.11	-34.54
	3/2013-11/2013	335	-3.78	-11.42
	11/2013-5/2014	423	-6.33	-32.98
	5/2014-12/2014	476	-5.33	-23.88
Holualoa	10/2012-3/2013	88	-3.79	-15.16
	3/2013-11/2013	141	-3.55	-11.9
	11/2013-5/2014	251	-5.67	-27.91
	5/2014-12/2014	291	-5.22	-23.06

Table A2.2. West Hawai‘i individual groundwater sample basic water quality parameters. Missing values indicate parameter not measured.

Group	Sample Location	Date	Time	Temperature (°C)	Salinity (PSU)	pH	DO (mg/L)
Kīholo Coastal	Hind Well	10/27/12	11:03	22.26	2.08	7.70	8.06
		3/31/12	8:57	21.46	2.05	7.74	8.43
	Kīholo Lava Tube	10/27/12	13:06	21.42	1.80	7.70	8.12
		3/31/12	10:17	21.68	1.84	7.80	8.42
	5352-01	10/26/11	13:38	22.70	1.19	8.03	8.01
		3/21/11	16:10	22.46	1.55		8.56
		3/29/12	15:05	22.51	1.82	8.04	8.02
Kīholo Upland	4950-01	10/26/11	11:36	22.73	0.25	8.20	7.77
		3/23/11	10:55	22.63	0.25		8.08
		3/29/12	13:10	22.72	0.24	8.26	7.84
	4850-01	10/25/11	13:30	23.26	0.18	8.10	7.36
		3/23/11	9:43	23.58	0.19		8.08
		3/29/12	12:18	23.78	0.19	8.28	8.04
	4650-01	10/25/11	14:22	23.60	0.08	8.22	7.26
		3/23/11	8:15	23.59	0.12		7.43
Ka‘ūpūlehu Coastal	4859-01	3/28/12	13:30	26.01	2.06	6.88	1.76
	King's Pond Well	10/28/11	15:34	24.44	19.83	7.68	5.88
		3/26/12	14:15	23.68	18.60	7.65	6.61
	Waiokane Piezometer	10/28/11	9:00	23.29	8.64	7.63	6.27
Ka‘ūpūlehu Middle	4757-01	3/27/12	12:50	20.99	1.53	6.97	6.91
		10/27/11	14:24	21.20	1.05	6.88	6.09
		3/24/11	11:00	20.88	1.58		4.71
	4757-02	10/27/11	12:47	19.92	0.46	6.98	6.42
		3/24/11	10:10	19.04	0.78		6.49
		3/27/12	12:10	19.31	0.78	7.14	6.47
	4856-01	3/27/12	11:20	21.21	0.80	7.41	6.49
		3/24/11	8:40	20.91	0.82		6.59
	4856-02	3/27/12	13:40	23.68	1.04	7.48	5.63
		10/27/11	13:41	23.84	0.84	7.34	5.58
		3/24/11	9:28	23.57	1.29		5.60
Ka‘ūpūlehu Upland	4658-01	3/27/12	8:55	21.45	0.73	7.14	6.21
	4658-02	10/27/11	9:02	21.24	0.81	6.98	6.20
		3/24/11	12:04	21.28	0.78		6.57
	4657-01	10/27/11	11:48	21.69	1.02	6.96	5.77
	4657-02	3/27/12	9:36	22.47	0.72	7.26	6.54
		3/24/11	12:50	22.56	0.73		10.41

Table A2.2 (Cont.)

Group	Sample Location	Date	Time	Temperature (°C)	Salinity (PSU)	pH	DO (mg/L)
Kaʻūpūlehu Upland (Cont.)	4657-03	3/27/12	8:10	20.57	0.65	7.13	6.48
		10/27/11	10:12	20.62	0.75	6.91	6.23
		3/24/11	13:40	20.50	0.71		6.57
	4656-01	10/27/11	10:56	21.07	0.51	6.92	4.65
		3/27/12	10:23	20.83	0.34	7.13	4.74
	4656-02	3/28/12	8:08	18.42	0.28	7.10	6.07
Kohanaiki North	4161-04	10/24/11	8:42	19.47	7.77	7.95	8.64
		3/30/12	6:47	19.36	7.78	7.93	8.77
	4161-05	10/24/11	9:20	20.15	8.06	7.90	8.40
		3/30/12	11:33	19.42	7.78	7.86	8.63
	4161-06	10/24/11	9:51	19.25	7.80	7.85	8.33
	4161-07	3/30/12	7:15	18.79	9.52	7.84	7.78
	4161-08	10/24/11	11:15	19.22	8.46	7.66	7.99
		3/30/12	7:40	18.82	8.12	7.86	8.17
Kohanaiki South	4162-06	10/30/12	12:20	20.75	11.76	7.11	7.12
	4162-07	10/24/11	15:42	20.97	10.33	7.27	7.73
		10/30/12	11:28	20.84	11.42	7.45	7.43
	4162-04	10/24/11	12:15	21.53	10.50	6.94	7.53
		10/30/12	10:20	21.38	10.02	6.84	7.22
	4161-11	10/24/11	14:02	21.41	8.31	6.91	7.33
		10/30/12	9:28	21.09	8.88	7.16	7.43
	4161-12	10/24/11	14:40	21.49	8.64	7.43	7.96
		10/30/12	8:06	19.49	8.51	7.61	7.92
		3/30/12	8:19	20.13	7.91	7.64	8.12
Kaloko-Honokōhau	Expansion Well 2	10/26/11	15:29	23.24	4.59	6.94	3.05
		10/27/12	8:45	22.65	5.17	6.90	2.67
		3/25/12	15:44	22.65	6.11	6.88	2.75
	4161-01	10/29/12	9:40	20.30	6.09	7.10	5.46
	4161-02	10/29/12	12:40	20.93	4.93	7.55	6.31
	4061-01	10/29/12	11:40	21.07	11.10	6.76	4.93
Keauhou North High Level	4158-02	10/26/11	9:50	21.88	0.10	7.86	7.79
		3/22/11	9:45	21.79	0.10		7.71
		3/29/12	10:45	21.80	0.10	7.94	7.88
	4258-03	3/22/11	8:50	20.99	0.11		
	4358-01	3/22/11	7:50	23.02	0.13		6.81
		10/26/11	10:40	23.26	0.13	7.91	6.84
		3/29/12	11:15	23.15	0.13	7.98	6.90

Table A2.2 (Cont.)

Group	Sample Location	Date	Time	Temperature (°C)	Salinity (PSU)	pH	DO (mg/L)
Keauhou South Basal	3657-01	3/22/11	12:45	20.80	0.21		
		3/29/12	7:53	20.62	0.23	8.04	8.65
	3557-04	3/22/11	13:55	20.18	0.36		
Keauhou South High Level	4057-01	10/26/11	8:55	21.02	0.06	8.04	8.20
		3/22/11	10:40	21.24	0.07		
		3/29/12	9:56	20.87	0.07	8.10	8.28
	3957-05	3/29/12	9:15	21.06	0.07	8.08	8.27
	3857-04	10/26/11	8:00	21.11	0.06	7.86	8.28
		3/22/11	11:18	21.16	0.06		
		3/29/12	8:40	21.18	0.06	8.18	8.35

Table A2.3. West Hawai‘i individual groundwater sample nutrient and DIC concentrations in units of μM. Missing values indicate parameter not measured.

Group	Sample Location	Date	Time	PO_4^{3-}	SiO_4^{4-}	NO_3^-	DIC
Kīholo Coastal	Hind Well	10/27/12	11:03	2.49	954	57.7	1408
		3/31/12	8:57	2.17	738	54.8	689
	Kīholo Lava Tube	10/27/12	13:06	2.40	880	48.0	1370
		3/31/12	10:17	1.92	745	45.9	1097
	5352-01	10/26/11	13:38	2.23	857	58.6	1283
		3/21/11	16:10	2.16	859	66.2	
		3/29/12	15:05	1.83	833	54.8	843
Kīholo Upland	4950-01	10/26/11	11:36	1.34	776	55.2	1250
		3/23/11	10:55	1.29	1004	61.6	
		3/29/12	13:10	1.05	752	52.2	927
	4850-01	10/25/11	13:30	2.09	767	80.1	1367
		3/23/11	9:43	2.05	760	91.0	
		3/29/12	12:18	1.85	747	76.8	1200
	4650-01	10/25/11	14:22	1.03	801	32.7	1175
		3/23/11	8:15	0.93	956	34.8	
Ka‘ūpūlehu Coastal	4859-01	3/28/12	13:30	0.30	760	107.6	4568
	King's Pond Well	10/28/11	15:34	5.49	433	77.0	2458
		3/26/12	14:15	5.60	486	84.9	
	Waiokane Piezometer	10/28/11	9:00	4.40	881	164.2	3017
Ka‘ūpūlehu Middle	4757-01	3/27/12	12:50	4.85	1270	113.5	3583
		10/27/11	14:24	5.15	1247	125.0	7433
		3/24/11	11:00	4.84	1338	131.5	
	4757-02	10/27/11	12:47	7.04	1172	200.3	4758
		3/24/11	10:10	6.67	1243	193.8	
		3/27/12	12:10	6.71	1171	166.9	2454
	4856-01	3/27/12	11:20	5.60	1159	140.7	3428
		3/24/11	8:40	5.62	1199	210.6	
	4856-02	3/27/12	13:40	3.98	1089	195.7	2043

Table A2.3 (Cont.)

Group	Sample Location	Date	Time	PO_4^{3-}	SiO_4^{4-}	NO_3^-	DIC
Ka‘ūpūlehu Middle (Cont.)	4856-02 (Cont.)	10/27/11	13:41	4.39	1097	232.8	3892
		3/24/11	9:28	4.19	1133	229.1	
Ka‘ūpūlehu Upland	4658-01	3/27/12	8:55	2.80	1030	185.4	4710
	4658-02	10/27/11	9:02	2.76	1020	239.5	6242
		3/24/11	12:04	2.54	996	263.7	
	4657-01	10/27/11	11:48	2.83	1071	205.1	7100
	4657-02	3/27/12	9:36	1.85	1080	219.7	3183
		3/24/11	12:50	2.30	1070	302.3	
	4657-03	3/27/12	8:10	4.07	1171	184.7	4329
		10/27/11	10:12	4.46	1182	214.2	5283
		3/24/11	13:40	4.38	1243	214.9	
	4656-01	10/27/11	10:56	5.72	1264	123.7	7142
		3/27/12	10:23	5.49	1291	112.3	3906
	4656-02	3/28/12	8:08	5.94	1250	153.7	4240
Kohanaiki North	4161-04	10/24/11	8:42	3.21	673	77.6	1408
		3/30/12	6:47	2.88	631	75.3	451
	4161-05	10/24/11	9:20	3.14	673	75.1	1292
		3/30/12	11:33	3.03	631	70.5	508
	4161-06	10/24/11	9:51	3.54	678	81.7	1425
	4161-07	3/30/12	7:15	3.25	603	69.6	
	4161-08	10/24/11	11:15	3.71	669	70.0	1367
		3/30/12	7:40	3.61	614	67.6	509
Kohanaiki South	4162-06	10/30/12	12:20	3.21	708	100.8	1706
	4162-07	10/24/11	15:42	2.91	595	98.5	1533
		10/30/12	11:28	3.45	656	76.1	1559
	4162-04	10/24/11	12:15	3.30	610	101.6	1442
		10/30/12	10:20	3.67	683	317.7	1550
	4161-11	10/24/11	14:02	3.61	644	95.4	1517
		10/30/12	9:28	4.09	714	81.3	1503
	4161-12	10/24/11	14:40	3.83	656	69.8	1267
		10/30/12	8:06	4.22	688	72.1	1371
		3/30/12	8:19	3.83	617	68.1	1276
Kaloko-Honokōhau	Expansion Well 2	10/26/11	15:29	102.08	573	260.0	1467
		10/27/12	8:45	125.59	624	244.0	1547
		3/25/12	15:44	96.23	606	657.9	982
	4161-01	10/29/12	9:40	4.97	794	75.9	1202
	4161-02	10/29/12	12:40	5.39	819	97.9	1138
	4061-01	10/29/12	11:40	4.52	681	63.9	1373
Keauhou North High Level	4158-02	10/26/11	9:50	3.97	860	72.9	1242
		3/22/11	9:45	3.93	862	82.4	
		3/29/12	10:45	3.75	846	68.8	1093
	4258-03	3/22/11	8:50	4.26	864	71.8	
	4358-01	3/22/11	7:50	3.89	924	73.0	
		10/26/11	10:40	3.98	909	63.5	1667
		3/29/12	11:15	3.76	905	60.1	1193
Keauhou South Basal	3657-01	3/22/11	12:45	3.77	770	70.2	

Table A2.3 (Cont.)

Group	Sample Location	Date	Time	PO_4^{3-}	SiO_4^{4-}	NO_3^-	DIC
Keauhou Sout Basal (Cont.)	3657-01 (Cont.)	3/29/12	7:53	3.70	754	58.7	637
	3557-04	3/22/11	13:55	4.36	814	86.0	
Keauhou South High Level	4057-01	10/26/11	8:55	3.83	811	79.8	967
		3/22/11	10:40	3.79	808	90.6	
		3/29/12	9:56	3.63	790	75.4	914
	3957-05	3/29/12	9:15	3.74	791	63.7	1070
	3857-04	10/26/11	8:00	4.19	813	69.8	958
		3/22/11	11:18	4.15	978	80.5	
		3/29/12	8:40	4.09	791	65.8	790

Table A2.4. West Hawai‘i individual groundwater sample stable isotope parameters in units of ‰ VSMOW ($\delta^{18}O$ and δ^2H of H_2O), ‰ VAIR ($\delta^{15}N$ of NO_3^-), and ‰ VPDB ($\delta^{13}C$ of DIC). Missing values indicate parameter not measured.

Group	Sample Location	Date	Time	$\delta^{15}N$ of NO_3^-	$\delta^{13}C$ of DIC	$\delta^{18}O$ of H_2O	δ^2H of H_2O
Kīholo Coastal	Hind Well	10/27/12	11:03	2.20	-1.85	-7.33	-47.00
		3/31/12	8:57	13.39	-0.84	-7.38	-47.08
	Kīholo Lava Tube	10/27/12	13:06	4.14	-2.30	-7.40	-47.97
		3/31/12	10:17	6.60	0.10	-7.58	-48.47
	5352-01	10/26/11	13:38	6.00	2.69	-7.71	-52.68
		3/21/11	16:10	4.11		-7.91	-53.90
		3/29/12	15:05	6.39	1.12	-8.11	-53.44
Kīholo Upland	4950-01	10/26/11	11:36	5.40	0.49	-8.25	-54.72
		3/23/11	10:55	0.97		-7.78	-50.54
		3/29/12	13:10	5.63	-0.39	-8.30	-54.05
	4850-01	10/25/11	13:30	3.57		-7.98	-51.60
		3/23/11	9:43	5.31		-7.78	-50.54
		3/29/12	12:18	3.94	-1.22	-7.92	-51.10
	4650-01	10/25/11	14:22	6.41		-8.24	-53.48
		3/23/11	8:15	0.62		-8.02	-53.17
Ka‘ūpūlehu Coastal	4859-01	3/28/12	13:30	6.49	-1.19	-5.50	-30.08
	King's Pond Well	10/28/11	15:34	7.45	-2.22	-2.13	-11.22
		3/26/12	14:15	6.78	-2.54	-2.63	-13.06
	Waiokane Piezometer	10/28/11	9:00	3.91	-1.84	-4.37	-23.21
Ka‘ūpūlehu Middle	4757-01	3/27/12	12:50	4.55	-1.98	-5.81	-31.81
		10/27/11	14:24	7.58	-2.86	-5.68	-30.95
		3/24/11	11:00	1.96		-5.48	-30.91
	4757-02	10/27/11	12:47	6.30	-2.45	-5.75	-31.23
		3/24/11	10:10	2.84		-5.48	-30.62
		3/27/12	12:10	3.63	-1.67	-5.83	-31.27
	4856-01	3/27/12	11:20	2.81	-1.91	-5.69	-30.84
		3/24/11	8:40	7.17		-5.47	-30.77
	4856-02	3/27/12	13:40	2.77	-2.46	-5.63	-30.75
		10/27/11	13:41	4.92	-2.46	-5.57	-30.76
		3/24/11	9:28	0.74		-5.42	-30.98

Table A2.4 (Cont.)

Group	Sample Location	Date	Time	$\delta^{15}N$ of NO_3^-	$\delta^{13}C$ of DIC	$\delta^{18}O$ of H_2O	$\delta^{2}H$ of H_2O
Kaʻūpūlehu Upland	4658-01	3/27/12	8:55	3.47	-1.83	-5.54	-29.25
	4658-02	10/27/11	9:02	5.76	-1.20	-5.44	-29.55
		3/24/11	12:04	2.56		-5.31	-28.53
	4657-01	10/27/11	11:48	5.98	-1.44	-5.61	-29.57
	4657-02	3/27/12	9:36	3.83	-2.72	-5.56	-30.00
		3/24/11	12:50	0.85		-5.31	-29.76
	4657-03	3/27/12	8:10	2.46	-2.03	-5.63	-30.35
		10/27/11	10:12	4.62	-1.50	-5.52	-30.81
		3/24/11	13:40	2.26		-5.40	-30.17
	4656-01	10/27/11	10:56	7.20		-5.81	-32.43
		3/27/12	10:23	4.29	-1.35	-5.86	-32.37
	4656-02	3/28/12	8:08	3.23	-1.26	-5.85	-31.39
Kohanaiki North	4161-04	10/24/11	8:42	4.78	-1.55	-5.10	-29.89
		3/30/12	6:47	11.50	-1.78	-5.17	-30.17
	4161-05	10/24/11	9:20	5.40	-1.09	-5.16	-29.65
		3/30/12	11:33	11.35	-1.80	-4.96	-28.90
	4161-06	10/24/11	9:51	4.46	-1.12	-4.82	-27.65
	4161-07	3/30/12	7:15	11.32	-1.39	-4.47	-24.88
	4161-08	10/24/11	11:15	5.18	-0.86	-4.51	-24.54
		3/30/12	7:40	12.32	-1.74	-4.42	-24.17
Kohanaiki South	4162-06	10/30/12	12:20	3.11	-3.68	-4.06	-23.14
	4162-07	10/24/11	15:42	5.45	-0.92	-4.15	-23.11
		10/30/12	11:28	2.47	-2.80	-4.09	-23.69
	4162-04	10/24/11	12:15	5.39	-3.10	-3.97	-21.90
		10/30/12	10:20	1.71	-6.23	-4.04	-22.32
	4161-11	10/24/11	14:02	5.02	-3.46	-4.20	-22.56
		10/30/12	9:28	2.14	-5.32	-4.20	-22.57
	4161-12	10/24/11	14:40	4.87	-1.14	-4.30	-23.34
		10/30/12	8:06	3.76	-3.48	-4.25	-22.58
		3/30/12	8:19	11.57	-2.36	-4.36	-23.65
Kaloko-Honokōhau	Expansion Well 2	10/26/11	15:29	43.08	-8.11	-3.47	-19.45
		10/27/12	8:45	42.75	-11.44	-3.56	-18.67
		3/25/12	15:44	28.82	-9.01	-3.77	-19.13
	4161-01	10/29/12	9:40	3.83	-5.24	-4.05	-19.47
	4161-02	10/29/12	12:40	4.92	-5.21	-3.81	-18.20
	4061-01	10/29/12	11:40	3.36		-3.56	-18.21
Keauhou North High Level	4158-02	10/26/11	9:50	6.37		-7.02	-43.98
		3/22/11	9:45	1.01		-6.79	-41.78
		3/29/12	10:45	3.96		-7.12	-42.77
	4258-03	3/22/11	8:50	2.88		-7.12	-44.16
	4358-01	3/22/11	7:50	1.74		-6.63	-40.86
		10/26/11	10:40	6.52	-5.33	-6.77	-41.32
		3/29/12	11:15	4.88	-3.33	-6.80	-40.94
Keauhou South Basal	3657-01	3/22/11	12:45	1.99		-4.05	-17.95
		3/29/12	7:53	5.81	-8.92	-4.14	-18.69
	3557-04	3/22/11	13:55	0.33		-5.18	-28.01

Table A2.4 (Cont.)

Group	Sample Location	Date	Time	$\delta^{15}N$ of NO_3^-	$\delta^{13}C$ of DIC	$\delta^{18}O$ of H_2O	$\delta^{2}H$ of H_2O
Keauhou South High Level	4057-01	10/26/11	8:55	5.47	-7.96	-5.65	-30.85
		3/22/11	10:40	-2.15		-5.51	-30.19
		3/29/12	9:56	4.24		-5.65	-31.06
	3957-05	3/29/12	9:15	4.21	-8.58	-5.22	-26.30
	3857-04	10/26/11	8:00	7.84		-5.38	-28.34
		3/22/11	11:18	2.07		-5.10	-26.56
		3/29/12	8:40	4.58		-5.38	-28.85

REFERENCES

Aravena, R., and Robertson, W. D., 1998, Use of multiple isotope tracers to evaluate denitrification in ground water: study of nitrate from a large-flux septic system plume. Ground Water, 36(6), 975-982.

Armstrong, F., Stearns, C., and Strickland, J., 1967, The measurement of upwelling and subsequent biological process by means of the Technicon Autoanalyzer and associated equipment. Deep-Sea Res., 14(3), 381-389.

Bauer, G.R., 2003, A study of ground-water conditions in North and South Kona and South Kohala districts: Island of Hawaii, 1991-2002. Final report submitted to the Commission on Water Resource Management, State of Hawaii, 95 p.

Beck, A.J., Tsukamoto, Y., Tovar-Sanchez, A., Huerta-Diaz, M., Bokuniewicz, H.J., and Sanudo-Wilhelmy, S.A., 2007, Importance of geochemical transformations in determining submarine groundwater discharge-derived trace metal and nutrient fluxes. Applied Geochemistry, v. 22, p. 477-490.

Bishop, J.M., Glenn, C.R., Amato, D.W., and Dulai, H., 2015, Effect of land use and groundwater flow path on submarine groundwater discharge nutrient flux. J. Hydrol.: Reg. Stud., http://dx.doi.org/10.1016/j.ejrh.2015.10.008.

Böhlke, J.K., and Coplen, T.B., 1995, Interlaboratory comparison of reference materials for nitrogen-isotope-ratio measurements, in Reference and intercomparison materials for stable isotopes of light elements. Vienna, International Atomic Energy Agency, IAEA-TECDOC-825, 51-66.

Bowles, S.P., 2007, Evidence and implications of saline cold ground-water, Honokohau, Hawaii. Report by Waimea Water Service Inc., appendix G-2 in Kona Kai Ola environmental impact statement, 7 p.

Bricker, S., Longstaff, B., Dennison, W., Jones, A., Boicourt, K., Wicks, C. and Woerner, J., 2007, Effects of nutrient enrichment in the nation's estuaries: a decade of change. NOAA Coastal Ocean Program Decision Analysis Series No. 26., National Centers for Coastal Ocean Science, Silver Spring, MD, 328 p.

Bruno, J. F. and Selig, E. R., 2007, Regional decline of coral cover in the Indo-Pacific: timing, extent, and subregional comparisons. PLoS ONE, 2(8), e711. http://dx.doi.org/10.1371/journal.pone.0000711

Burnett, W.C., H. Bokuniewicz, M. Huettel, W.S. Moore, and Taniguchi, M., 2003, Groundwater and porewater inputs to the coastal zone. Biogeochemistry, 66, 3-33.

Burnett, W.C., and Dulaiova, H., 2003, Estimating the dynamics of groundwater input into the coastal zone via continuous radon-222 measurements. Journal of Environmental Radioactivity, 69, 21-35.

Clark, I.D., and Fritz, P., 1997, Environmental isotopes in hydrology. New York, CRC Press, 328 p.

Clark, I.D., Fritz, P., Michael, F.A., and Souther, J.G., 1982, Isotope hydrogeology and geothermometry of the Mount Meager geothermal area. Canadian Journal of Earth Sciences, 19(7), 1454-1473

Craig, H., 1961. Isotopic variations in meteoric waters. Science 133 (3465), 1702–1703. http://dx.doi.org/10.1126/science.133.3465.1702.

Cyronak, T., Santos, I.R., Erler, D.V., and Eyre, B.D., 2013, Groundwater and porewater as major sources of alkalinity to a fringing coral reef lagoon (Muri Lagoon, Cook Islands). Biogeosciences, 10, 2467-2480.

Cyronak, T., Santos, I.R., Erler, D.V., Maher, T., and Eyre, B.D., 2014, Drivers of pCO2 variability in two contrasting coral reef lagoons: The influence of submarine groundwater discharge, Global Biogeochem. Cycles, 28, http://dx.doi.org 10.1002/2013GB004598.

Dailer, M.L., Knox, R.S., Smith, J.E., Napier, M., and Smith, C.M., 2010, Using 15N values in algal tissue to map locations and potential sources of anthropogenic nutrient inputs on the island of Maui, Hawai‘i, USA. Marine Pollution Bulletin, 60, 655-671.

Dailer, M.L., Ramey, H.L., Saephan, S., and Smith, C.M., 2012, Algal δ15N values detect a wastewater effluent plume in nearshore and offshore surface waters and three-dimensionally model the plume across a coral reef on Maui, Hawai‘i, USA. Marine Pollution Bulletin, 64, 207-213.

Dansgaard, W., 1964. Stable isotopes in precipitation. Tellus, 5, 461-469.

Deenik, J., and McClellan, A.T., 2007, Soils of Hawai‘i. University of Hawai‘i at Manoa, College of Tropical Agriculture and Human Resources Publication SCM-20, 12 p. http://www.ctahr.Hawai‘i.edu/oc/freepubs/pdf/SCM-20.pdf

DeGeorges, A., Goreau, T.J., and Reilly, B., 2010, Land-sourced pollution with an emphasis on domestic sewage: lessons from the Caribbean and implications for coastal development on Indian ocean and Pacific coral reefs. Sustainability, 2, 2919-2949.

Dollar, S., and Andrews, C., 1997, Algal blooms off west Maui—assessing causal linkages between land and the coast ocean. Final Report for National Oceanic and Atmospheric Administration Coastal Ocean Program Office and University of Hawai‘i Sea Grant College Program, Honolulu, HI.

Dollar, S. J., and Atkinson, M.J., 1992, Effects of nutrient subsidies from groundwater to neatshore marine ecosystems off the island of Hawai‘i: Estuar. Coast. Shelf Sci. 35: 409–424, http://dx.doi.org/10.1016/S0272-7714(05)80036-8

Dubrovsky, N.M., Burrow, K.R., Clark, G.M., Gronberg, J.M., Hamilton, P.A., Hitt, K.J., Mueller, D.K., Munn, M.D., Nolan, B.T., Puckett, L.J., Rupert, M.G., Short, T.M., Spahr, N.E., Sprague, L.A., and Wilber, W.G., 2010, The quality of our nation’s water – nutrients in the nation’s streams and groundwater, 1992-2004. U.S. Geological Sruvey Circular 1350, 174 p.

Engott, J.A., 2011. A water-budget model and assessment of groundwater recharge for the Island of Hawai‘i. United States Geological Survey Water-Resources Investigations Report, 2011–5078.

Engott, J.A., and Vana, T.T., 2007, Effects of Agricultural Land-Use Changes and Rainfall on Ground-Water Recharge in Central and West Maui, Hawai‘i, 1926-2004. U.S. Geological Survey Scientific Investigations Report 2007-5103, 56 p.

Fackrell, J.K., and Glenn, C.R., 2014. How much do high-level aquifers impact SGD and the coastal zone in Hawai‘i? Unscrambling the mix with water isotopes. February 23–28, 2014 Ocean Science Meeting, Honolulu, HI. http://www.sgmeet.com/osm2014/static/files/osm2014-program-low.pdf

Faust, S. D., and Aly, O. M., 1998, Chemistry of water treatment, second edition. Boca Raton, Florida, CRC Press, 587 p.

Flinders, A.F., Ito, G., Garcia, M.O., Sinton, J.M., Kauahikaua, J., and Taylor, B., 2013. Intrusive dike complexes, cumulate cores, and the extrusive growth of Hawaiian volcanoes. Geophys. Res. Lett. 40 (13), 3367–3373, http://dx.doi.org/10.1002/grl.50633.

Frans, L.M., Rupert, M.G., Hunt, C.D., and Skinner, K.D., 2012, Groundwater quality in the Columbia plateau, Snake River plain, and Oahu basaltic rock and basin fill aquifers in the northwestern United States and Hawai‘i, 1992-2010. U.S. Geological Survey Scientific Investigations Report 2012-51523, 84p.

Froelich P. N., Klinkhammer G. P., Bender M. L., Luedtke N., Heath G. R., Cullen D., Dauphin P., Hammond D., Hartman B., and Maynard V., 1979, Early oxidation of organic matter in pelagic sediments of the eastern equatorial Atlantic: suboxic diagenesis. Geochim. Cosmochim. Acta, 43, 1075–1090.

Garrison, G.H., Glenn, C.R., and McMurtry, G.M., 2003, Measurement of submarine groundwater discharge in Kahana Bay, O‘ahu, Hawai‘i. Limnology and Oceanography, 48(2), 920-928.

Gerlach, T.M., and Thomas, D.M., 1986, Carbon and sulphur isotopic composition of Kilauea parental magma. Nature, 319, 480-483.

Giambelluca, T.W., Chen, Q., Frazier, A.G., Price, J.P., Chen, Y.-L., Chu, P.-S., Eischeid, J.K., andDelparte, D.M., 2013, Online rainfall atlas of Hawai’i. B. Am.Meteor. Soc. 94, 313–316, http://dx.doi.org/10.1175/BAMS-D-11-00228.1.

Giambelluca, T.W., Sanderson, M., 1993. The water balance and climatic classification. In: Sanderson, M. (Ed.), Prevailing Trade Winds: Weather and Climate in Hawai‘i. University of Hawaii Press, Honolulu, pp. 56–72.

Giambelluca, T.W., Shuai, X., Barnes, M.L., Alliss, R.J., Longman, R.J., Miura, T., Chen, Q., Frazier, A. G., Mudd, R.G., Cuo, L., Businger, A.D., 2014. Evapotranspiration of Hawai‘i. Final report submitted to the U.S. Army Corps of Engineers—Honolulu District, and the Commission on Water Resource Management, State of Hawaii. http://evapotranspiration.geography.hawaii.edu/

Gingerich, S. B., and Engott, J.A., 2012, Groundwater availability in the Lahaina district, West Maui, Hawai‘i. U.S. Geological Survey Scientific Investigations Report 2012-5010, 90 p.

Glenn, C.R., Whittier, R.B., Dailer, M.L., Dulaiova, H., El-Kadi, A.I., Fackrell, J., Kelly, J.L., and Waters, C.A., 2012, Lahaina Groundwater Tracer Study – Lahaina, Maui, Hawai‘i.

Final Interim Report prepared for the State of Hawai‘i Department of Health, the U.S. Environmental Protection Agency, and the U.S. Army Engineer Research and Development Center. http://www.epa.gov/region9/water/groundwater/uic-pdfs/lahaina02/lahaina-final-interim-report.pdf

Glenn, C.R., Whittier, R.B., Dailer, M.L., Dulaiova, H., El-Kadi, A.I., Fackrell, J., Kelly, J.L., Waters, C.A., and Sevadjin, J, 2013, Lahaina Groundwater Tracer Study – Lahaina, Maui, Hawai‘i. Final Report prepared for the State of Hawai‘i Department of Health, the U.S. Environmental Protection Agency, and the U.S. Army Engineer Research and Development Center. http://www.epa.gov/region9/water/groundwater/uic-pdfs/lahaina02/lahaina-gw-tracer-study-final-report-june-2013.pdf

Gonneea, M.E., and Charette, M.A., 2014, Hydrologic controls on nutrient cycling in an unconfined coastal aquifer. Environmental Science and Technology, v. 48, p. 14178-14185.

Granger, J., Sigman, D. M., Lehmann, M. F., and Torell, P.D., 2008, Nitrogen and oxygen fractionation during dissimilatory nitrate reduction by denitrifying bacteria. Limnology and Oceanography, 53(6), 2533-2545.

Granger, J., Sigman, D. M., Prokopenko, M., Lehmann, M. F., and Tortell, P. D., 2006, A method for nitrite removal in nitrate N and O isotope analysis. Limnology and Oceanography: Methods, 4, 205-212.

Grasshoff K., Ehrhardt M., and Kremling K., 1983, Methods of Seawater Analysis, second revised and extended edition, Weinheim, Verlag Chemie GmbH, 447 p.

Griffith, D.R., Barnes, R.T., and Raymond, R.A., 2009, Inputs of fossil carbon from wastewater treatment plants to U.S. rivers and oceans. Environmental Science and Technology, 43(15), 5647-5651.

Hawaii Commission on Water Resource Management, 2008, Groundwater index wells database for the main Hawaiian islands.

Henley, R.W., and Ellis, A.J., 1983, Geothermal systems ancient and modern: a geochemical review. Earth Science Reviews, 19, 1-50.

Henze, M., Harremoes, P., Arvin, E., and la Cour Jansen, J., 2002, Wastewater treatment: biological and chemical processes, third edition. Berlin, Springer-Verlag, 433 p.

Hoegh-Guldberg, O., Mumby, P.J., Hooten, A.J., Steneck, R.S., Greenfield, P., Gomez, E., Harvell, C.D., Sale, P.F., Edwards, A.J., Caldiera, K., Knowlton, N., Eakin, C.M., Iglesias-Prieto, R.,Muthiga, N., Bradbury, R.H., Dubi, A., and Hatziolos, M.E., 2007, Coral reefs under rapid climate change and ocean acidification. Science, 318, 1737-1742.

Hoellein, T.J., Bruesewitz, D.A., and Hamilton, D.P., 2012, Are geothermal streams important sites of nutrient uptake in an agricultural and urbanising landscape (Rotorua, New Zealand)? Freshwater Biology, 57, 116-128, http://dx.doi.org/10.1111/j.1365-2427.2011.02702.x

Holloway, J.A., Nordstrom, D.K., Böhlke, J.K., McCleskey, R.B., and Ball., J.W., 2011, Ammonium in thermal waters of Yellowstone National Park: processes affecting speciation and isotope fractioination. Geochimica et Cosmochimica Acta, 75, 4611-4636, http://dx.doi.org/10.1016/j.gca.2011.05.036

Howarth, R. W., and Marino, R., 2006, Nitrogen as the limiting nutrient for eutrophication in coastal marine ecosystems: evolving views over three decades. Limnology and Oceanography, 51(1-2), 364-376.

Hunt, C.D., Jr., 2014, Baseline water-quality sampling to infer nutrient and contaminant sources and Kaloko-Honokōhau National Historical Park, island of Hawai‘i, 2009. U.S. Geological Survey Scientific Investigations Report 2014-5158, 52 p.

Hunt, C.D., Jr., and Rosa, S.N., 2009, A Multitracer approach to detecting wastewater plumes from municipal injection wells in near shore marine waters at Kihei and Lahaina, Maui, Hawai‘i. U.S. Geological Survey Scientific Investigations Report 2009-5253, 166 p.

Hwang, D.W., Kim, G., Lee, Y.W., Yang, H.S., 2005, Estimating submarine inputs of groundwater and nutrients to a coastal bay using radium isotopes. Marine Chemistry, 96(1), 61-71.

Johnson, A. G., Glenn, C. R., Burnett, W. C., Peterson, R. N., and Lucey, P. G., 2008, Aerial infrared imaging reveals large nutrient-rich groundwater inputs to the ocean: Geophysical Research Letters, 35, http://dx.doi.org 10.1029/2008GL034574.

Izuka, S.K., Engott, J.A., Bassiouni, M., Johnson, A.G., Miller, L.D., Rotzoll, K.,and Mair, M, 2016, Volcanic aquifers of Hawaii – hydrogeology, water budgets, and conceptual models. U.S. Geological Survey Scientific Investigations Report 2015-5164, 158 p., http://dx.doi.org/10.3133/sir20155164.

Kauahikaua, J., Hildenbrand, T., Webring, M., 2000, Deep magmatic structures of Hawaiian volcanoes, imaged by three-dimensional gravity models. Geology, 28, 883-886. http://dx.doi.org/10.1130/0091-7613(2000)28<883:DMSOHV>2.0.CO;2

Kay, E. A., Lau, L.S., Stroup, E.D., Dollar, S.J., Fellows, D.P., and Young, R.H.F., 1977, Hydrologic and ecologic inventories of the coastal waters of west Hawai‘i: Technical Report 105. Sea Grant Cooperative Report UNIHI-SEAGRANT-CR-77-02.

Kehew, A.E., 2000, Applied chemical hydrogeology. Upper Saddle River, New Jersey, Prentice Hall, 368 p.

Kelly, J.L., Glenn, C.R., 2015. Chlorofluorocarbon apparent ages of groundwaters from west Hawaii, USA. J. Hydrol. 527, 355-366, http://dx.doi.org/10.1016/j.jhydrol.2015.04.069

Kendall, C., 1998, Tracing nitrogen sources and cycling in catchments. In: Kendall, C., and McDonnell, J.J. (Eds.), Catchment Hydrology. Amsterdam, Elsevier Science, pp. 519-576.

Kendall, C., and Aravena, R., 2000, Nitrate isotopes in groundwater systems. In: Cook, P., and Herczeg, A. L., eds., Environmental Tracers in Subsurface Hydrology: Boston, Kluwer Academic Publishers, p. 261-297.

Knee, K.L., Street, J.H., Grossman, E.E., Boehm, A.B., and Paytan, A., 2010, Nutrient inputs to the coastal ocean from submarine groundwater discharge in a groundwater-dominated system: Relation to land use (Kona coast, Hawai‘i, U.S.A.), Limnology and Ocenaography, 55(3), 1105-1122, http://dx.doi.org/10.4319/lo.2010.55.3.1105.

Kroeger, K.D., and Charette, M.A., 2008, Nitrogen biogeochemistry of submarine groundwater discharge. Limnology and Oceanography, 53(3), 1025-1039.

Kroeger, K.D., Cole, M.L., York, J.K., and Valiela, I., 2006, Nitrogen loads to estuaries from waste water plumes: modeling and isotopic approaches. Groundwater, 44(2), 188- 200.

Kuenen, J.G., 2008, Anammox bacteria: from discovery to application. Nature Rev. Microbiology, v. 6, no. 4, p. 320-326, http://dx.doi.org/10.1038/nrmicro1857.

Kuypers, M.M.M., Lavik, G., Woebken, D., Schmid, M., Fuchs, B.M., Amann, R., Jørgensen, B.B., and Jetten, M.S.M., 2005, Massive nitrogen loss from the Benguela upwelling system through anaerobic ammonium oxidation, Proc. Natl. Acad. Sci. USA, 102, 6478–6483, http://dx.doi.org/10.1073/pnas.0502088102.

Kwon, E.Y., Kim, G., Primeau, F., Moore, W.S., Cho, H. M., DeVries, T., Sarmiento, J.L., Charette, M.A., and Cho, Y.K., 2014, Global estimate of submarine groundwater discharge based on an observationally constrained radium isotope model. Geophysical Research Letters, 41: 8438-8444, http://dx.doi.org/10.1002/2014GL061574.

LaPointe, B.E., Clark, M.W., 1992, Nutrient inputs from the watershed and coastal eutrophication in the Florida Keys. Estuaries, 15(4), 465-476.

Lapointe, B.E., O'Connell, J.D., and Garrett, G.S., 1990, Nutrient couplings between on-site sewage disposal systems, groundwaters, and nearshore surface waters of the Florida Keys. Biogeochemisry, 10, 289-307.

Laws, E.A., Brown, D., and Peace, C., 2004, Coastal water quality in the Kihei and Lahaina districts of the island of Maui, Hawai'ian Islands. Impacts from physical habitat and groundwater seepage: implications for water quality standards. International Journal of Environment and Pollution, 22, 531-547.

Lee, Y., Hwang, D., Kim, G., Lee, W., and Oh., H, 2009, Nutrient inputs from submarine groundwater discharge (SGD) in Masan Bay, an embayment surrounded by heavily industrialized cities, Korea. Science of the Total Environment, 407, 3181-3188.

Lincoln, N., Chadwick, O., and Vitousek, P., 2014, Indicators of soil fertility and opportunities for precontact agriculture in Kona, Hawai'i. Ecosphere, 5(4), 42, http://dx.doi.org/10.1890/ES13-00328.1

Lipman, P.W., and Coombs, M.L., 2006, North Kona slump: Submarine flank failure during the early(?) tholeiitic shield stage of Hualalai Volcano, Journal of Volcanology and Geothermal Research, 151, 189-236, http://dx.doi.org/10.1016/j.jvolgeores.2005.07.029

McCook, L., 1999, Macroalgae, nutrients and phase shifts on coral reefs: scientific issues and management consequences for the Great Barrier Reef. Coral Reefs, 18(4), 357-367.

Moore, J.G., and Clague, D.M., 1992. Volcano growth and evolution of the island of Hawaii. Geol. Soc. Am. Bull.,104 (11), 1471-1484, http://dx.doi.org/10.1130/00167606(1992)104<1471:VGAEOT>2.3.CO;2

Moore, W.S., 1999, The subterranean estuary: a reaction zone of ground water and sea water. Marine Chemistry, 65, 111-125.

Moore, W.S., 2006, The role of submarine groundwater discharge in coastal biogeochemistry. Journal of Geochemical Exploration, 88(1-3), 389-393.

Mulder, A., van de Graaf, A.A., Robertson, L.A., and Kuenen, J.G., 1995, Anaerobic ammonium oxidation discovered in a denitrifying fluidized-bed reactor. FEMS Microbiol Ecol, 16, 177–183.

Murphy, J., and Riley, J., 1962, A modified single solution method for the determination of phosphate in natural waters. Analytica Chimica Acta, 27, 31-36.

Nance, T., 2013. Assessment of the potential impact of the proposed Kaloko Makai project on water resources. Report by Tom Nance Water Resource Engineering, appendix C in Kaloko Makai draft environmental impact statement, 23 p.

Ning, R. Y., 2002, Discussion of Silica Speciation, Fouling, Control and Maximum Reduction. Desalination,151, 67.

National Cooperative Soil Survey (NCSS), 2013, National cooperative soil characterization database. USDA-NRCS, http://ncsslabdatamart.sc.egov.usda.gov (accessed 21 June 2016).

National Oceanic and Atmospheric Administration (NOAA), 2012, Coastal Change Analysis Program Regional Land Cover (C-CAP) Hawai‘i 2005 Land Cover. NOAA Ocean Service, Office for Coastal Management. http://coast.noaa.gov/digitalcoast/data/ccapregional.

Oki, D.S., 1999. Geohydrology and numerical simulation of the ground-water flow system of Kona, island of Hawaii. United States Geological Survey Water-Resources Investigations Report, 99–4073.

Paerl, H.W., 1997, Coastal eutrophication and harmful algal blooms; importance of atmospheric deposition and groundwater as “new” nitrogen and other nutrient sources. Limnology and Oceanography, 42(5-2), 1154-1165.

Paytan, A., Shellenbarger, G.G., Street, J.H., Gonneea, M.E., Davis, K., Young , M.B. ,and Moore, W.S., 2006, Submarine groundwater discharge: an important source of new inorganic nitrogen to coral reef ecosystems. Limnology and Oceanography, 51, 343-348.

Peterson, R.N., Burnett, W.C., Glenn, C.R., and Johnson, A.G., 2007, A box model to quantify groundwater discharge along the Kona coast of Hawai‘i using natural tracers: IAHS Publ. 312, 142-149.

Peterson, R.N., Burnett, W.C., Glenn, C.R., and Johnson, A.G., 2009, Quantification of point-source groundwater discharges to the ocean from the shoreline of the Big Island, Hawai‘i: Limnology and Oceanography, 54(3), 890-904, http://dx.doi.org,10.4319/lo.2009.54.3.0890.

Pringle, C.M., and Triska, F.J., 1991, Effects of geothermal groundwater on nutrient dynamics of a lowland Costa Rican stream. Ecology, 72(3), 951-965.

Prouty, N.G., Swarzenski, P.W., Fackrell, J.K., Johannesson, K., and Palmore, C.D., 2015, Groundwater-derived nutrient and trace element transport to a nearshore Kona coral ecosystem: experimental mixing model results. J. Hydrol.: Reg. Stud., http://dx.doi.org/10.1016/j.ejrh.2015.12.058

Rich, J. J., Dale, O. R., Song, B., Ward, B. B., 2008, Anaerobic ammonium oxidation (anammox) in Chesapeake Bay sediments. Microb. Ecol., 55, 311–320.

Richardson, C.M., Dulai, H., and Whittier, R.B., 2015, Sources and spatial variability of groundwater derived nutrients in Maunalua Bay, Oahu, Hawai‘i. J. Hydrol.: Reg. Stud., http://dx.doi.org/10.1016/j.ejrh.2015.11.006

Salata, G.G., Roelke, L.A., and Cifuentes, L.A., 2000, A rapid and precise method for measuring stable carbon isotope ratios of dissolved inorganic carbon. Marine Chemistry, 69, 153-161.

Sano, Y., Takahata, N., Nishio, Y., Fischer, T.P., and Williams, S.N., 2001, Volcanic flux of nitrogen from the earth. Chemical Geology, 171, 263-271.

Santoro, A.E., 2010, Microbial nitrogen cycling at the saltwater-freshwater interface. Hydrogeology Journal, 18(1), 187-202, http://dx.doi.org/10.1007/s10040-009-0526-z.

Scavia, D., and Bricker, S.B., 2006, Coastal eutrophication assessment in the United States. Biogeochemistry, http://dx.doi.org/10.1007/s10533-006-9011-0.

Scholl, M.A., Gingerich, S.B., Tribble, G.W., 2002. The influence of microclimates and fog on stable isotope signatures used in interpretation of regional hydrology, East Maui, Hawai‘i. J. Hydrol., 264(1-4), 170–184, http://dx.doi.org/10.1016/S0022-1694(02).

Scholl, M.A., Ingebritsen, S.E., Janik, C.J., Kauahikaua, J.P., 1996. Use of precipitation and groundwater isotopes to interpret regional hydrology on a tropical volcanic island: Kilauea volcano area, Hawai‘i. Water Resour. Res. 32, 3525–3537, http://dx.doi.org/10.1029/95wr02837.

Schopka, H.H., and Derry, L.A., 2012, Chemical weathering fluxes from volcanic islands and the importance of groundwater: the Hawai‘ian example. Earth and Planetary Science Letters, 339-340, 67-78, http://dx.doi.org/10.1016/j.epsl.2012.05.028

Sherrod D.R., Sinton, J.M., Watkins, S.E., Brunt, K.M., 2007. Geologic map of the state of Hawai‘i. United States Geological Survey Open File Report, 2007–1089.

Sigman, D. M., Casciotti, K. L., Andreani, M., Barford, C., Galanter, M., and Bohlke, J. K., 2001, A bacterial method for the nitrogen isotopic analysis of nitrate in seawater and freshwater: Analytical Chemistry, 73(17), 4145-4153.

Sigman, D. M., Granger, J., DiFiore, P, J., Lehmann, M.M., Ho, R., Cane, G, and van Geen, A., 2005, Coupled nitrogen and oxygen isotope measurements of nitrate along the eastern North Pacific margin. Global Biogeochemistry Cycles, 19, GB4022.

Slomp, C.P., and Van Cappellen, P., 2004, Nutrient inputs to the coastal ocean through submarine groundwater discharge: controls and potential impact. Journal of Hydrology, 295, 64-86, http://dx.doi.org/10.1016/j.jhydrol.2004.02.018.

Smith, S., Kimmerer, W.J., Laws, E.A., Brock, R.E., Walsh, T.W., 1981, Kaneohe Bay sewage diversion experiment: perspectives on ecosystem responses to nutritional perturbation. Pacific Science, 35, 279–402.

Soicher, A.J., 1996, Assessing non-point pollutant discharge to the coastal waters of West Maui, Hawai‘i [M.S. thesis]. Honolulu, University of Hawai‘i, 98 p.

Soicher, A.J., and Peterson, F.L., 1997, Terrestrial nutrient and sediment fluxes to the coastal waters of West Maui, Hawai‘i. Pacific Science, 51, 221-232.

Sonthiphand, P., Hall, M. W., and Neufeld, J. D., 2014, Biogeography of anaerobic ammonia-oxidizing (anammox) bacteria. Frontiers in Microbiology, 5(399), http://dx.doi.org/10.3389/fmicb.2014.00399

Souza, W.R., 1981, Ground-water status report, Lahaina District, Maui, Hawai‘i, 1980. U.S. Geological Survey Open File Report 81–549, 2 map sheets.

Spiteri, C., Slomp, C.P., Charette, M.A.,Tuncay, K., and Meile, C., 2008, Flow and nutrient dynamics in a subterranean estuary (Waquoit Bay, MA, USA): field data and reactive transport modeling. Geochim. et Cosmochim. Acta, 72, 3398-3412.

State of Hawai‘i Office of Planning, 2008, Geothermal resource coverage for the state of Hawai‘i. http://planning.Hawai‘i.gov/gis/download-gis-data/ (last accessed April 13, 2016).

Stearns, H.T., and MacDonald, G.A., 1942, Geology and Groundwater resources of the island of Maui, Hawai‘i, Hawai‘i (Territory) Division of Hydrography Bulletin, 7, 344 p.

Stearns, H.T., and MacDonald, G.A., 1946, Geology and Groundwater resources of the island of Hawai‘i, Hawai‘i (Territory) Division of Hydrography Bulletin, 9, 363 p.

Street, J.H., Knee, K. L., Grossman, E.E., and Paytan, A., 2008, Submarine groundwater discharge and nutrient addition to the coastal zone and coral reefs of leeward Hawai'i: Marine Chemistry, 109(3-4), 355-378, doi: 10.1016/j.marchem.2007.08.009.

Stumm W., and Morgan J. J., 1996, Aquatic Chemistry. Wiley, New York, 1022 p.

Swain, L. A., 1973, Chemical quality of ground water in Hawai‘i: U.S. Geological Survey Report R48, 54 p.

Swanberg, C.A., and Morgan, P., 1978, Silica content of groundwater and regional heat flow. Pageoph, 117, 227-241.

Swarzenski, P.W., Storlazzi, C.D., Presto, M.K., Gibbs, A.E., Smith, C.G., Dimova, N.T., Dailer, M.L., and Logan, J.B., 2012, Nearshore morphology, benthic structure, hydrodynamics, and coastal groundwater discharge near Kahekili Beach Park, Maui, Hawai‘i. U.S. Geological Survey Open File Report 2012-1166, 34 p.

Szmant, A.M., 2002, Nutrient enrichment on coral reefs: is it a major cause of coral reef decline? Estuaries, 25(4b), 743-766.

Terada, A., Zhou, S., and Hosomi, M., 2011, Presence and detection of anaerobic ammonium-oxidizing (anammox) bacteria and appraisal of anammox processes for high-strength nitrogenous wastewater treatment: a review. Clean Tech. Environ. Policy, 13, 759-781.

Tetra Tech, Inc., 1993. Preliminary Assessment of Possible Anthropogenic Nutrient Sources in the Lahaina District of Maui – Final. Prepared for USEPA Region 9, the Hawai‘i Department of Health, and the County of Maui. July 1993, 116 p. plus appendixes.

Tetra Tech, Inc., 1994, Effluent fate study, Lahaina wastewater reclamation facility, Maui, Hawai‘i. Prepared for U.S. Environmental Protection Agency Region 9, 73 p. plus appendixes.

Thomas, D. M., 1986, Geothermal resources assessment in Hawai‘i. Geothermics, 15(4), 435-514.

Thomas, D., Haskins, H., Wallin, E., and Pierce, H., 2015. New insights into the influence of structural controls affecting groundwater flow and storage within an ocean island volcano,

Mauna Kea, Hawai‘i. December 14-18, 2015 AGU Fall Meeting, San Francisco, CA, https://agu.confex.com/agu/fm15/meetingapp.cgi/Paper/84879

Tillman, F.D., Oki, D.S., Johnson, A.G., Barber, L.B., and Beisner, K.R., 2014. Investigation of geochemical indicators to evaluate the connection between inland and coastal groundwater systems near Kaloko-Honokōhau National Historical Park, Hawai‘i. Appl. Geochem., 51, 278–292, http://dx.doi.org/10.1016/j.apgeochem.2014.10.003.

UNESCO, 1994, Protocols for the Joint Ocean Global Flux Study (JGOFS) core measurements. IOC Manual and Guides, 29.

United States Environmental Protection Agency, 1999a, Wastewater technology fact sheet: chlorine disinfection. Washington D.C., Office of Water, 7 p.

United States Environmental Protection Agency, 1999b, Wastewater technology fact sheet: ultraviolet disinfection. Washington D.C., Office of Water, 7 p.

Vitousek, P, 2004, Nutrient cycling and limitation: Hawai‘i as a model system. Oxford and Princeton, Princeton University Press, 223 p.

Wakida, F.T., and Lerner, D.N., 2004, Non-agricultural souces of groundwater nitrate: a review and case study. Water Research, 39, 3-16, http://dx.doi.org/10.1016/j.watres.2004.07.026

Ward, M.H., deKok, T.M., Levallois, P., Brender, J., Gulis, G., Nolan, B.T., and VanDerslice, J.,2005, Workgroup report: drinking-water nitrate and health-recent findings and research needs. Environmental Health Perspectives, 113, 1607-1614, http://dx.doi.org/10.1289/ehp.8043

Whittier, R.B., and El-Kadi, A.I., 2009, Human and Environmental Risk Ranking of Onsite Sewage Disposal Systems. Final report submitted to State of Hawai‘i Department of Health, Safe Drinking Water Branch, Honolulu, Hawai‘i, 72 p.

Whittier, R., and El-Kadi, A.I., 2014, Human and Environmental Risk Ranking of Onsite Sewage Disposal Systems: Molokai, Maui, and Hawai‘i. Final Report submitted to State of Hawai'i Department of Health, Safe Drinking Water Branch, Honolulu, Hawai‘i, 258 p.

Wilkinson, C., 2008, Status of coral reefs of the world: 2008. Global Coral Reef Monitoring Network and Reef and Rainforest Centre, Townsville, Australia, 296 p.

Williams, I., and Sparks, R., 2008, Status and trends of benthic and fish communities around Maui. In: Vermeij, M. (Ed.), Coral reefs of Maui: status, stressors, and suggestions, San Francisco, Blurb, Inc., p. 8-12.

Zhu, G., Wang, S., Wang, W., Wang, Y., Zhou, L., Jiang, B., Hubb., J.M.O.D.C., Risgaard-Petersen, N., Schwark, L., Peng, Y., Hefting., M.M., Jetten, M.S.M., and Yin, C., 2013, Hotspots of anaerobic ammonium oxidation at land-freshwater interfaces. Nature Geoscience, 6, 103-107.

Zhou, S., 2007, Stoichiometry of biological nitrogen transformations in wetlands and other ecosystems. Biotechnology Journal, 2, 497-507, http://dx.doi.org/10.1002/biot.200600078.